Finite Element Simulation and Assessment of Single-Degree-of-Freedom Prediction Methodology for Insulated Concrete Sandwich Panels Subjected to Blast Loads

by

Charles Michael Newberry

A thesis submitted to the Graduate Faculty of
Auburn University
in partial fulfillment of the
requirements for the Degree of
Master of Civil Engineering

Auburn, Alabama
May 9, 2011

Keywords: insulated sandwich panel, single-degree-of-freedom,
finite element modeling

Approved by

James S. Davidson, Chair, Associate Professor of Civil Engineering
Justin D. Marshall, Assistant Professor of Civil Engineering
Robert W. Barnes, James J. Mallett Associate Professor of Civil Engineering

Abstract

This report discusses simulation methodologies used to analyze large deflection static and dynamic behavior of foam-insulated concrete sandwich wall panels. Both conventionally reinforced cast-on-site panels and precast/prestressed panels were considered. The experimental program used for model development and validation involved component-level testing as well as both static and dynamic testing of full-scale wall panels. The static experiments involved single spans and double spans subjected to near-uniform distributed loading. The dynamic tests involved spans up to 30 ft tall that were subjected to impulse loads generated by an external explosion. Primary modeling challenges included: (1) accurately simulating prestressing initial conditions in an explicit dynamic code framework, (2) simulating the concrete, reinforcement, and foam insulation in the high strain rate environment, and (3) simulating shear transfer between wythes, including frictional slippage and connector rupture. Correlation challenges, conclusions and recommendations regarding efficient and accurate modeling techniques are highlighted. The modeling methodologies developed were used to conduct additional behavioral studies and help to assess single-degree-of-freedom prediction methodology developed for foam-insulated precast/prestressed sandwich panels for blast loads.

Acknowledgments

This work was sponsored in part by the Air Force Research Laboratory and a research fellowship grant from the Precast/Prestressed Concrete Institute (PCI). The static tests from which the model validation data was generated were conducted at the University of Missouri Remote Testing Facility under the direction of Professor Hani Salim. Professor Clay Naito of Lehigh University was the lead technical advisor of the AFRL/PCI test program. The dynamic tests were conducted by the Engineering Mechanics and Explosives Effects Research Group, Force Protection Branch, Airbase Technologies Division, of the Air Force Research Laboratory (AFRL) at Tyndall Air Force Base Florida. The AFRL test program was coordinated by John Hoemann of Applied Research Associates, Inc. The test program also involved other employees of ARA and Black & Veatch, Federal Services Division. Dr. Jun Suk Kang, Postdoctoral Research Assistant, Auburn University, provided valuable technical assistance with the development of the many finite element models involved in the project.

Table of Contents

List of Tables

List of Figures

CHAPTER 1

INTRODUCTION

1.1 Overview

Threats to structures and the people residing within are increasing. Since the attacks on the World Trade Center and the Pentagon on September 11, 2001, the realization of such threats has promoted research in the field of structures subjected to impulse loads. The study of structures subjected to impulse loads has existed for decades; however, a shift in the type of risks structures face has occurred due to the more localized manner of current threats. Also, most of the criteria for designing structural components subjected to impulse loads were created before many modern concrete components were introduced.

The behavior and design of structural components subjected to impulse loads differs from the behavior under static loads. Most loads such as wind and gravity loads are assumed to be static since the time in which they are applied is relatively large enough not to induce significant accelerations of structural components. Dynamic loads such as blasts last only a fraction of a second but may be quite large in magnitude and can induce significant accelerations and large displacements.

The design of structural components for impulse loads is also different from design for typical loads in that the failure of the structural component is acceptable

depending upon how the component failed. Components are not intended to necessarily be functional after an incident; the primary goal in blast design is the safety of the people residing within the structure. Often in attacks, fragmentation of structural components leads to injuries or fatalities of occupants of the structure.

A common type of modern exterior wall construction, the sandwich panel, contains two concrete wythes separated by a layer of foam insulation. The concrete wythes can be either conventionally reinforced or prestressed. Reinforcement allows the concrete to reach its full flexural strength and resist lateral, construction, and handling loads. Since these wall structures also serve the purpose of insulating the building, it is common for ties that connect concrete wythes to each other to be made of non-metallic materials (PCI, 2004).

1.2 Objectives

The objective of this project was to develop ways of predicting dynamic response of precast insulated concrete sandwich panels using high-fidelity finite element (FE) modeling. With these models, a detailed study of sandwich panel behavior under blast loads was completed. Also single-degree-of-freedom (SDOF) prediction methodology was examined. Finite element models were used for comparisons to SDOF prediction models.

1.3 Scope and Methodology

Due to the high costs associated with full-scale dynamic tests, the use of finite element models is crucial to understanding failure modes, energy dissipation, and damage

of sandwich panels subjected to impulse loads. Loading-tree tests conducted at the University of Missouri were used to validate the FE modeling approach and input parameters. Static tests used for validation consisted of (1) simple reinforced concrete beams, (2) conventionally reinforced sandwich panels, and (3) prestressed sandwich panels. Also, shear tests involving a variety of connectors were conducted to assess the shear transfer through ties and its impact on composite action. High-fidelity, dynamic FE models were developed, and full-scale dynamic tests conducted by the Air Force Research Laboratory (AFRL) were used to validate the dynamic analysis approach. Once the dynamic FE models were validated, behavioral studies were conducted that examined concentrated reinforcement strain at hinge locations, energy attenuation, and dynamic reactions. Single-degree-of-freedom (SDOF) models developed with Microsoft Excel to provide predictions for sandwich panels subjected to blast loads. FE models were used to expand the data points used for comparison against SDOF predictions.

1.4 Report Organization

This report consists of six chapters. Chapter 1 lists the objectives, scope, methodology, and report organization. Chapter 2 provides a literature review and background of relevant history and analytical information. Chapter 3 discusses the model developments and validation. Chapter 4 consists of behavioral observations. Chapter 5 describes the assessment of single-degree-of-freedom prediction models and comparison to full-scale dynamic tests. Chapter 6 summarizes the report and provides conclusions and recommendations for possible future work.

CHAPTER 2

TECHNICAL BACKGROUND

2.1 Overview

Heightened risks globally have motivated interest in the effects of structural components subjected to impulse loads. Throughout the Cold War, vast amounts of research were conducted on the effects of blasts on structures, leading to a majority of the current understanding of structures subjected to impulse loads. Design of structures subjected to blast loads is greatly influenced by the research motivated by the threat of large, nuclear airbursts. With the end of the Cold War came awareness of new, more localized threats. Attacks in which explosives in vehicles placed next to structures increased in frequency, the most known such attack being that of the Murrah Federal Building in Oklahoma City in 1995 (NRC, 1995). Overseas, attacks such as that which targeted the Khobar Towers in Riyadh, Saudi Arabia, killed 19 marines and injured hundreds others (Jamieson, 2008).

With increased consciousness of more localized threats came increased funding for blast resistance of a diverse spectrum of structural components. A common type of component, the sandwich panel, is comprised of two precast concrete wythes separated by a layer of foam insulation. Cladding is the most common use of the sandwich panel; they also serve the purpose of insulating the building. For this reason, it is common for ties that connect concrete wythes to be made of non-metallic materials to keep the

thermal resistance of the panel at a maximum. Reinforcement can be conventional or prestressed. Reinforcement allows the concrete to reach its full flexural strength and resist lateral loads and transportation loads of the panels.

The sandwich panel was introduced into the market after most research on concrete structural components was completed and design criteria were in place. It is anticipated that the present research fills this vacuum of understanding.

2.2 Blast Loading

An explosion is a violent load scenario that occurs due to the release of large amounts of energy in a very short amount of time. This energy could come in the form of a chemical reaction as in explosive ordnances or from the rupture of high pressure gas cylinders (Tedesco, 1999). Trinitrotoluene (TNT) equivalence is used to compare the effects of different explosive charge materials. The equation used for calculating the TNT equivalence based on weight is as follows:

$$W_E = \frac{H^D{}_{EXP}}{H^D{}_{TNT}} \cdot W_{EXP} \tag{2-1}$$

where W_E is the TNT equivalent weight, W_{EXP} is the weight of the explosive, $H^D{}_{EXP}$ is the heat of detonation of the explosive, and is the heat of detonation of TNT.

When an explosion occurs, an increase in the ambient air pressure, called overpressure, presents itself as a shock front that propagates spherically from the source. When the shock front comes in contact with a surface normal to itself, an instantaneous reflected pressure is experienced by the surface that is twice the overpressure plus the dynamic pressure. The dynamic pressure is the component of reflected pressure that takes in account the density of air and the velocity of the air particles (Biggs, 1964). This peak

positive pressure can be quite large and decays nonlinearly to a pressure below the ambient air pressure. The time period of positive pressure that the surface experiences is called the positive phase. The negative phase occurs when the pressure experience by the surface is negative (i.e. suction). The negative phase, although much smaller in magnitude than the positive phase, affects the surface for a relatively extended amount of time compared to the positive phase (USACE PDC, 2006). Figure 2.1 illustrates the basic shape, relative magnitudes, and durations for the positive and negative phases of a pressure wave created by an explosion.

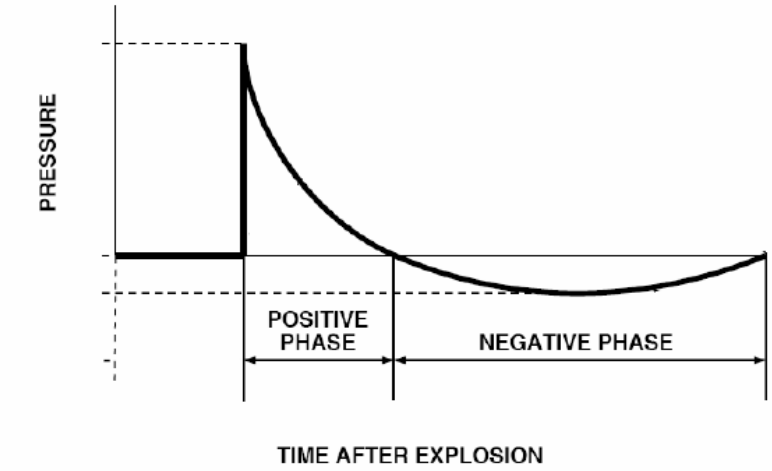

Fig. 2.1. Pressure vs. time description for an arbitrary explosion

Structures at risk are designed to resist the reflected pressure of a blast load. Peak positive pressure and impulse (area under the pressure vs. time curve) are the most important considerations in design of structures for impulse loads. A conservative assumption used in design is to only consider the positive phase, since neglect of the negative phase "will cause similar or somewhat more structural response", while taking

into account the “ratio of the blast load duration to the natural period of the structural component” (USACE PDC, 2006).

Due to the violent nature of blast loading, a select few variables can be determined in tests considering blast. Under the conditions of dust, debris, and vibration that come with blast testing, it is possible to record deflection histories of certain locations of test specimens, reflected pressure histories, and high-speed video. All of these methods were used in full-scale dynamic tests referenced in this report.

2.3 Precast/Prestressed Sandwich Wall Panels

The typical configuration of concrete sandwich wall panels is two wythes (i.e. layers) of reinforced concrete, either conventionally reinforced or prestressed, separated by a layer of insulating foam with some arrangement of connectors that secure the concrete wythes through the foam.

Sandwich panels are commonly used for both exterior and interior walls and also can be designed solely for cladding or as load-bearing members (PCI, 1997). Sandwich panels have become popular due to their energy efficiency. The amount of mass provided by the concrete layers along with the layer of foam provide the designer with a wide variety of thermally-efficient options for walls. In the past, connectors used as shear ties have primarily consisted of steel tie or solid concrete sections. However, these create thermal bridges that can lower the thermal efficiency of the panel and cause cool locations on the interior concrete wythe, leading to condensation. The desire for more thermally efficient structures has in turn produced a variety of thermally efficient shear connectors. The exterior layer of concrete can receive architectural finishes that bring an

aesthetic appeal to sandwich panels. Only panels used solely for cladding purposes were studied in this effort. All full-scale dynamic tests specimens used energy-efficient shear connectors made of either carbon fiber or fiberglass materials.

Sandwich panels are primarily designed to withstand handling, transportation, and construction loads. These conditions most often provide the largest stresses within the service life of the sandwich panel. The thermal efficiency desired can control the thickness of the concrete and insulation wythes; for instance, if the structure is used for cold storage, a required R-value (thermal efficiency index) will be needed (PCI, 1997). Once concrete and foam thickness have been chosen, the panel is checked against handling/erection loads. If the panel design withstands handling/construction stresses, the panel is then checked against an allowable deflection due to lateral loads (i.e. wind or seismic).

Depending upon the amount of shear transfer desired, the sandwich panel can be designed as either a non-composite or composite panel. When designing non-composite panels, the concrete wythes are considered to act independently of each other. Composite panels are designed such that the concrete wythes act dependently or fully composite; this is accomplished by providing full shear transfer between the wythes, most commonly with the use of solid concrete sections or shear connectors produced with the intention of allowing the two concrete wythes to resist load together.

> "Because present knowledge of the behavior of sandwich panels is primarily based on observed phenomena and limited testing, some difference of opinion exists among designers concerning such matters as degree of composite action and the resulting panel performance, the effectiveness of shear transfer connectors and the effect of insulation

type and surface roughness on the degree of composite action" (PCI, 2007).

Pessiki and Mlynarczyk (2003) investigated the flexural behavior of sandwich panels and the contribution to composite action of various shear transfer mechanisms. Shear mechanisms included regions of solid concrete, steel M-ties that passed through the insulation, and bond between concrete and insulation wythes. Four sandwich panel specimens were created with one panel having all three shear transfer mechanisms and the other three panels each having only one of the shear transfer mechanisms. Research showed that solid concrete sections provided the most strength and stiffness with steel M-tie connectors only moderately affecting the composite behavior of the panels. The affect of bond between concrete and foam wythes was virtually negligible. Through their research, Pessiki and Mlynarczyk found that panels with the most robust shear transfer mechanisms that behaved either fully composite or nearly fully composite did not behave consistently in regards to flexural cracking. Flexural tensile strengths of nearly fifty percent below the theoretical tensile strength of concrete in flexure arose, conceivably from a lack of localized composite action, causing larger amounts of stress at midspan.

2.4 Design of Precast/Prestressed Concrete Structures for Blast

The key blast design consideration of a structure is the safety of occupants of the structure. Much like the case of the attack on the Khobar Towers, Saudi Arabia in 1996, most injuries and fatalities occur due to building debris accelerated by the blast. Precast/prestressed components, along with their connections to the structure, should be designed to withstand the blast to prevent falling or flying debris, even if the structural component itself is damaged beyond repair or lost entirely (Alaoui and Oswald, 2007).

A common design technique of precast/prestressed concrete structures subjected to blasts is based on a single-degree-of-freedom (SDOF) methodology. “Structural components subject to blast loads can be modeled as an equivalent SDOF mass-spring system with a nonlinear spring” (USACE PDC, 2006). A manual by the Departments of the U.S. Army, Navy, and Air Force (1990) titled “Structures to Resist the Effects of Accidental Explosions” was written to support application of this method to different types of structures. The report is most commonly referenced by its U.S. Army report number, TM 5-1300 and has been published under the Unified Facilities Criteria system as UFC 3-340-02 (Department of Defense, 2008).

CHAPTER 3
MODEL DEVELOPMENT AND VALIDATION

3.1 Overview

The primary challenges associated with FE modeling of foam-insulated concrete sandwich panels include: accurately describing and incorporating the fracture and damage behavior of reinforced concrete, integrating foam constitutive models, accurately describing the transfer of shear between concrete wythes, incorporating strain rate effects on material behavior, and simulating initial conditions associated with the prestressed reinforcement strands. Validation of input parameters was accomplished in four parts: (1) simple reinforced concrete beams subjected to uniform loading, (2) static testing of shear connectors, (3) static testing of sandwich panels (prestressed and conventionally reinforced) subjected to uniform loading, and (4) full-scale dynamic tests of sandwich panels (prestressed and conventionally reinforced). An organizational chart of FE model validation can be seen in Figure 3.1. Component and material level test results were used to define appropriate constitutive model input. Direct shear tests were used to evaluate the shear resistance input required to simulate the various ties used in the full-scale sandwich panels specimens.

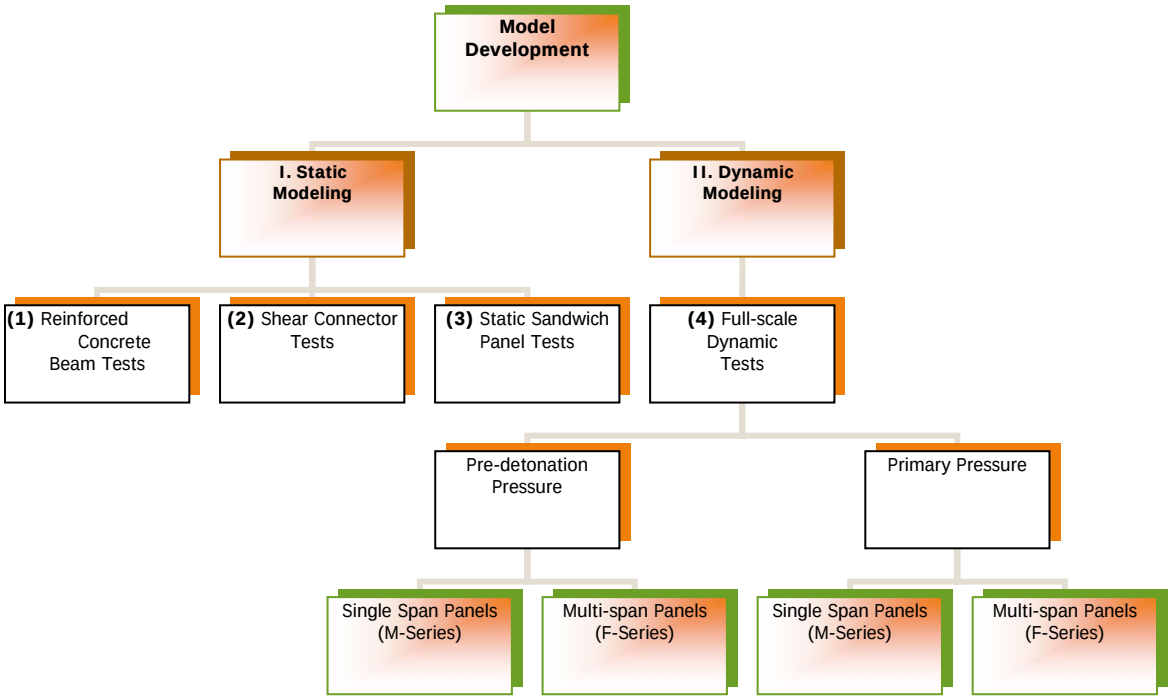

Fig. 3.1. Organizational chart of model development

3.2. Reinforced Concrete Beam Validation

Two conventionally reinforced concrete beam designs were tested under a near-uniform distributed load using the University of Missouri loading-tree apparatus shown in Figure 3.2. All samples were 18 inches wide, simply supported, with a 120 inch clear span. Two samples of each design were constructed and total load and midspan vertical displacement were recorded for each sample. The test matrix and reinforcement description are provided in Table 3.1 and Figure 3.3. Concrete cylinders were cast and compressive strengths obtained via ASTM C39/C39M were used in the development of the concrete damage model. Reinforcements (steel and welded wire) were tested for tensile capacity using standards provided by ASTM E8. It should be noted that the

purpose of these reinforced beam tests was not finite element validation. These test results were selected since they provided flexural resistance data obtained using the same loading-tree apparatus later used in static tests of sandwich panel specimens.

Fig. 3.2. University of Missouri loading-tree apparatus setup and reinforced concrete beam validation sample

3.2.1 Concrete Model and Parameters

A numerical strategy for solving any boundary value problem with location of fracture should consider complex constitutive modeling. It is necessary to identify a large number of parameters if a structural, heterogeneous material such as concrete is taken into account. Concrete is comprised of a wide range of materials, whose properties are quantitatively and qualitatively different. The ABAQUS Concrete Damage Plasticity (CDP) constitutive model used in this study is based on the assumption of scalar

(isotropic) damage and is designed for applications where the concrete is subjected to arbitrary loading conditions, including cyclic loading (ABAQUS, 2008). The model takes into consideration the degradation of the elastic stiffness induced by plastic straining both in tension and compression. The model is a continuum plasticity-based damage model that assumes that the primary failure mechanisms are tensile cracking and compressive crushing of the concrete material.

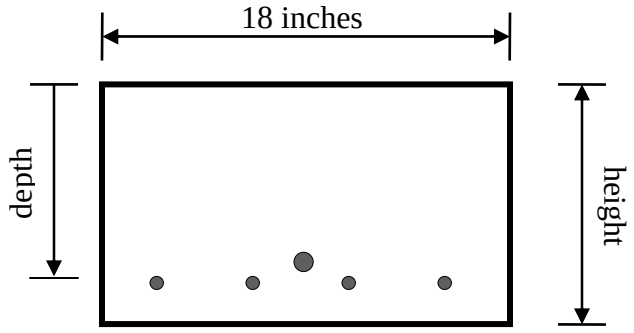

Figure 3.3. Layout of reinforced concrete beam specimens

Table 3.1. Description of reinforced concrete beam samples

Name	***Height (inch)***	***Reinforcement/depth***
RC Beam Design 1	11.5	Welded-Wire W4 x W4 /10” # 8/ 9.5”
RC Beam Design 2	6	Welded-Wire W4 x W4 / 3.25” # 4/ 3”

3.2.2 Mechanical Behavior and Concrete Plasticity

The evolution of the yield (or failure) surface is controlled by two hardening variables, tensile and compressive equivalent plastic strains ($\tilde{\varepsilon}_t^{pl}$ and $\tilde{\varepsilon}_c^{pl}$), linked to failure mechanisms under tension and compression loading, respectively.

The model assumes that the uniaxial tensile and compressive response of concrete

is characterized by damaged plasticity, as shown in Figure 3.4. Under uniaxial tension the stress-strain response follows a linear elastic relationship until the value of the failure stress, σ_{t0}, is reached. The failure stress corresponds to the onset of micro-cracking in the concrete material. Beyond the failure stress, the formation of micro-cracks is represented macroscopically with a softening stress-strain response, which induces strain localization in the concrete structure. Under uniaxial compression, the response is linear until the value of initial yield, σ_{c0}, is reached. In the plastic regime, the response is typically characterized by stress hardening followed by strain softening beyond the ultimate stress, σ_{cu}. This representation, although somewhat simplified, captures the main features of the response of concrete.

It is assumed that the uniaxial stress-strain curves can be converted into stress versus plastic-strain curves. This conversion is performed automatically by ABAQUS from the user-provided stress versus "inelastic" strain data. As shown in Figure 3.4, when the concrete specimen is unloaded from any point on the strain softening branch of the stress-strain curves, the unloading response is weakened: the elastic stiffness of the material appears to be damaged (or degraded). The degradation of the elastic stiffness is characterized by two damage variables, d_t and d_c, which are assumed to be functions of the plastic strains, temperature, and field variables:

$$d_t = d_t\left(\tilde{\varepsilon}_t^{pl}, \theta, f_i\right); \; 0 \le d_t \le 1, \tag{3-1}$$

$$d_c = d_c\left(\tilde{\varepsilon}_c^{pl}, \theta, f_i\right); \; 0 \le d_c \le 1 \tag{3-2}$$

The damage variables can take values from zero, representing the undamaged material, to one, which represents total loss of strength. If E_0 is the initial (i.e. undamaged) elastic

stiffness of the material, the stress-strain relations under uniaxial tension and compression loading are, respectively:

$$\sigma_t = (1-d_t)E_0(\varepsilon_t - \bar{\varepsilon}_t^{pl}), \tag{3-3}$$

$$\sigma_c = (1-d_c)E_0(\varepsilon_c - \bar{\varepsilon}_c^{pl}) \tag{3-4}$$

The "effective" tensile and compressive cohesion stresses are defined as follows:

$$\bar{\sigma}_t = \frac{\sigma_t}{(1-d_t)} = E_0(\varepsilon_t - \bar{\varepsilon}_t^{pl}), \tag{3-5}$$

$$\bar{\sigma}_c = \frac{\sigma_c}{(1-d_c)} = E_0(\varepsilon_c - \bar{\varepsilon}_c^{pl}) \tag{3-6}$$

The effective cohesion stresses determine the size of the yield (or failure) surface.

Concrete plasticity can be simulated by defining flow potential, yield surface, and viscosity parameters as follows:

The effective stress is defined as

$$\bar{\sigma} = \mathrm{D}_0^{el} : (\varepsilon - \varepsilon^{pl}) \tag{3-7}$$

where D_0^{el} is the initial (undamaged) elasticity matrix

The plastic flow potential function and the yield surface make use of two stress invariants of the effective stress tensor, namely the hydrostatic pressure stress,

$$\bar{p} = -\frac{1}{3}\mathrm{trace}(\bar{\sigma}), \tag{3-8}$$

and the von Mises equivalent effective stress,

$$\bar{q} = \sqrt{\frac{3}{2}(\bar{\mathrm{S}}:\bar{\mathrm{S}})}, \tag{3-9}$$

where $\bar{\mathrm{S}}$ is the effective stress deviator, defined as

$$\bar{\mathrm{S}} = \bar{\sigma} + \bar{p}\mathrm{I} \tag{3-10}$$

The concrete damaged plasticity model assumes non-associated potential plastic flow. The flow potential G used for this model is the Drucker-Prager hyperbolic function (Drucker et al., 1952):

$$G = \sqrt{(\varepsilon \sigma_{t0} \tan\psi)^2 + \bar{q}^2} - \bar{p} \tan\psi \tag{3-11}$$

where $\psi(\theta, f_i)$ is the dilation angle measured in the *p*–*q* plane at high confining pressure:

$$\sigma_{t0}(\theta, f_i) = \sigma_t\big|_{\tilde{\varepsilon}_t^{pl}=0, \dot{\tilde{\varepsilon}}_t^{pl}=0} \tag{3-12}$$

is the uniaxial tensile stress at failure, taken from the user-specified tension stiffening data; $\varepsilon(\theta, f_i)$ is a parameter, referred to as the eccentricity, that defines the rate at which the function approaches the asymptote (the flow potential tends to a straight line as the eccentricity tends to zero). This flow potential, which is continuous and smooth, ensures that the flow direction is always uniquely defined. The function approaches the linear Drucker-Prager flow potential asymptotically at high confining pressure stress and intersects the hydrostatic pressure axis at 90°. The default flow potential eccentricity is $\varepsilon = 0.1$, which implies that the material has almost the same dilation angle over a wide range of confining pressure stress values. Increasing the value of ε provides more curvature to the flow potential, implying that the dilation angle increases more rapidly as the confining pressure decreases. Values of ε that are significantly less than the default value may lead to convergence problems if the material is subjected to low confining pressures because of the very tight curvature of the flow potential locally where it intersects the *p*-axis.

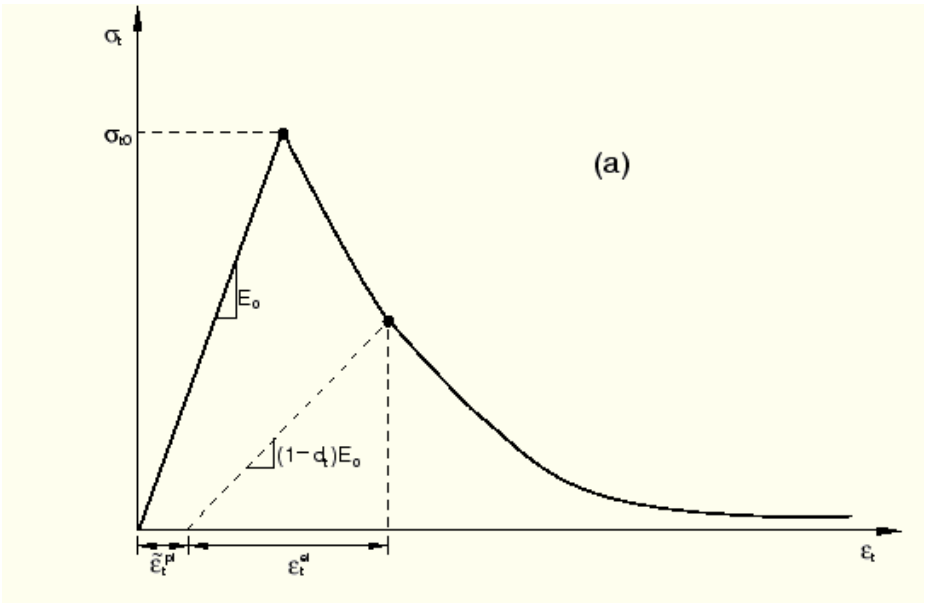

Fig. 3.4. Response of concrete to uniaxial loading in (a) tension and (b) compression (ABAQUS, 2008)

3.2.3 Yield Function

The model made use of the yield function of Lubliner et al. (1989), with the modifications proposed by Lee and Fenves (1998) to account for different evolution of strength under tension and compression. The evolution of the yield surface is controlled

by the hardening variables, $\tilde{\varepsilon}_t^{pl}$ and $\tilde{\varepsilon}_c^{pl}$. In terms of effective stresses, the yield function takes the form

$$F = \frac{1}{1-\alpha}\left(\bar{q} - 3\alpha\bar{p} + \beta\left(\tilde{\varepsilon}_t^{pl}\right)\left\langle\hat{\bar{\sigma}}_{\max}\right\rangle - \gamma\left\langle-\hat{\bar{\sigma}}_{\max}\right\rangle\right) - \bar{\sigma}_c\left(\tilde{\varepsilon}_c^{pl}\right) = 0 \tag{3-13}$$

with

$$\alpha = \frac{\left(\sigma_{b0}/\sigma_{c0}\right)-1}{2\left(\sigma_{b0}/\sigma_{c0}\right)-1}; 0 \le \alpha \le 0.5, \tag{3-14}$$

$$\beta = \frac{\bar{\sigma}_c\left(\tilde{\varepsilon}_c^{pl}\right)}{\bar{\sigma}_t\left(\tilde{\varepsilon}_t^{pl}\right)}(1-\alpha) - (1+\alpha), \tag{3-15}$$

$$\gamma = \frac{3(1-K_c)}{2K_c - 1} \tag{3-16}$$

Where $\hat{\bar{\sigma}}_{\max}$ is the maximum principal effective stress; σ_{b0}/σ_{c0} is the ratio of initial equibiaxial compressive yield stress to initial uniaxial compressive yield stress (the default value is 1.16); K_c is the ratio of the second stress invariant on the tensile meridian, *q*(TM), to that on the compressive meridian, *q*(CM), at initial yield for any given value of the pressure invariant *p* such that the maximum principal stress is negative, $\hat{\sigma}_{\max} < 0$ (see Figure 3.4); it must satisfy the condition $0.5 < K_c \le 1.0$ (the default value is 2/3); $\bar{\sigma}_t\left(\tilde{\varepsilon}_t^{pl}\right)$ is the effective tensile cohesion stress; and $\bar{\sigma}_c\left(\tilde{\varepsilon}_c^{pl}\right)$ is the effective compressive cohesion stress. Typical yield surfaces are shown in Figure 3.5 on the deviatoric plane.

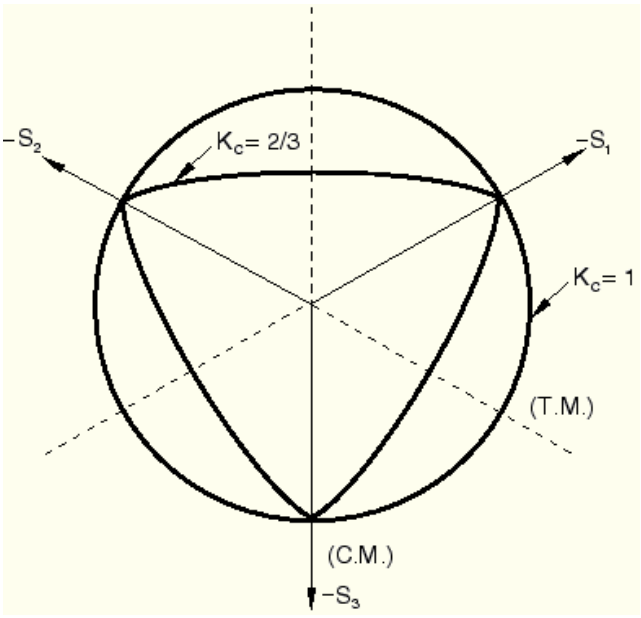

Fig. 3.5. Yield surfaces in the deviatoric plane, corresponding to different values of K_c (ABAQUS, 2008)

3.2.4 Material Parameters of Concrete Damage Plasticity Model

The material parameters of the concrete damage plasticity model are presented in Table 3.2. For the identification of the constitutive parameters of the CDP model, the following laboratory tests are necessary (Jankowiak, et al., 2005): 1) uniaxial compression, 2) uniaxial tension, 3) biaxial failure in plane state of stress , 4) triaxial test of concrete (superposition of the hydrostatic state of stress and the uniaxial compression stress). These tests are necessary to identify the parameters, which determine the shape of the flow potential surface in the deviatoric and meridian plane and the evolution rule of the material parameters (the hardening and the softening rule in tension and compression).

Table 3.2. Material parameters of concrete damage plasticity model

Concrete		Parameters of CDP model	
E(psi)	3.6E+6	ψ , dilation angle	30°
ν	0.18	ε , flow potential eccentricity	0.1
Density (pcf)	150	$\sigma_{b0} / \sigma_{c0}$ *	1.16
Compressive strength (psi)	4,000	K_c **	0.667
Tensile strength (psi)	300	μ , Viscosity parameter	0.0
Concrete Compression Hardening		Concrete Tension Stiffening	
Yield stress (psi)	Crushing strain	Remaining stress after cracking (psi)	Cracking strain
3,500	0.0	300	0.0
4,000	0.0005	0	0.002
2,500	0.0012	-	-

* The ratio of initial equibiaxial compressive yield stress to initial uniaxial compressive yield stress.
** The ratio of the second stress invariant on the tensile meridian, *q*(TM), to that on the compressive meridian, *q*(CM).

3.2.5 Reinforcements (Rebar and Welded Wire Reinforcement)

Reinforcement in concrete structures is typically provided by means of reinforcing bars (rebar), which are modeled as one-dimensional rods that can be defined singly or embedded in oriented surfaces. Rebar is typically used with metal plasticity models to describe the behavior of the rebar material and is superposed on a mesh of standard element types used to model the concrete. With this modeling approach, the concrete behavior is considered independently of the rebar. Effects associated with the rebar/concrete interface, such as bond slip and dowel action, are modeled approximately by introducing "tension stiffening" into the concrete modeling to simulate load transfer across cracks through the rebar. In this study, rebar and welded wire reinforcement (WWR) were modeled using beam elements and the embedded element technique in

ABAQUS. The rebar and WWR strength parameters were based upon laboratory testing of reinforcement samples used in construction of the samples. Table 3.3 summarizes material parameters for rebar (Figure 3.6) and WWR (Figure 3.7).

Table 3.3. Material strengths for reinforcements

	Modulus of elasticity (psi)	Poisson's ratio	Density (pcf)	Yield strength (psi)
Rebar	2.9E+7	0.3	490	69,710*
WWR	2.9E+7	0.3	490	94,000**

*See Figure 3.6 ** See Figure 3.7

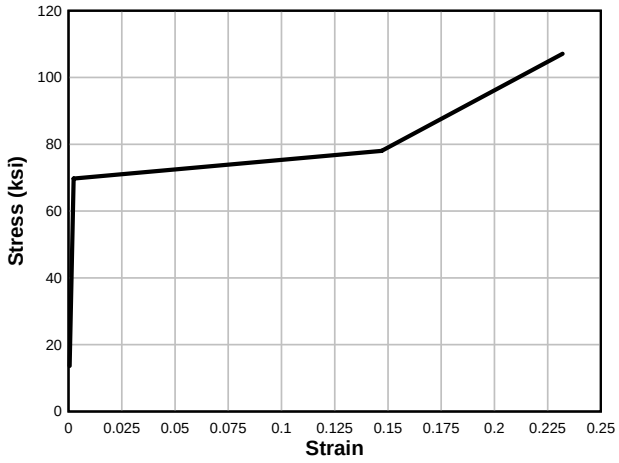

Fig. 3.6. Stress-strain relationship of rebar used in the analyses

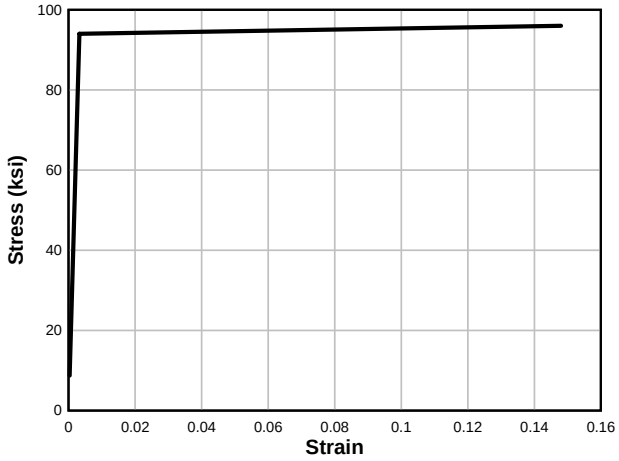

Fig. 3.7. Stress-strain relationship of WWR used in the analyses

3.2.6. Geometry, Elements, Loading, and Boundary Conditions.

An example of the RC beam models developed in ABAQUS is shown in Figure 3.8. The concrete and reinforcements (rebar and WWR) were modeled using solid element (C3D20; 20-node quadratic brick) and truss element (T3D3; 3-node quadratic truss), respectively. The rebar and WWR were embedded by using *Embedded Element option in ABAQUS. The interface properties between concrete and reinforcements were assumed to be fully-bonded. As with the RC samples, FE models were simply supported and uniformly loaded across a clear span of 120 in.

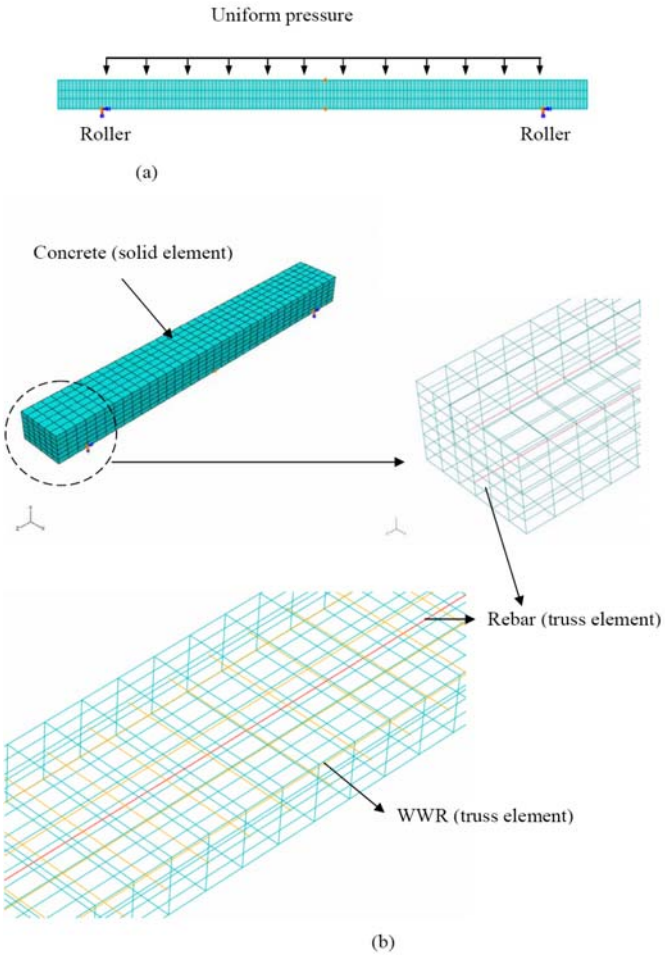

Fig. 3.8. FE Models: (a) loading and boundary conditions and (b) concrete, rebar and WWR elements

3.2.7. Nonlinear Incremental Analysis

Geometrically nonlinear static problems sometimes involve buckling or collapse behavior, where the load-displacement response shows a negative stiffness and the structure must release strain energy to remain in equilibrium. This study used Riks method to predict geometrical nonlinearity and material nonlinearity of reinforced concrete structures. The Riks method uses the load magnitude as an additional unknown; it solves simultaneously for loads and displacements. Therefore, another quantity must be used to measure the progress of the solution; ABAQUS uses the "arc length," along the static equilibrium path in load-displacement space. This approach provided solutions regardless of whether the response is stable or unstable (ABAQUS, 2008).

3.2.8 Static RC Flexure Test and FE Results Comparison

As shown in Figure 3.9, the results from FE analyses were generally in good agreement with test results. The initial stiffness of the FE models was slightly higher than that of the test beams, which is likely due to 1) cracking of samples that occurred prior to testing, 2) seating of the support conditions during testing, and/or 3) approximations used for the compressive and tensile strength of the concrete. After yielding, models continued to predict load/displacement behavior within the acceptable margin of error for such nonlinear analyses. The ability to predict concrete behavior at large displacements is important due to the large displacements experience by concrete components subjected to blast loads.

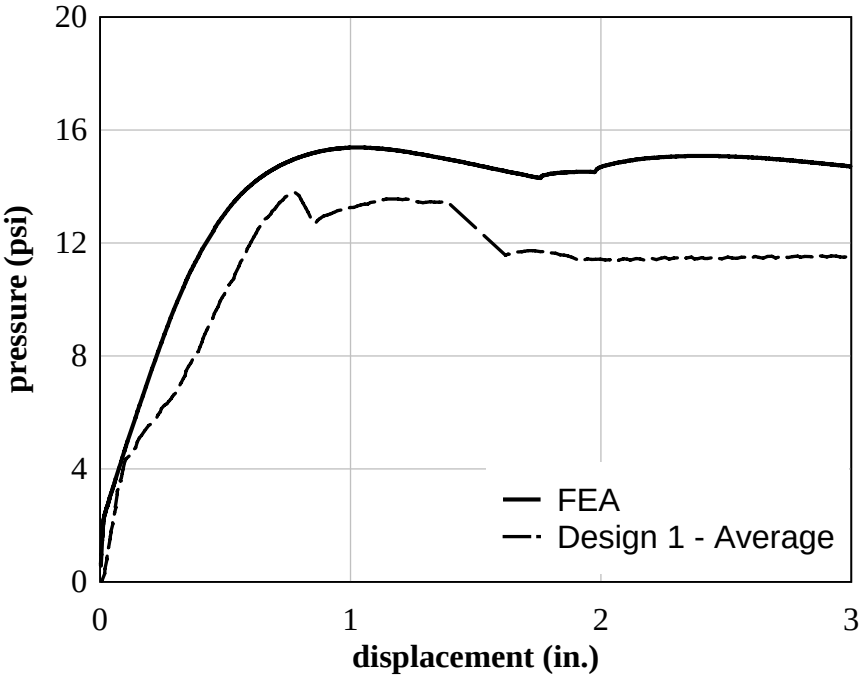

(a)

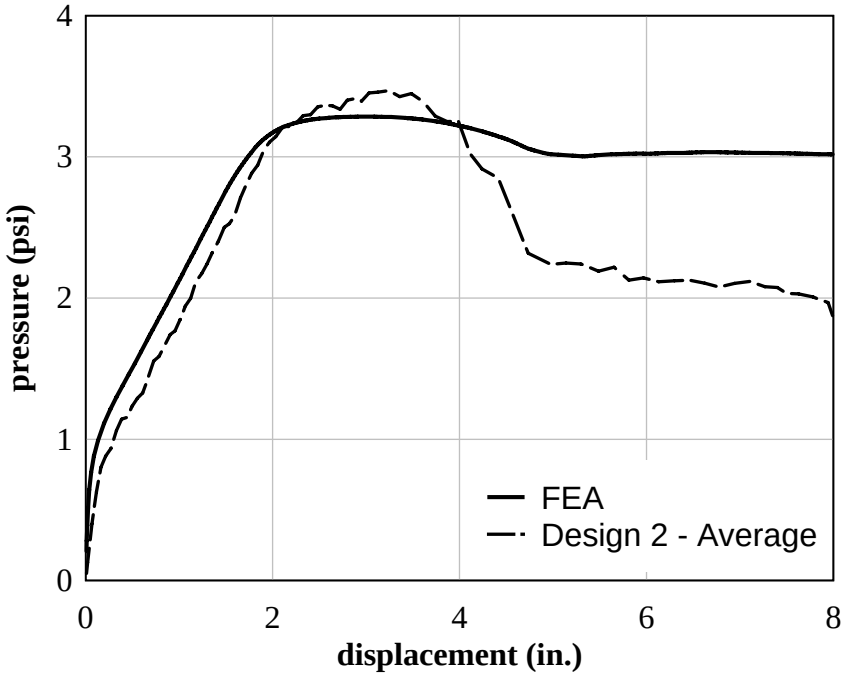

(b)

Fig. 3.9 (a) RC Beam Design 1 vs. FEA, (b) RC Beam Design 2 vs. FEA

3.3 Static Tests of Sandwich Panels

Static tests of prestressed and conventionally reinforced sandwich panels were also conducted under uniform distributed loading (Naito et al. 2010a). Important strength and stiffness design parameters included: configuration of concrete and foam layers, the type of insulation foam used, and reinforcement (prestressed or conventional). Figure 3.10 displays the design parameters of a conventionally reinforced sandwich panel specimen. Direct shear tests of various shear ties were completed to better understand shear tie behavior and provide a means for modeling (Naito et al. 2009a). Insulating foams included expanded polystyrene (EPS), extruded expanded polystyrene (XPS), and polyisocyanurate (PIMA). Compressive testing of insulating foams employed as construction materials was used to define the stress/strain material property input for foam elements (Jenkins 2008). Total load and vertical displacement of the midspan were recorded.

3.3.1 Shear Connectors

There are several means of transferring shear between concrete wythes in precast sandwich panels. Solid concrete regions that pass through the foam and various steel connectors have been used in the industry for quite some time for connecting concrete layers and transferring shear. Solid concrete regions provide good points for attached hardware used in handling, transportation, and construction. Steel connectors, such as C-clips and M-clips, are also inexpensive and widely available options for connecting concrete layers. The drawback for both solid concrete regions and steel connectors is they allow for a thermal bridge through the insulation, decreasing the thermal efficiency of the

panel. Energy-efficient shears ties were developed from materials such as fiberglass and carbon fiber and are currently being used in modern energy-efficient construction. Shear ties can also be categorized as non-composite or composite, depending upon the amount of composite action required for the service life of the sandwich panel being designed.

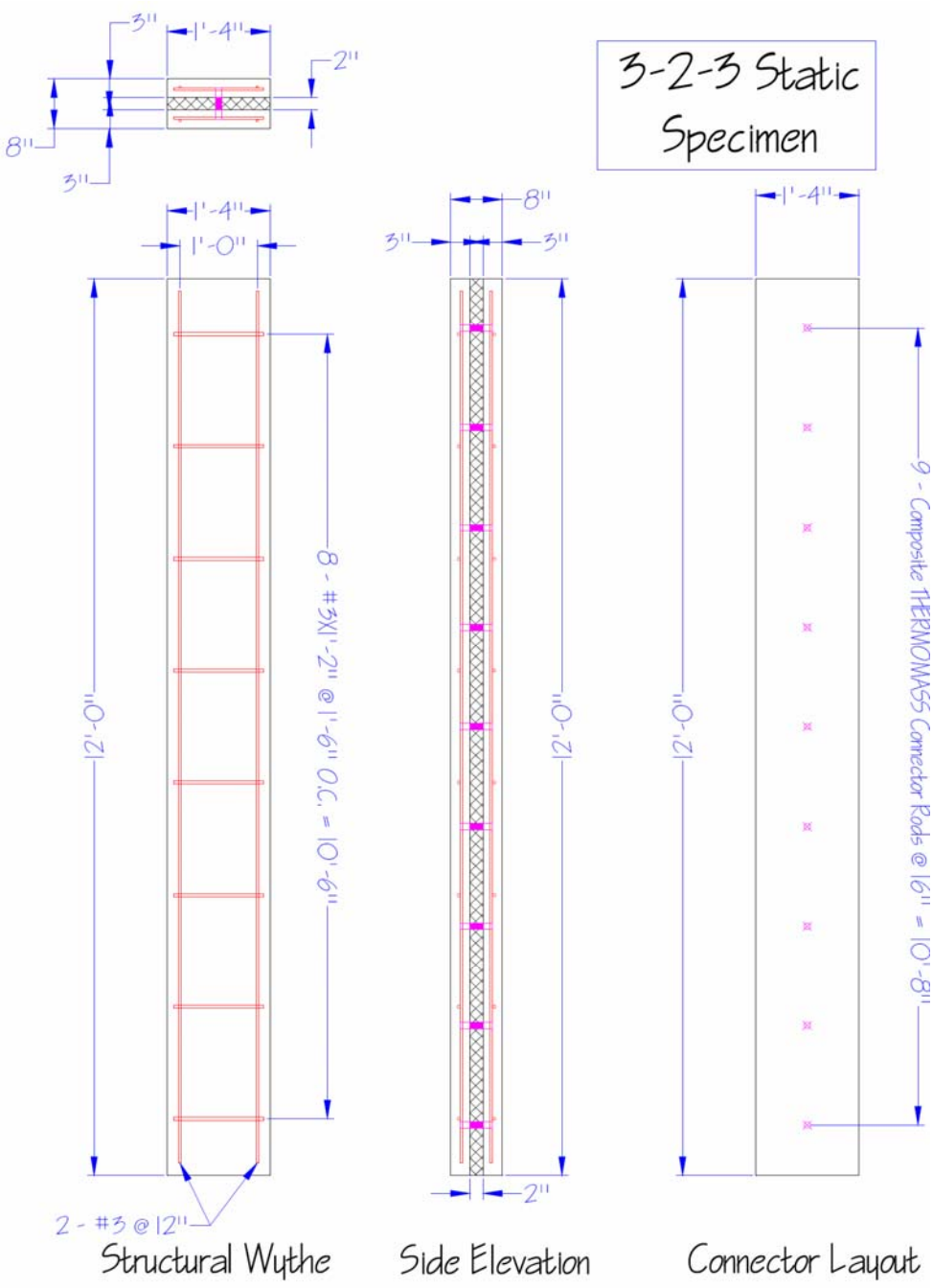

Fig. 3.10 Conventionally reinforced 3-2-3 static sandwich panel specimen

3.3.2 Static Shear Tie Tests

Static shear tie test results were used to define shear resistance of ties between the wythes of the sandwich panels. The testing configuration consisted of three concrete layers, two shear ties, and two layers of foam as shown in Figure 3.11. The symmetrical test configuration was chosen to minimize eccentricity. The outer two concrete wythes were fixed at the bottom, and the middle layer of concrete was pulled vertically. Total vertical load and vertical displacement were recorded. Since the system consisted of two ties, total load was divided by two to provide an accurate resistance for a single tie. Extreme differences in resistances provided by commercially available shear ties were observed (Naito et al. 2009a).

3.3.3 Shear Tie Modeling Methodology

The results from the shear tie tests were used to establish multipoint constraint (MPC) input for tying the concrete wythes together. The direct shear tests were also modeled explicitly in ABAQUS as shown in Figure 3.12. A spring with a bilinear strength was used to model the axial resistance of the ties. The nonlinear SPRING1 elements were used to simulate the shear resistance of nodes coupled between wythes, and SPRING2 elements were used to simulate the axial behavior of ties. These models used the same concrete and rebar material properties used for the RC models. Figure 3.13 compares tested shear resistances with shear resistances using the MPC approach and illustrates that the MPC approach provides an efficient and accurate representation of the shear resistance of various sandwich panel ties without having to explicitly model intricate shear connector systems.

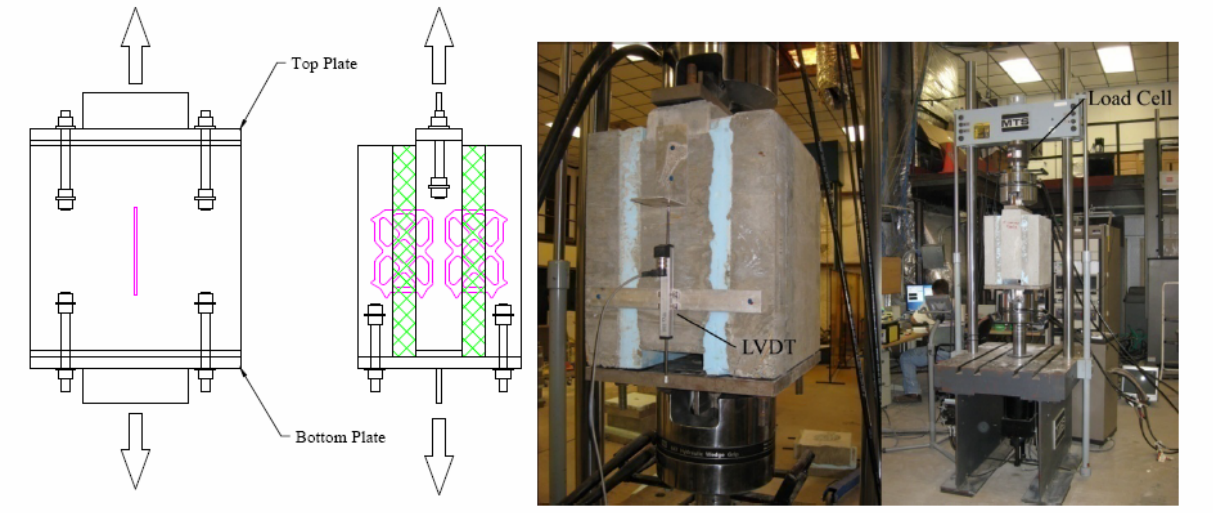

Fig. 3.11. Shear tie static test configuration

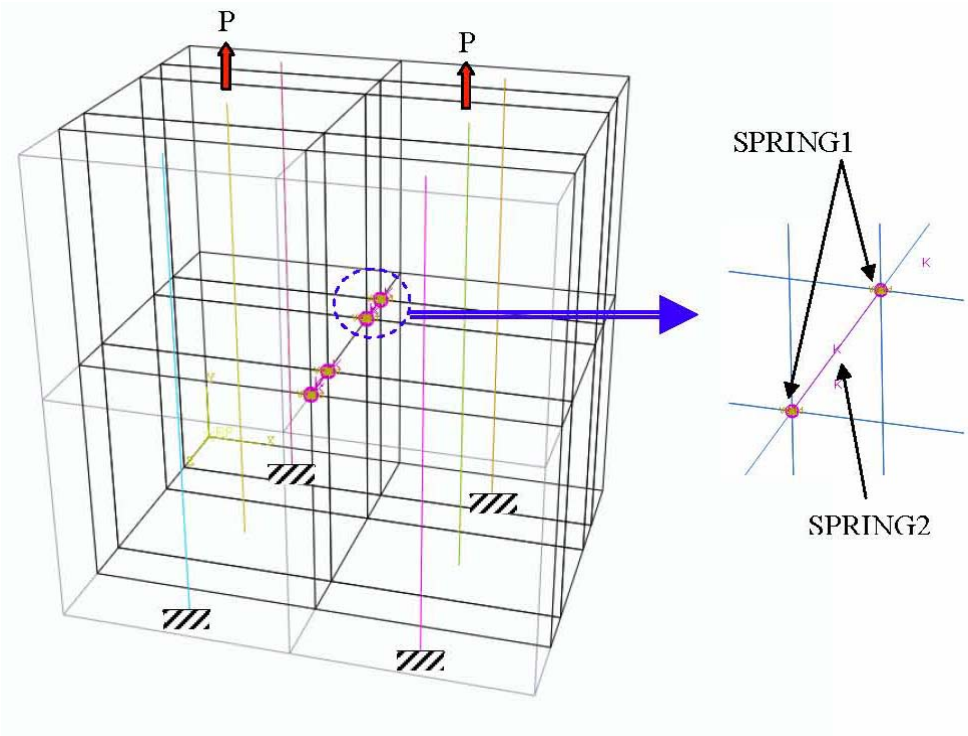

Fig. 3.12. Shear tie MPC validation model configuration

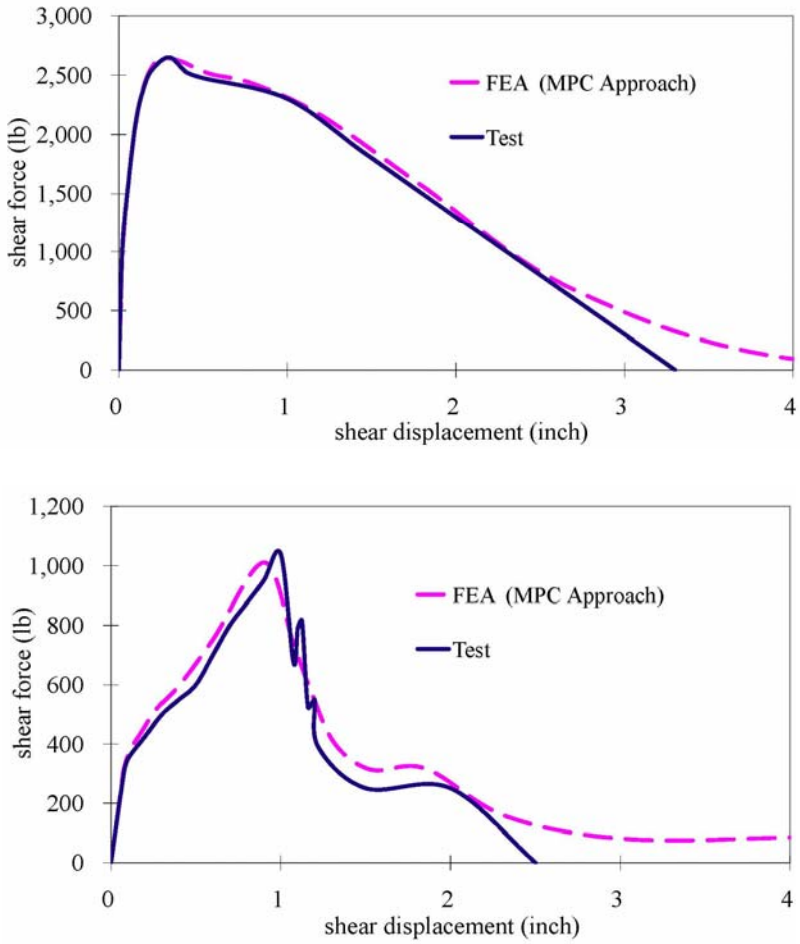

Fig. 3.13. Validation of MPC approach: (a) composite shear tie (b) non-composite shear tie.

3.3.4 Implementation of the MPC Approach into Sandwich Panel Models

The MPC approach described above was incorporated into the sandwich panel models. Generalized shear resistances used in the MPC approach introduced in sandwich panels models are displayed in Figure 3.14. A model simulating the loading-tree tests was created in ABAQUS (Figure 3.15). The interface properties between concrete and foam did not include friction since the resistance data collected in the shear tie static tests indirectly included friction resistance. The shear resistance for all concrete sandwich panels, therefore, was provided by nonlinear spring elements that represent each individual shear tie. It was noted for many static samples that the shear ties would begin

to fail at one end of the panel. This could be attributed to the inherent construction variability of the system; it is highly improbable that corresponding shear ties at opposite ends would fail at precisely the same time during testing, even though the model could be developed to be numerically, perfectly symmetric. This unbalanced variability was simulated by decreasing the resistance of the shear tie farthest from the midspan on one side by fifty percent, resulting in unsymmetrical failure patterns. As shear increased, this reduced tie failed before the corresponding tie on the opposite end, resulting in the unzipping failure mode observed in many of the full-scale static tests.

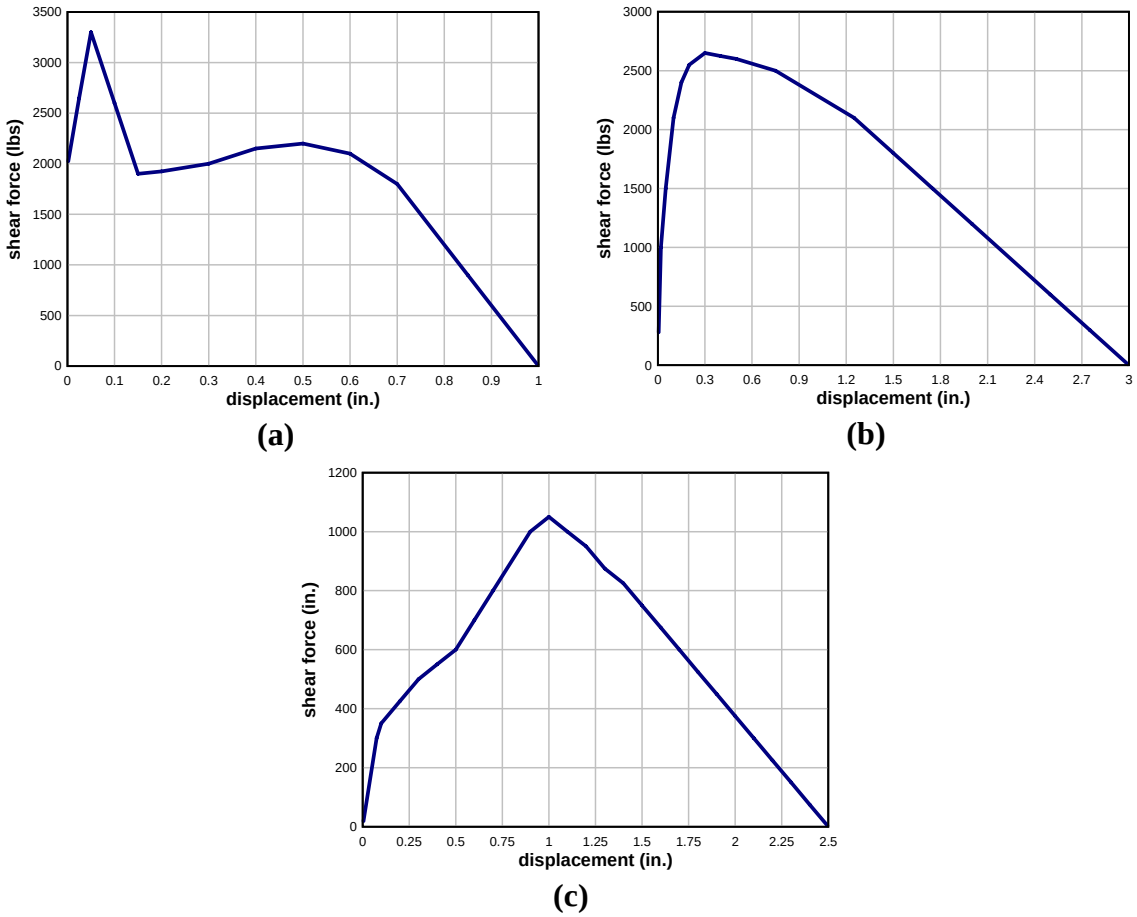

Fig. 3.14. Generalized shear tie resistances used in the MPC approach: a) composite carbon fiber; b) composite fiberglass; c) non-composite fiberglass

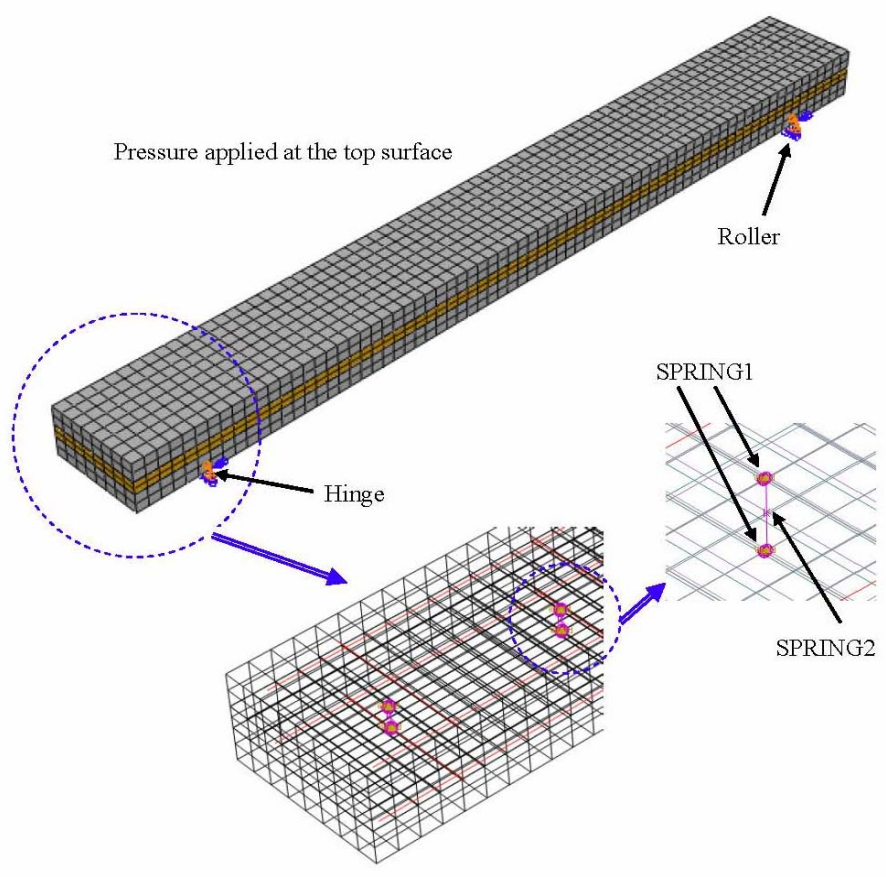

Fig. 3.15. FE model of sandwich panel utilizing MPC for shear tie behavior

3.3.5 Simulation of Prestressing Effects in Sandwich Panel Models

Initial conditions can be used to model prestressing effects in reinforcement of prestressed sandwich panels. The structure must be brought to a state of equilibrium before it is actively loaded by means of an initial static analysis step with no external loads applied. If prestress is defined in the reinforcement and unless the prestress is held fixed, it will be allowed to change during an equilibrating static analysis step; this is a result of the straining of the structure as the self-equilibrating stress state establishes itself. An example is the pretension type of concrete prestressing in which reinforcing

tendons are initially stretched to a desired tension before being covered by concrete. After the concrete cures and bonds to the reinforcement, release of the initial prestressing strand tension transfers load to the concrete, introducing compressive stresses in the concrete. The resulting deformation in the concrete reduces the stress in the strand. Initial Conditions, a keyword in ABAQUS, was used to define prestress for reinforcement (ABAQUS, 2008).

In this study, prestressed reinforcement was modeled using beam elements and the embedded element technique in ABAQUS. The prestressed strand strength (Figure 3.16) was based upon published values (Nawy, 1996).

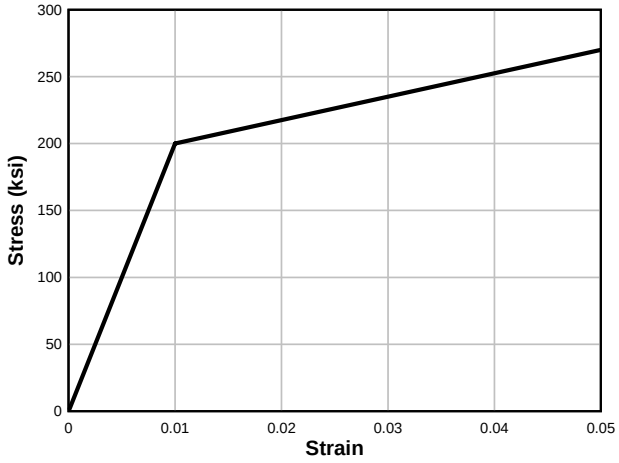

Fig. 3.16. Stress-strain relationship of prestressing strand used in the analyses

3.3.6 Insulation Foam Modeling

Stress-strain data from compressive testing of insulating foams used as construction materials was used for the material model input for the foam elements (Figure 3.17, Jenkins 2008). Significant sandwich panel resistance differences can occur due solely to foam type, as illustrated in Fig. 3.18 for extruded-expanded polystyrene (XPS) and polyisocyanurate (PIMA). The static sandwich panel specimens both failed in

a similar manner as implied by the similar shapes of their resistance curves. However, the difference in overall resistance is apparent given that the resistance of the PIMA insulated panel was consistently significantly lower than that of the XPS insulated panel.

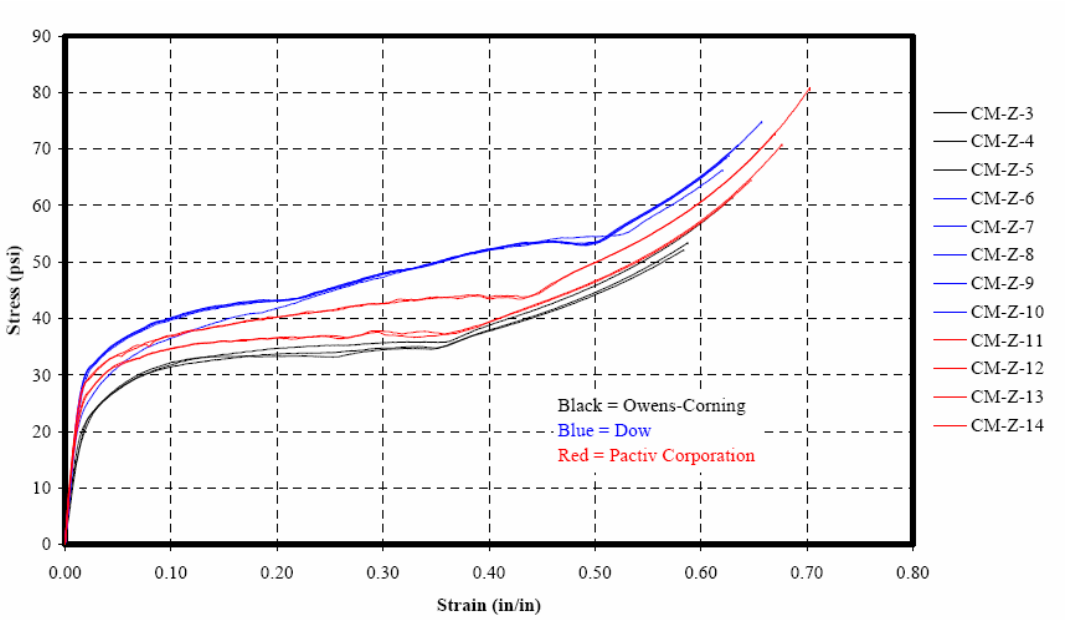

Fig. 3.17. Comparison of stress-strain response of various extruded polystyrene products (Jenkins, 2008)

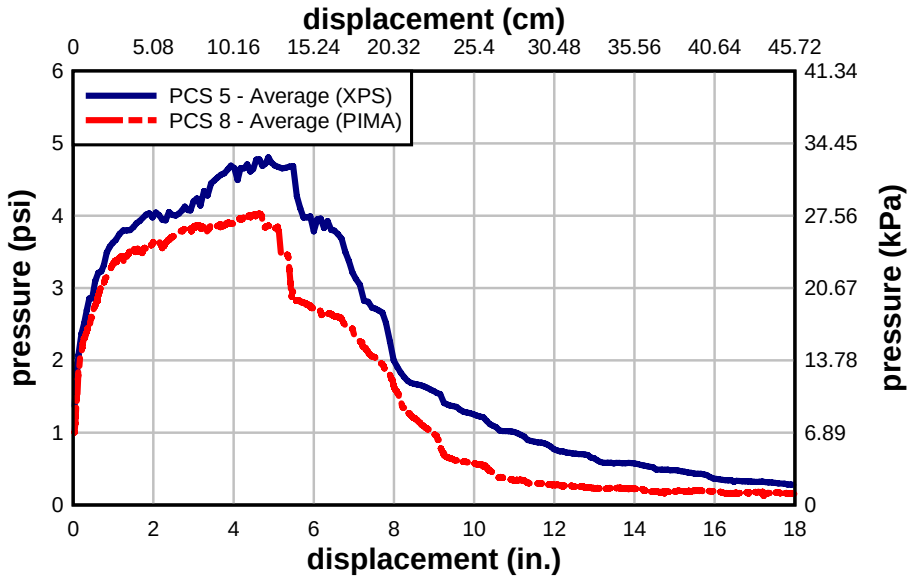

Fig. 3.18. Comparison of similar panel resistances with different foam insulation

Additional static testing of cylindrical foam samples was conducted to better understand resistance of insulation materials. Three types of foam insulation are commonly used in sandwich panel construction: expanded polystyrene (EPS), extruded expanded polystyrene (XPS), and polyisocyanurate (PIMA). Samples of various diameters were compressed, with stroke and total load used to calculate stress and strain (Figure 3.19). The amount of strain foam samples exhibited was limited due to the stroke of the test apparatus. Also, an attempt was made to study Poisson's effect on all insulating foam samples by measuring transverse displacement, however, results were not definitive.

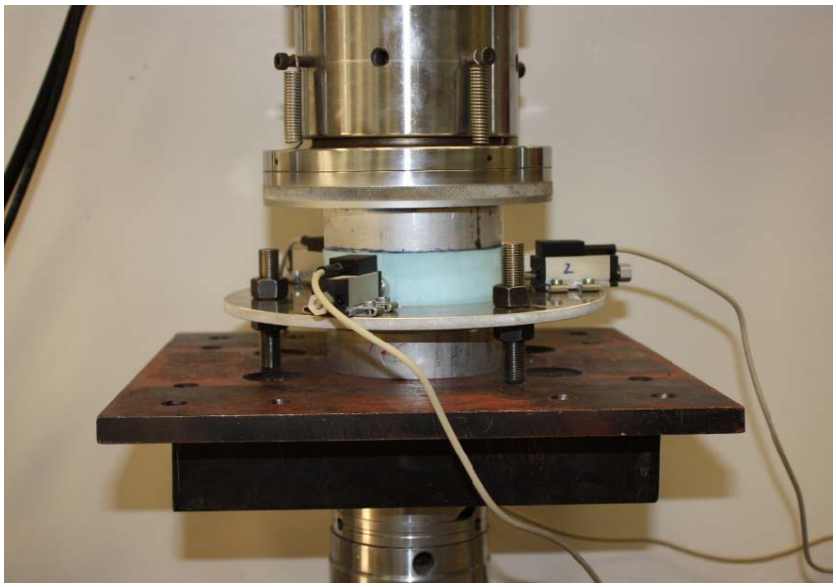

Fig. 3.19. Test setup for static testing of insulation foam materials

In static compressive testing of foam materials, strain was recorded as engineering strain. It is evident in Figures 3.20 through Figure 3.22 that if the sandwich panel system allows the foam to become compressed, theoretically, a large amount of energy will be absorbed due to the large stresses absorbed by the foam. However, the sandwich panel

system and response behavior does not support foam in becoming a major source of energy dissipation. Rigid shear ties such as the fiberglass connectors used in dynamic tests discussed later transfer force axially from exterior to interior concrete wythe until inertia due to the acceleration of mass becomes the controlling component of response. It is recommended that future research continues to study the strength of insulation foam including flexural resistance tests.

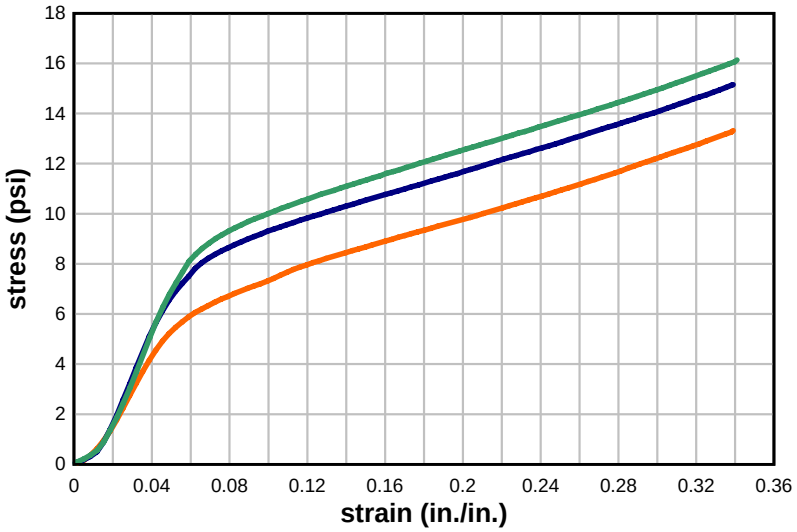

Fig. 3.20. Stress-strain curve of expanded polystyrene insulation foam samples

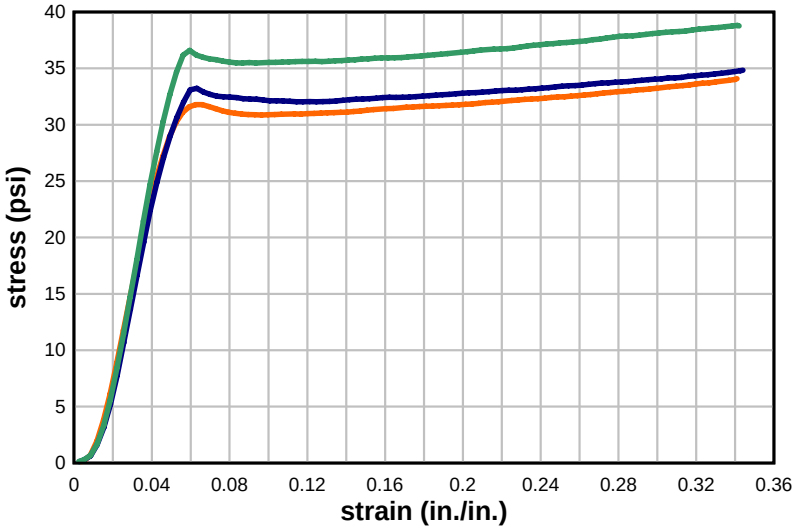

Fig. 3.21. Stress-strain curve of polyisocyanruate insulation foam samples

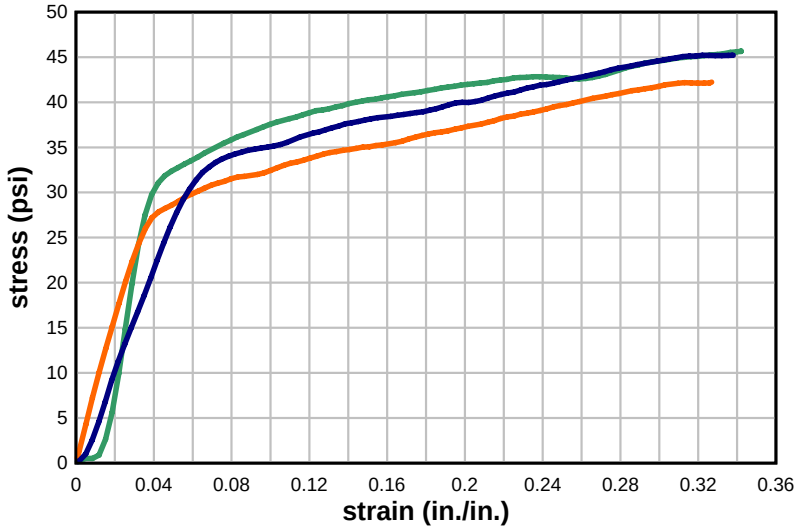

Fig. 3.22. Stress-strain curve of extruded expanded polystyrene insulation foam samples

3.3.7 Static Sandwich Panel Tests and Modeling Comparisons

Table 3.4 describes the sandwich panels used to validate static FE models. Primary strength and geometric variables included foam insulation, wythe configurations, reinforcement (prestressed or conventional), and shear connectors (Naito et al., 2010a). Figure 3.23 illustrates the comparison between the FE models and the static tests results of each representative static specimen. All models compared relatively well, especially in the early stages of loading where the initial stiffness of the models impacts behavior. After loss of initial stiffness, there is some disparity between static testing results and FEM models Static 2 and 4. This is primarily due to approximations involved in simulating composite action between concrete wythes; much is still unknown about the "effectiveness of shear transfer connectors and the effect of insulation type and surface roughness on the degree of composite action" (PCI, 1997). The natural variance of failure in discrete shear ties within a system, especially those connectors designated as creating a non-composite panel, is another area that makes modeling of such systems difficult. For

instance, it was noted in static testing that often shear ties would begin to fail on one side of the panel, creating unsymmetrical stresses on the panels. Although creating the nonsymmetrical tie condition described above provided failure modes that better compared with the failure of test samples, the approach is highly approximate. Furthermore, although the static shear connector test data proved to be helpful in understanding shear transfer of connectors, the tests only took into account direct shear. Uncertainty from the use of this data arises from the fact that shear ties are part of a flexural system and not only subjected to direct shear.

Table 3.4. Static sandwich panel validation matrix

Specimen	Reinforcement Type	Wythe Conf.	Insulation	Panel Reinforcement (Longitudinal/Transverse)	Shear Ties
Static 1	conventionally reinforced	323	XPS	# 3 /#3	fiberglass composite
Static 2	conventionally reinforced	623	XPS	# 3 / WWR	fiberglass non-composite
Static 3	prestressed	333	XPS	3/8 strand / # 3	fiberglass composite
Static 4	prestressed	333	XPS	3/8 strand / # 3	steel c-clip non-composite
Static 5	prestressed	323	EPS	3/8 strand / WWR	carbon-fiber composite
Static 6	prestressed	323	EPS	3/8 strand / WWR	steel c-clip non-composite

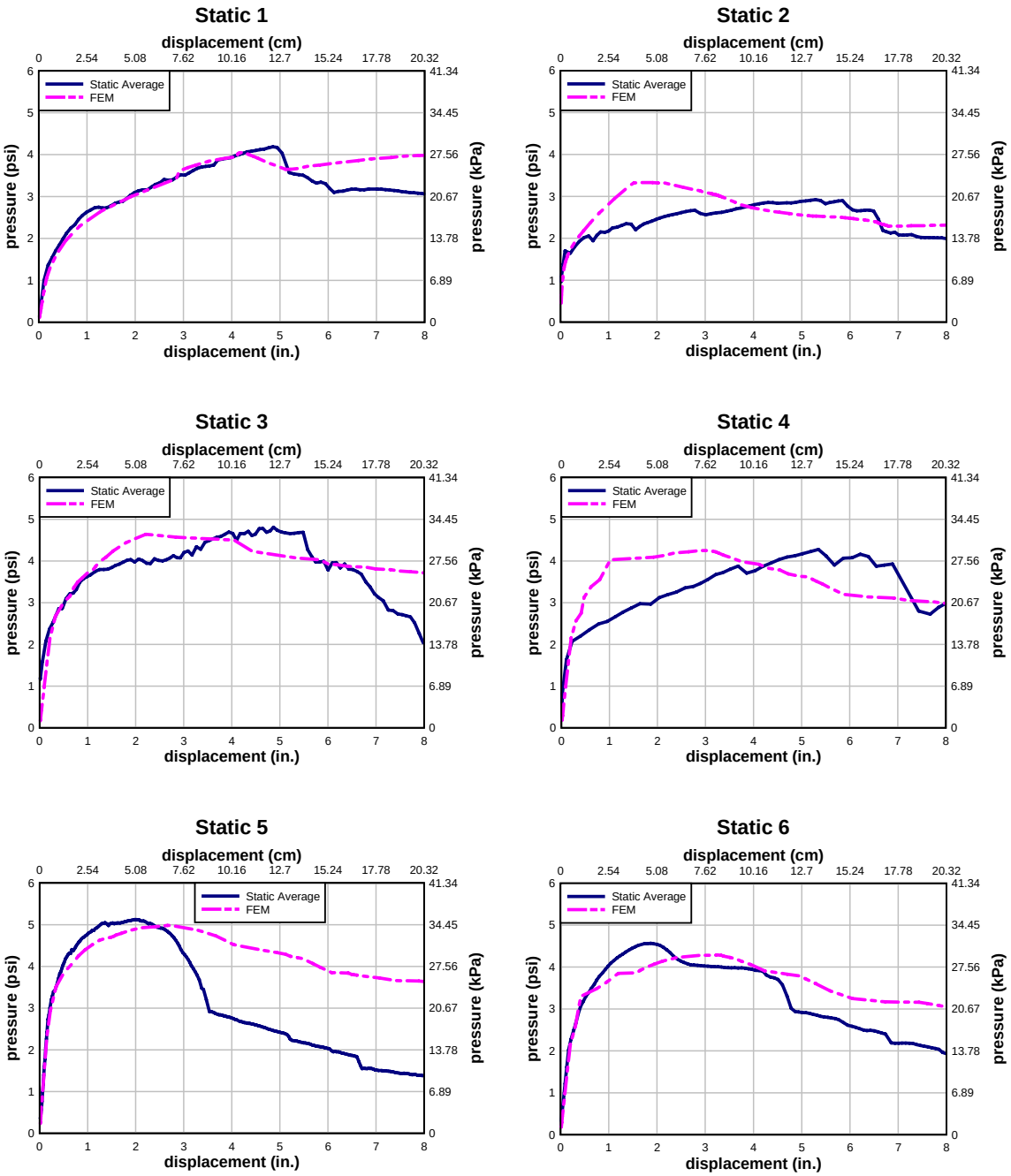

Fig. 3.23 Static test results vs. finite element model comparisons

3.4 Dynamic Modeling and Experimental Comparisons

Full-scale dynamic tests were completed of both prestressed and conventionally reinforced sandwich panels. Dynamic FE models were created using approaches

developed in static modeling stages and results were compared against full-scale test data.

3.4.1 Full-scale Dynamic Tests

Full-scale dynamic experiments were broken into two parts: Dynamic Series I (Naito et al., 2009a) and Dynamic Series II (Naito et al., 2010b). All experiments were conducted by the Airbase Technologies Division of the Air Force Research Laboratory at Tyndall Air Force Base, Florida. Dynamic Series I was not focused upon in finite element simulation; however, experimental data was used for comparison purposes for SDOF prediction methodology later discussed. For each Dynamic Series II experiment, eight sandwich panels (four single span panels and four multi-span panels) were subjected to a small pre-detonation load and a large primary detonation. An overall view of the test arena used for full-scale dynamic tests is shown in Figure 3.24. The purpose of the pre-detonation load was to excite the elastic natural frequencies of the panels so that the frequencies could be compared to those of respective FE models. The primary detonation loading was designed to deform the panels well beyond their elastic limit and, if possible, close to their ultimate strength. Dynamic tests consisted of both single span and multi-span precast sandwich panels, with either prestressed or conventional reinforcement. All panels were designed to be thermally efficient by using either glass fiber or carbon fiber reinforced shear connectors (Naito et al. 2010b). Foam insulation consisted of either expanded polystyrene (EPS) or extruded expanded polystyrene (XPS). Midspan deflections and reflected pressures were recorded. Reflected pressures on the single span reaction structure were recorded in three locations along the midspan. Multi-span reaction

structure reflected pressure gauges were located longitudinally and transversely in three locations for a total of nine locations of pressure recordings. Dynamic deflections were also recorded at the middle of each span, which were used as the predominant comparison between testing and FE data.

Table 3.5 provides an overview of the panel designs used in the full-scale dynamic experiments. Single span specimens were tested in the single span reaction structure; therefore specimens are referenced by an "SS" followed by the specimen identification number. Multi-span panels were tested in the multi-span reaction structure; therefore multi-span panels are referenced with an "MS" followed by the specimen identification number. For each detonation, a representative reflected pressure was created by averaging the recorded pressures to obtain a pressure curve with both a comparable peak pressure and peak impulse. The four different load regimes involved in the tests (which provide a basic understanding of the time domain involved) are non-dimensionally represented in Figure 3.25 and Table 3.6 using the lowest peak pressure and impulse as the basis.

Table 3.5. Dynamic test specimen details

Specimen No.	Wythe Configuration	Tie Type	Insulation Type	Reinforcement Type
SS1 & MS1	3-2-3	carbon-fiber composite	EPS	prestressed
SS2 & MS2	3-2-3	fiberglass composite	XPS	prestressed
SS3 & MS3	3-2-3	fiberglass composite	XPS	conventionally reinforced
SS4 & MS4	6-2-3	fiberglass non-composite	XPS	conventionally reinforced

Fig. 3.24. Test set up for full-scale dynamic tests with single span reaction structure (left) and multi-span reaction structure (right)

Table 3.6. Primary detonation normalized pressures and impulses

		Maximum Normalized Pressure	Maximum Normalized Impulse
Experiment 1	single span	1.99	1.53
	multi-span	1.00	1.00
Experiment 2	single span	2.76	1.89
	multi-span	2.25	1.69

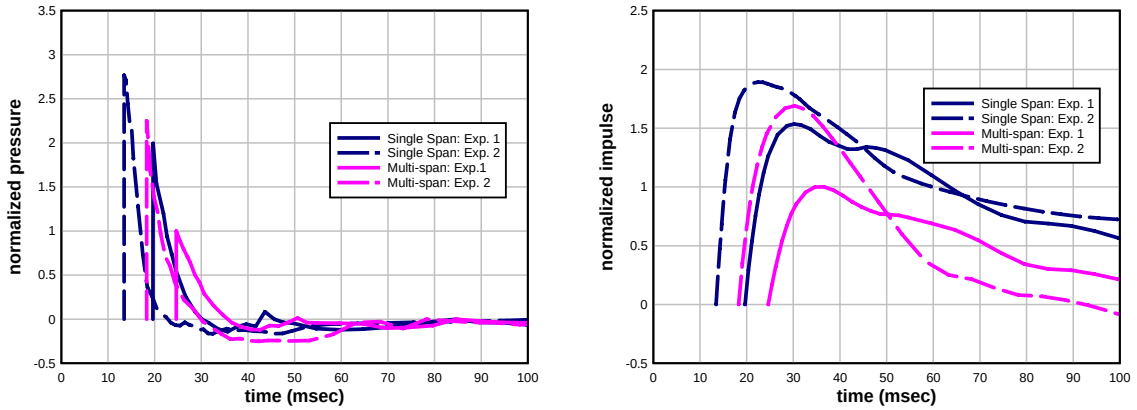

(a) (b)

Fig. 3.25. (a) Average primary detonation reflected pressure curves both experiments and reactions structures. (b) Average impulse curves associated with the average reflected pressure curves

3.4.2 Dynamic Finite Element Models

All dynamic models were created using the statically validated parameters and methods, including material models, the concrete damage plasticity model, and the multipoint constraint approach for the modeling of shear connectors. Models were developed and analyzed using LS-DYNA, an advanced general purpose finite element code capable of solving complex nonlinear mechanics problems (LSTC, 2009). The "MAT_CONCRETE_DAMAGE_R3" concrete model was used for concrete elements, and steel elements were modeled using the "MAT_PLASTIC_KINEMATIC" material model. The "MAT_072R3" concrete element was used in LS-DYNA for concrete elements. Steel elements were modeled using the "MAT_003" element in LS-DYNA. Rigid elements were used for boundary conditions. Transient pressures were applied uniformly across the exterior surface of the panel. Overall, the modeling approach was designed to focus on the flexural response of the sandwich panel system, and care was taken so that the models would not become unstable due to local punching at the supports, although punching failure was noted in some of the multi-span tests.

3.4.3 Simulation of Prestressing Effects in LS-DYNA

LS-DYNA provides several methods for including initial conditions prior to a transient load application. For simulating prestressing in concrete structures, the "CONTROL_DYNAMIC_RELAXATION" feature provides a procedure for combining the initial static loading with a subsequent dynamic load case. The dynamic relaxation method was used in this study to initialize the stress in the panel systems due to the prestressing strand elements, and then the dynamic load case was run based on this initial

condition. Definition of the initial stress in truss elements was made by setting ELFORM=3, and assigning values to RAMPT (ramp time for stress initialization by dynamic relaxation), and STRESS (initial stress in truss elements) in the keyword card "SECTION_BEAM". The initial stress was initialized by setting IDRFLG=-1 in the "CONTROL_DYNAMIC_RELAXATION" card. Then, after stress initialization, the load case was applied dynamically by setting IMFLAG=0 in the "CONTROL_IMPLICIT_GENERAL" card.

3.4.4 Simulation of Dynamic Increase Factors

The sudden nature of dynamic loading and the acceleration of structural mass result in high rates of strain. At these higher strain rates, the strength of both concrete and steel can increase. The ratio of the dynamic to static strength is referred to as the dynamic increase factor (DIF) and is commonly reported as a function of strain rate.

Steel reinforcement used the Copper and Symonds model (Equation 3.17) which scales the yield stress depending upon the strain rate (Stouffer and Dame, 1996).

$$DIF = 1 + \left(\frac{\dot{\varepsilon}}{C} \right)^{1/P} \tag{3-17}$$

In the Copper Symonds model, $\dot{\varepsilon}$ represents strain rate. Also, C and P are parameters that depend upon the steel properties. Mild steel was considered in this study; therefore, C and P were 40 and 5, respectively.

A curve relating the dynamic increase factor of concrete vs. strain-rate provided within LS-DYNA was used as the basis for strain-rate effects. However, the flexural response proved very sensitive to the strain rate effects definition, and the input data associated with the range of strain rates observed from the modeling output was

magnified up to five times the LS-DYNA default to reflect the upper limits of previously published research (Malvar and Crawford, 1998; Malvar and Ross, 1998). Figure 3.26 demonstrates the default DIF curve used by LS-DYNA.

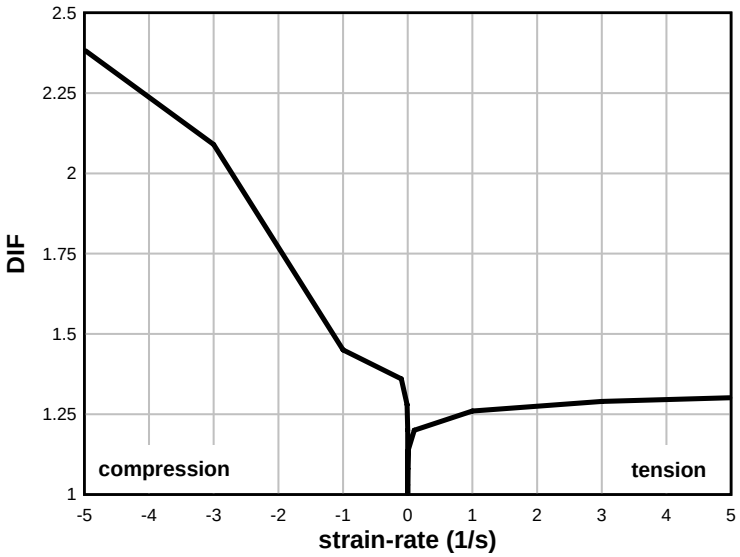

Fig. 3.26. LS-DYNA default curve for concrete DIF

3.4.5 Dynamic Sandwich Panel Experiment and FE Model Comparisons

Full-scale dynamic test results for Dynamic Series II were compared with the results of FE models subjected to similar loading. Loading curves were developed by analyzing recorded reflected pressures and creating a representative curve that would be similar in both peak positive and negative pressure as well as impulse. Single span dynamic models were completed first, followed by multi-span dynamic models. For comparison purposes, only pre-detonation loading from Experiment 1 was evaluated due to the similarities of pressure for both experiments. Both single span and multi-span models were compared against two primary detonation pressures.

3.4.6 Single Span Results and Comparisons

All single span models exhibited very similar initial response and maximum midspan displacement was within reasonable error. The reasons for variability include: inabililty to replicate boundary conditions exactly, variability of foam insulation, shear tie variability and ambiguities (i.e. response of shear ties in a high strain-rate environment), any local failures for which models were not created to exhibit, and DIF ambiguity. Single span primary detonation comparisons are displayed in Figure 3.27 and Figure 3.28 for Experiments 1 and Experiment 2 respectively.

As mentioned above, only Experiment 1 pre-detonation loading (Figure 3.29) was considered. Pre-detonation results (Figure 3.30) were fairly accurate for the first half sine wave of displacement. After the first half period, variance between the FE models and experimental damping are quite apparent. This is most likely due to the absence of damping characteristics such as real-world boundary conditions causing friction. Models were considered acceptable if the first half sine wave of displacement correlated well.

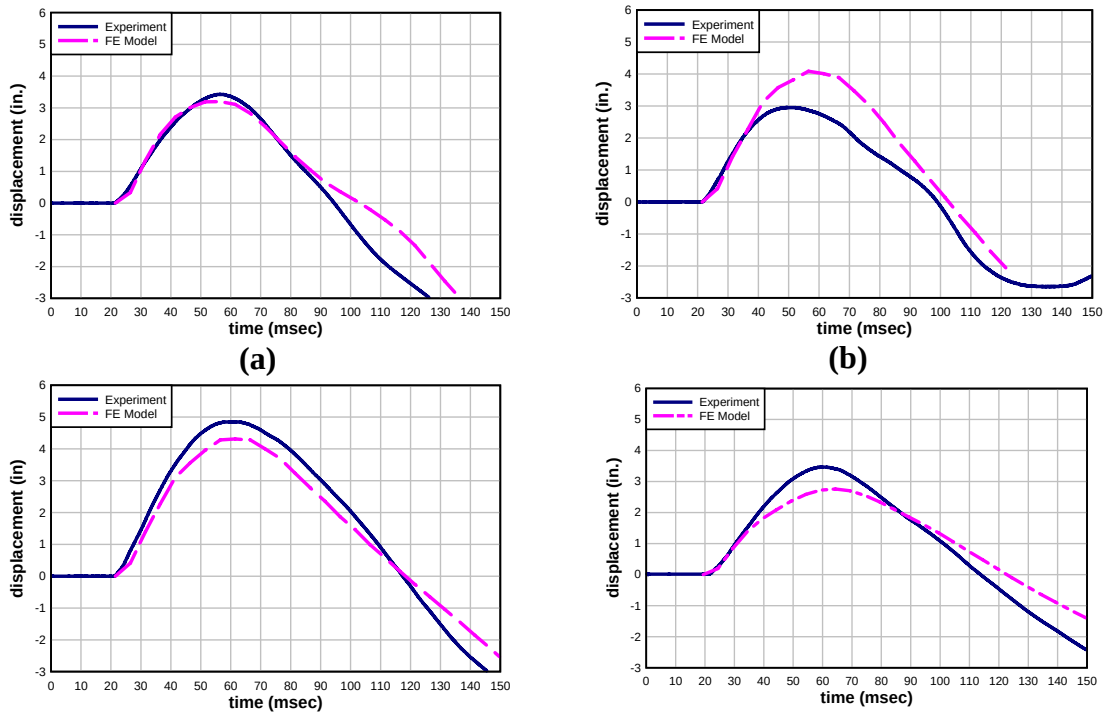

Fig. 3.27. Experiment 1 – Primary detonation measured midspan displacement vs. finite element midspan displacement comparison for (a) SS1, (b) SS2, (c) SS3, and (d) SS4

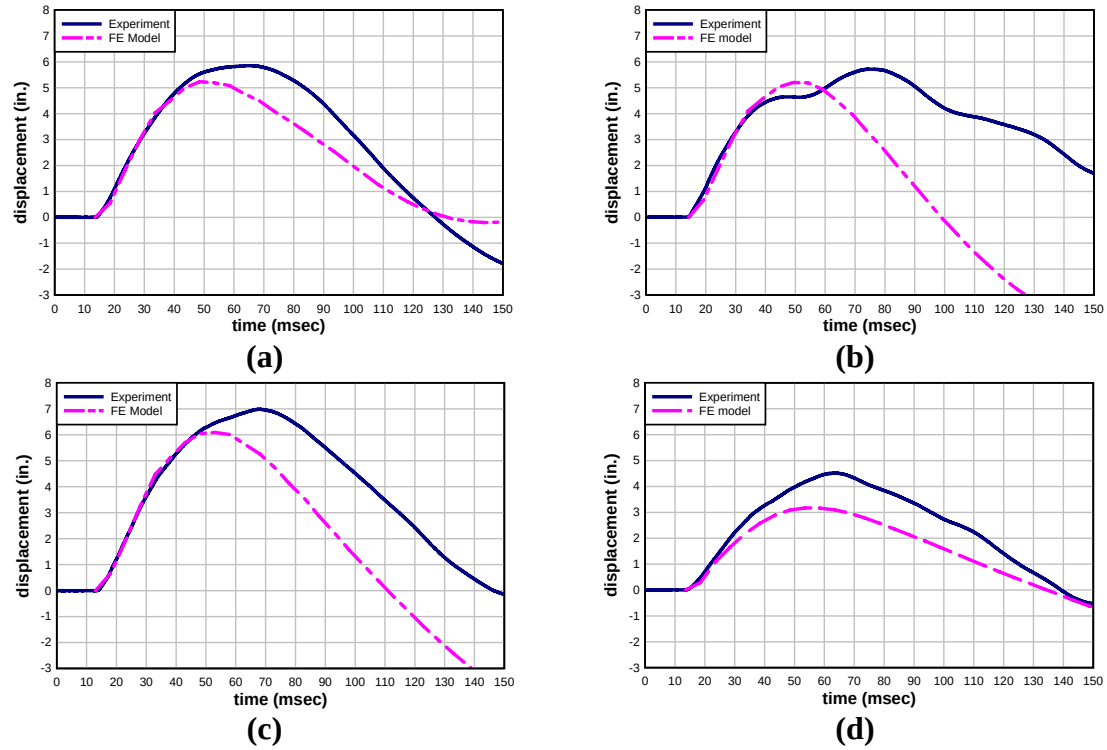

Fig. 3.28. Experiment 2 – Primary detonation measured midspan displacement vs. finite element midspan displacement comparison for (a) SS1, (b) SS2, (c) SS3, and (d) SS4

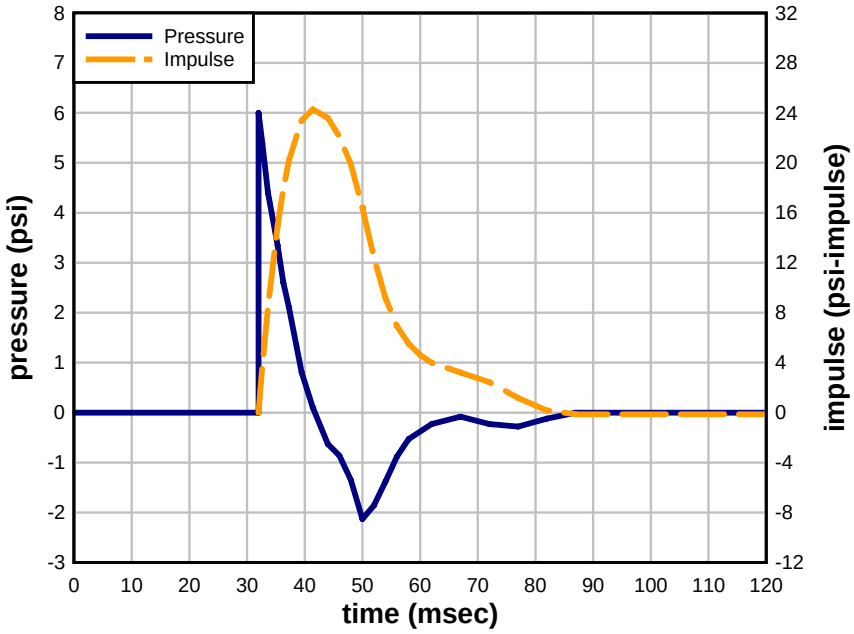

Fig. 3.29. Pre-detonation pressure and impulse for single span reaction structure – Experiment 1

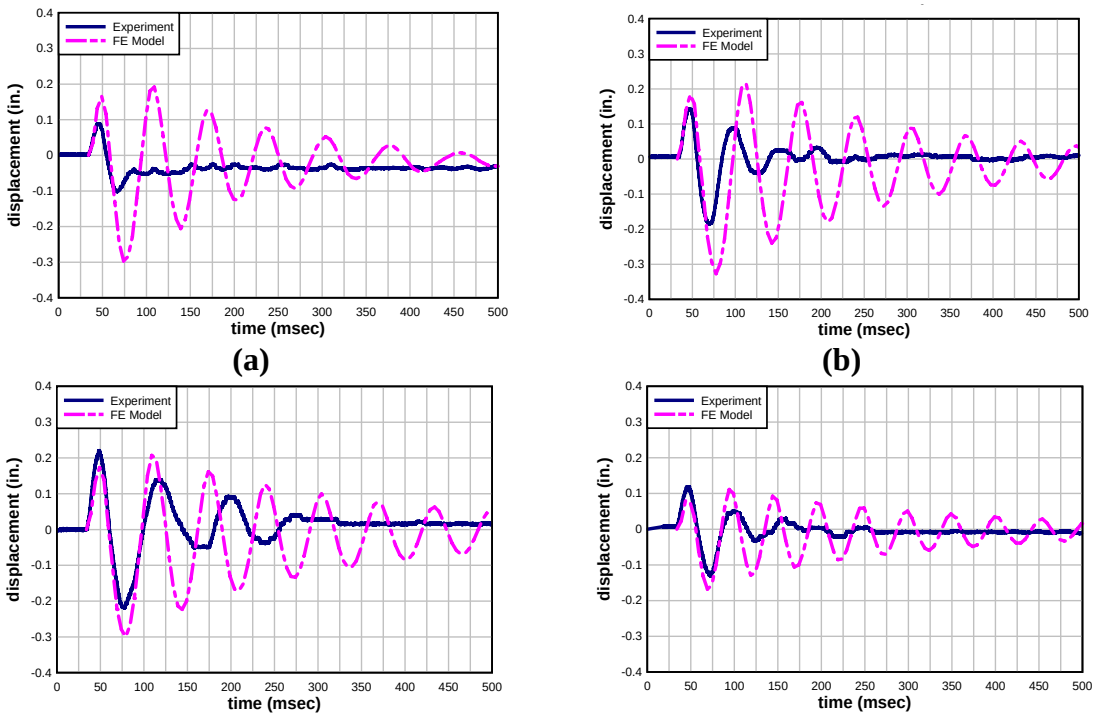

Fig. 3.30. Experiment 1 – Pre-detonation measured midspan displacement vs. finite element midspan displacement comparison for (a) SS1, (b) SS2, (c) SS3, and (d) SS4

Table 3.7. Pre-detonation comparison of single span experimental and FE model natural period

Panel	Experimental First Half Sine Wave, msec	FE Model First Half Sine Wave, msec	Error
SS1	30.0	34.5	15.0 %
SS2	20.0	23.7	18.5 %
SS3	25.1	24.5	2.4 %
SS4	23.2	21.2	8.6 %

3.4.7 Multi-span Results and Comparisons

Multi-span panels in general exhibited good correlation between FE models and experimental results, especially in regards to initial response. Multi-span primary detonation comparisons for Experiment 1 are displayed in Figure 3.31 and Figure 3.32; Multi-span primary detonation comparisons for Experiment 2 are displayed in Figure 3.33 and Figure 3.34. All variability issues involving single span validation are also true for multi-span validation. Multi-span FE models exhibited less local failures than the experimental panels; this is especially the case for panels tested in Experiment 2 due to its much larger reflected pressure. Local failures were most prevalent for second floor frame connections due to the large tributary area of the connections. For instance, the response of panel MS4 was influenced by the failure of its second floor connection. Examples of local failures are displayed in Figure 3.35.

Response due to multi-span pre-detonation pressure (Figure 3.36) was fairly accurate for the first quarter sine wave of displacement. Multi-span pre-detonation responses are displayed in Figure 3.37 and Figure 3.38. Due to the increased natural variance of multi-span connection system, pre-detonation results for multi-span panels experienced more variance. A second floor frame (Figure 3.39) was fabricated and intended to react like a second floor system would react under similar loading conditions.

All multi-span panels were connected to this frame; therefore, approximately after the first quarter-sine wave of midspan displacement, an interaction between experimental panel responses was apparent. FE models were created independently and used linear spring elements to approximate the resistance for the second floor frame in Figure 3.39, leading to the discrepancy between experimental and FE model pre-detonation response.

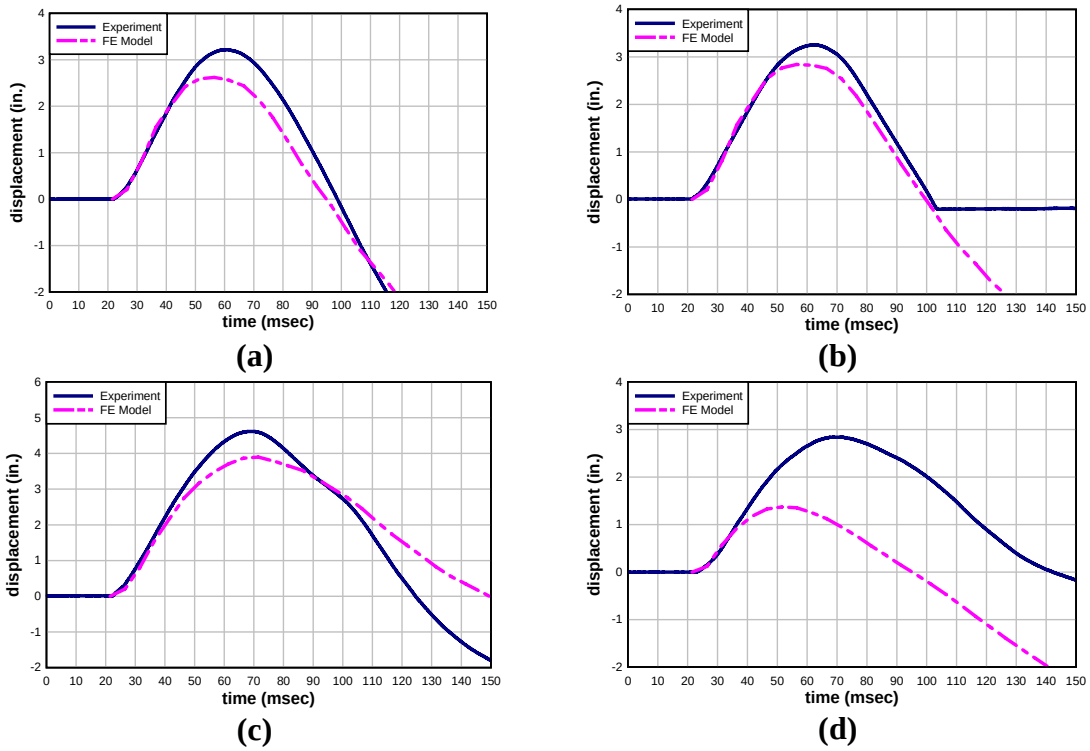

Fig. 3.31. Experiment 1 – Primary detonation measured first floor midspan displacement vs. finite element midspan displacement comparison for (a) MS1, (b) MS2, (c) MS3, and (d) MS4

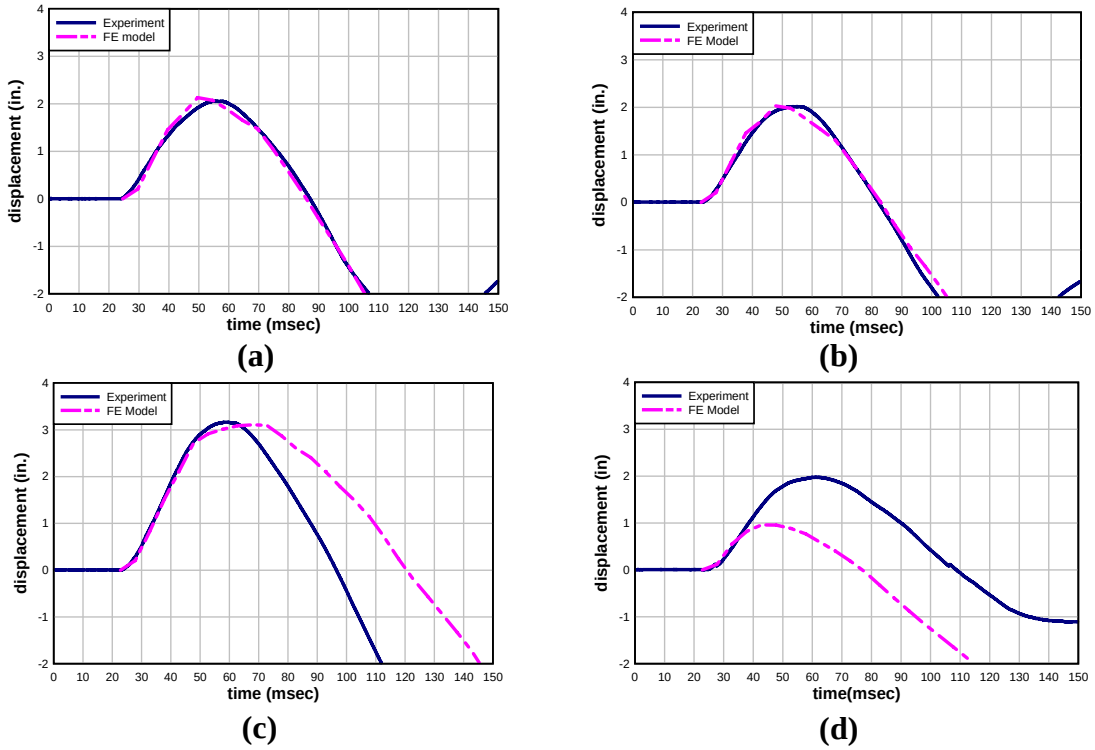

Fig. 3.32. Experiment 1 – Primary detonation measured second floor midspan displacement vs. finite element midspan displacement comparison for (a) MS1, (b) MS2, (c) MS3, and (d) MS4

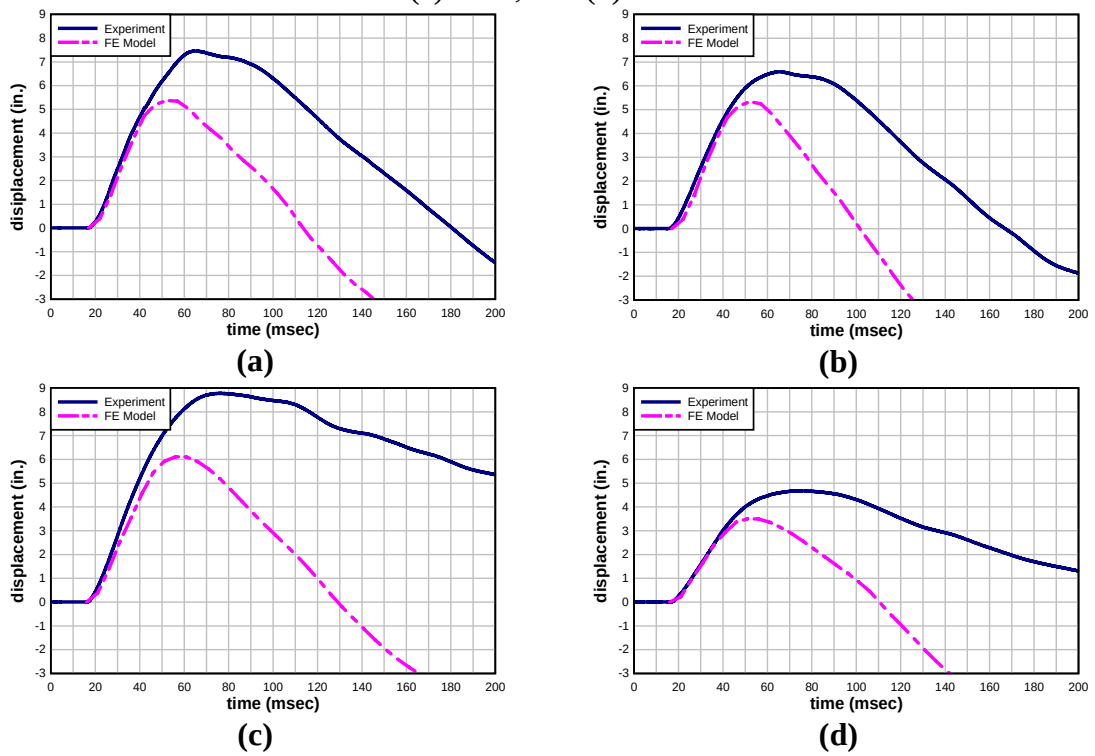

Fig. 3.33. Experiment 2 – Primary detonation measured first floor midspan displacement vs. finite element midspan displacement comparison for (a) MS1, (b) MS2, (c) MS3, and (d) MS4

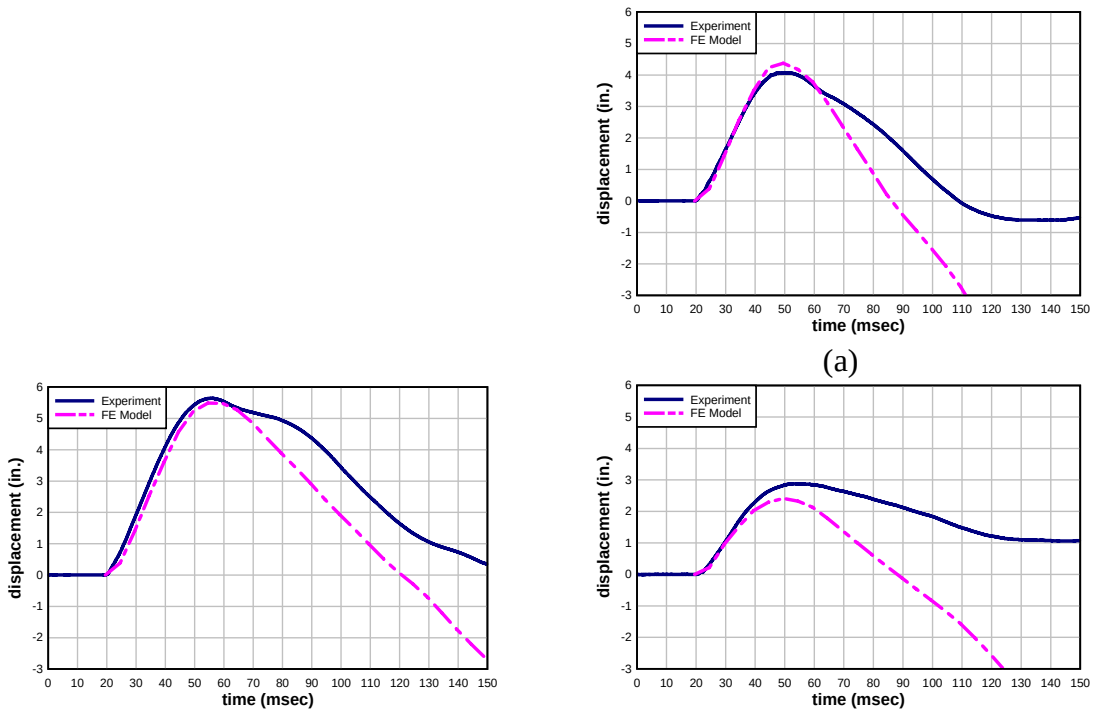

Fig. 3.34. Experiment 2 – Primary detonation measured second floor midspan displacement vs. finite element midspan displacement comparison for (a) MS2, (b) MS3, and (c) MS4

Fig. 3.35. Local failures examples along second floor support

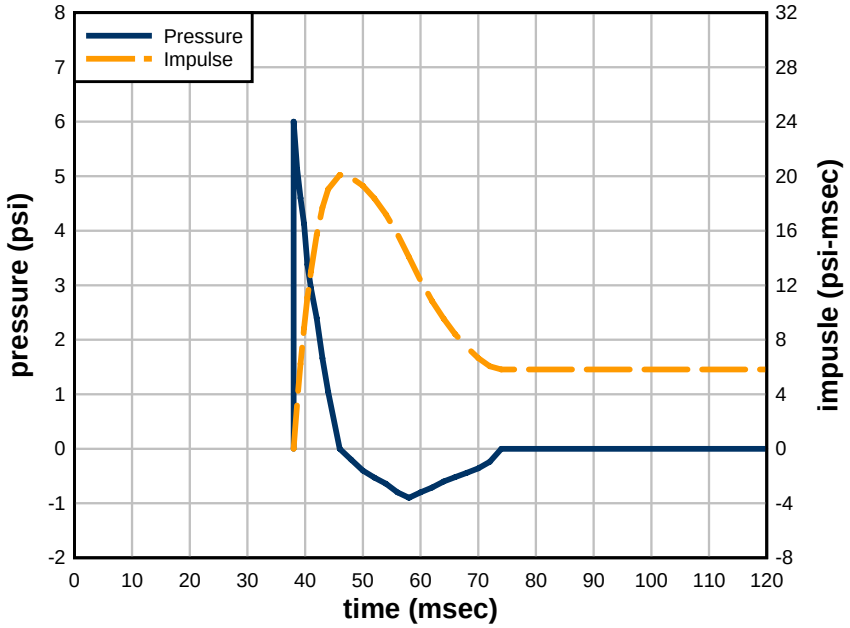

Fig. 3.36. Pre-detonation pressure and impulse for multi-span reaction structure - Experiment 1

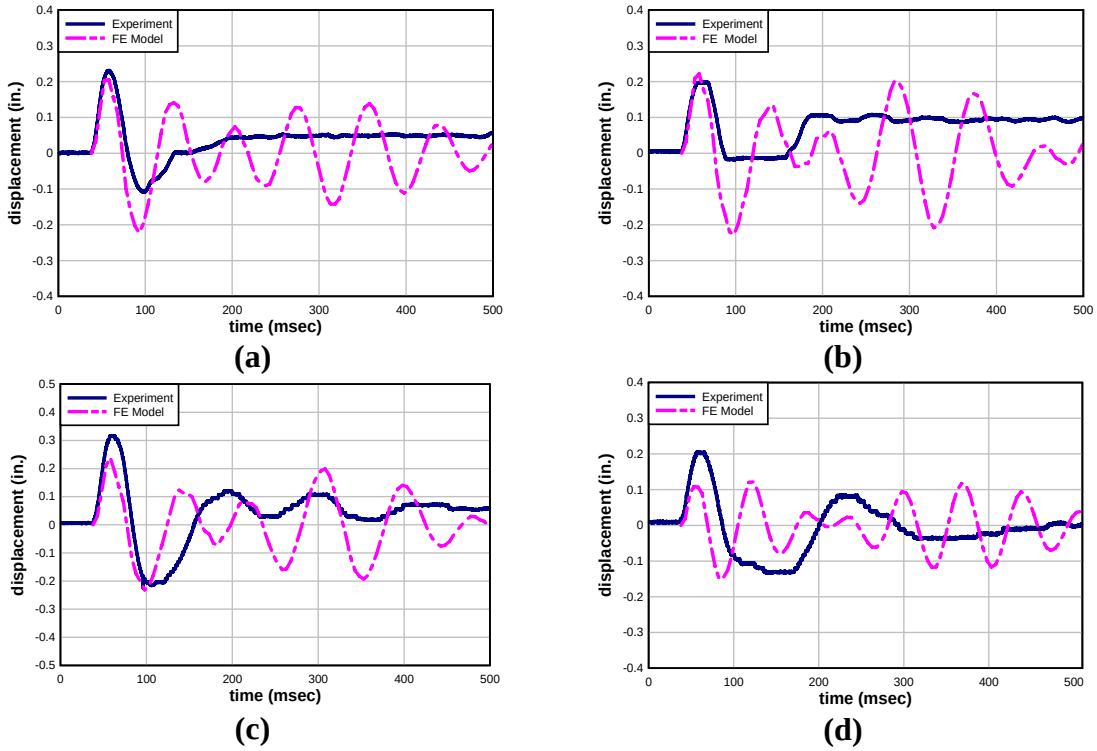

Fig. 3.37. Experiment 1 –Pre-detonation measured first floor midspan displacement vs. finite element midspan displacement comparison for (a) MS1, (b) MS2, (c) MS3, and (d) MS4.

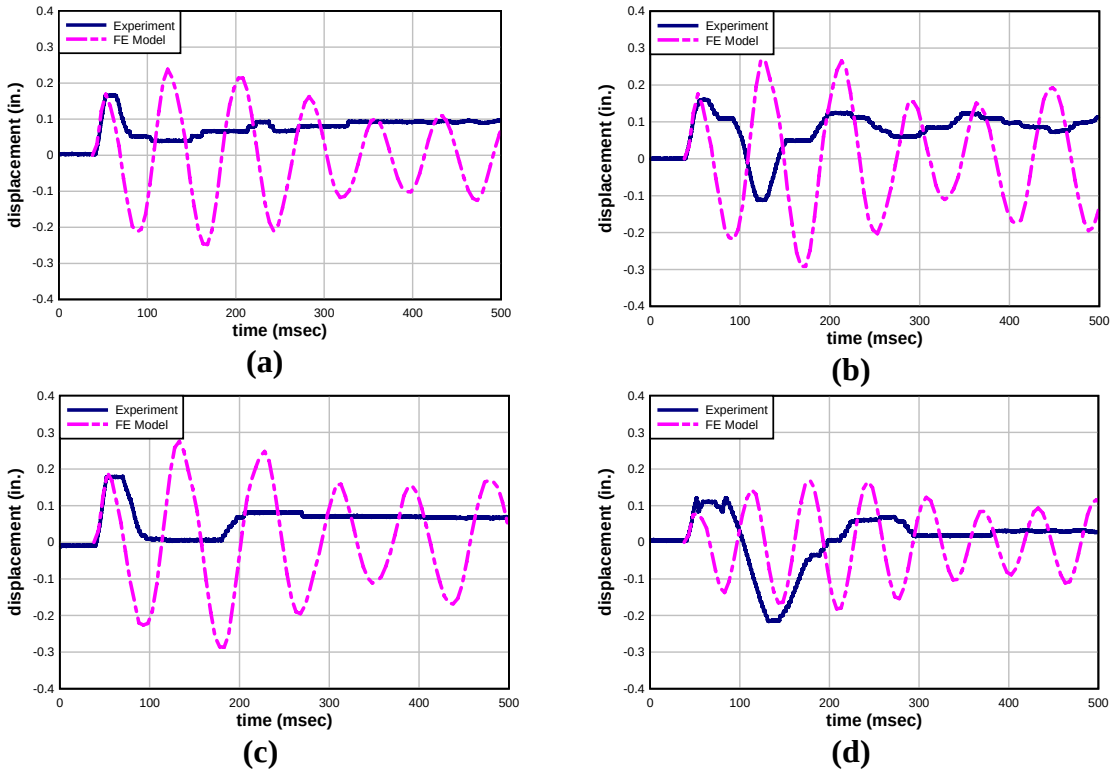

Fig. 3.38. Experiment 1 –Pre-detonation measured second floor midspan displacement vs. finite element midspan displacement comparison for (a) MS1, (b) MS2, (c) MS3, and (d) MS4.

Table 3.8. Pre-detonation comparison of multi-span experimental and FE model natural period

Panel	Experimental First Quarter Sine Duration, msec	FE Model First Quarter Sine Duration, msec	Error
MS1	~20.0	~17.5	~14 %
MS2	~19.1	~23.5	~23 %
MS3	~19.5	~24.0	~23%
MS4	~13.3	~15.0	~13%

Fig. 3.39. Second floor support frame allowing interaction between the behaviors of all multi-span panels attached

CHAPTER 4

STUDY OF BLAST RESPONSE BEHAVIOR OF SANDWICH PANELS

4.1 Introduction

Due to the high costs of full-scale dynamic testing, finite element simulation can serve as a crucial tool in evaluating behavior of structural components subjected to blast loads. After validation and comparisons of experimental data with FE models, the models were used to evaluate the failure mechanisms of sandwich panels subjected to impulse loads. The study consisted of energy plots, strain of reinforcement along height vs. time, and total reaction forces experienced. Energy plots were intended to display the "flow" of energy throughout time and help determine the importance of mass and the strain of reinforcement in sandwich panels. The reinforcement strain vs. time plot describes the development of hinges throughout time and their locations. Also, dynamic reactions were recorded in FE models.

4.2. Energy Dissipation

Energy provided by an impulse load on a sandwich panel can be dissipated in two ways: internal and external energy. Energy involving straining and/or failure of concrete wythes, steel reinforcement, foam insulation, or shear connectors is internal energy. External energy involves the kinetic energy of the mass of the sandwich panel that is

accelerated by the impulse load. Energy plots can give the researcher insight into the role each component takes in absorbing and dissipating energy.

The two components that are assured to impact energy absorption are the mass of the concrete wythes and the yielding of steel reinforcement. There is a vast amount of data studying the insulation capabilities of the foam; however, the absorption of energy by the insulating foam in a high-strain environment is unknown. Also unknown is the role of shear connectors in transferring energy between the concrete wythes. FE models indicated that early within the response of panels, shear connectors absorbed energy axially through the nonlinear spring of the MPC approach that represented the axial strength of the tie. This would signify brief displacement of the shear connector which would cause the external concrete wythe the opportunity to provide more energy across the entire surface of the foam.

4.2.1 Kinetic Energy

Kinetic energy plots of FE models display the significant role the mass of concrete plays in dissipating the energy of the system (Figure 4.1). Reinforcement and foam insulation play small roles as far as kinetic energy is concerned due to their small mass. It is key to notice the similarities between panels SS2 and SS3. Figure 4.1-b displays the kinetic energy of a prestressed sandwich panel with a 3-2-3 wythe configuration; Figure 4.1-c has the same 3-2-3 configuration but is conventionally reinforced. However, both models used an MPC approach that simulated a composite fiberglass shear connector. The kinetic energy plots of both panels have very similar maximum kinetic energy for both concrete wythes and behavior continues to appear

similar throughout response. This reinforces the idea that the shear connector resistance is a very crucial component on the overall behavior of the sandwich panel when subjected to blast loads due to the impact of shear connector resistance on composite action. As expected, the six-inch interior concrete wythe of panel SS4 displays the relatively large kinetic energy in comparison to the thee-inch exterior wythe due to the increased mass (Figure 4.1-d).

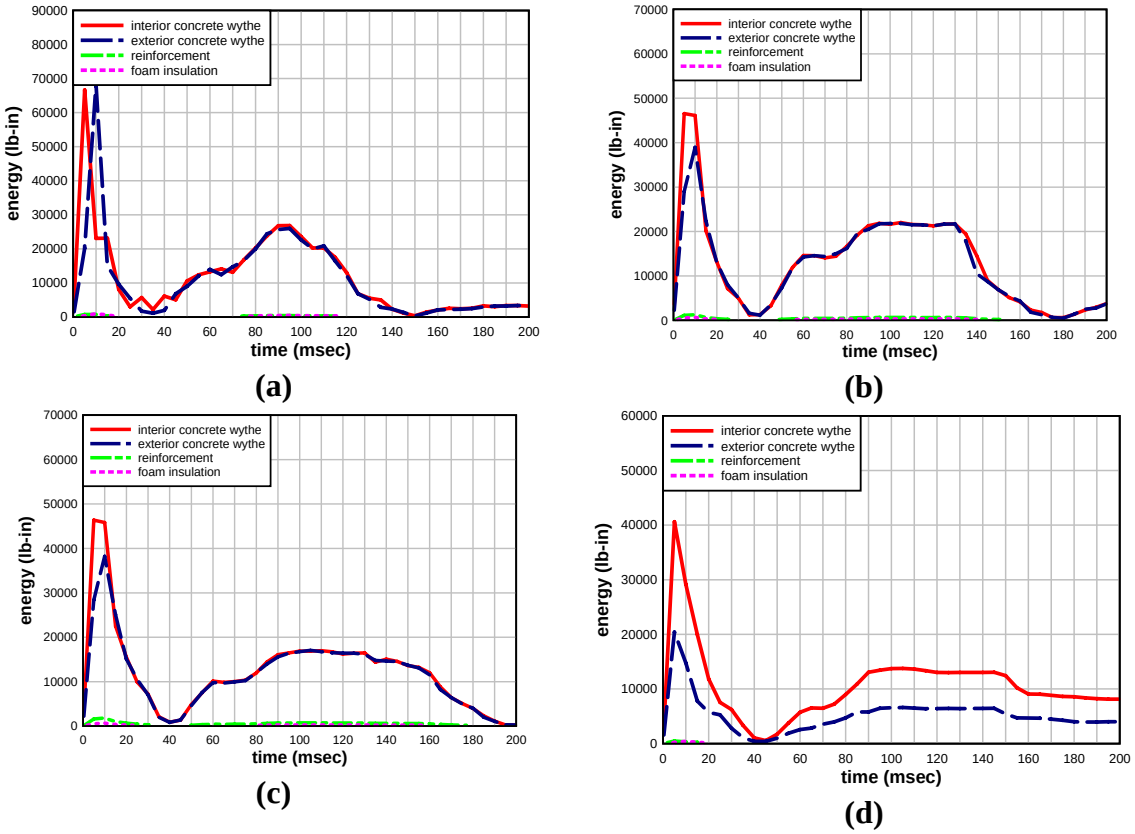

Fig 4.1. Kinetic energy of sandwich panel system components-Experiment 1; a) SS1, b) SS2, c) SS3, d) SS4

4.3 Strain Distribution

Strain of reinforcement was plotted across the height of one prestressed specimen and both conventionally reinforced models simulating Experiment 1, single span test

specimens. The strain was plotted every five milliseconds beginning at zero until the maximum strain of reinforcement was reached. As can be seen in Figures 4.2 through Figure 4.4, the strain for all specimens reaches maximum at a point in time past the positive phase of pressure in Figure 4.5. This is due to the mass of sandwich panel specimens accelerating due to the positive phase of pressure. The inertia due to the mass of the panel must be countered by the structural resistance of the panel. The yielding of reinforcement at midspan causes a hinge, which helps to dissipate energy.

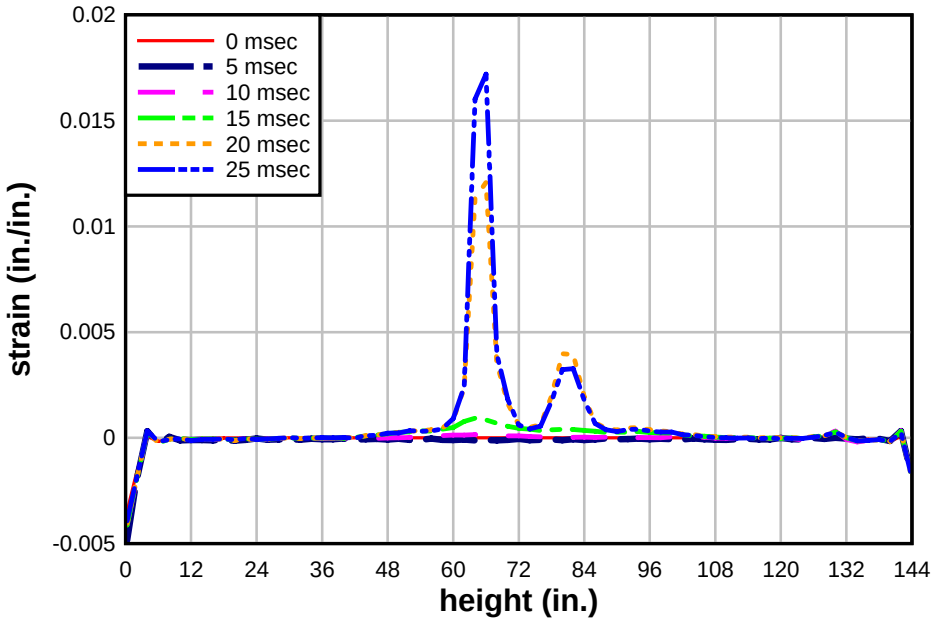

Fig. 4.2. SS1 – Experiment 1**:** Strain of reinforcement of interior concrete wythe across panel height over time

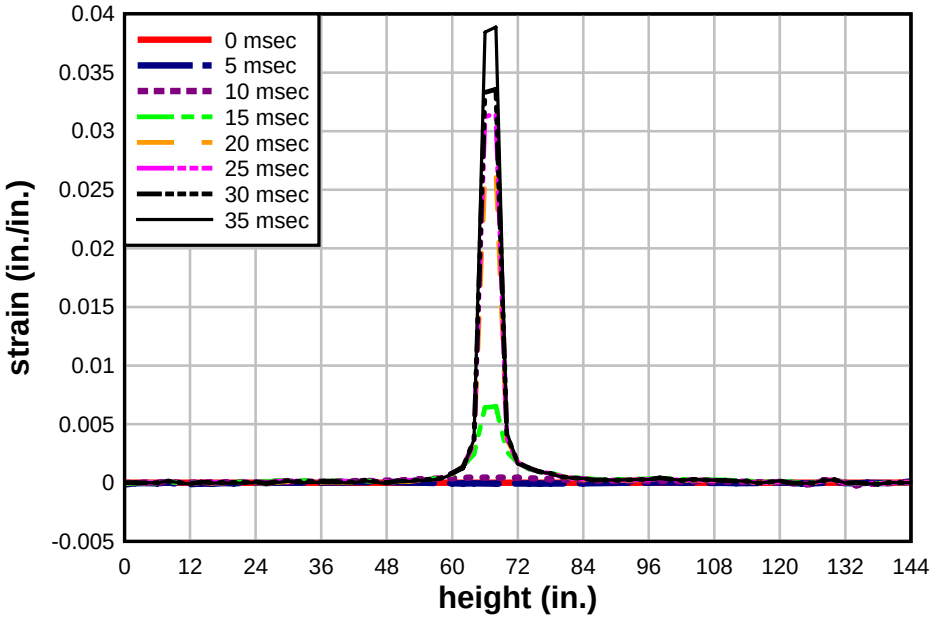

Fig. 4.3. SS3 – Experiment 1**:** Strain of reinforcement of interior concrete wythe across panel height over time

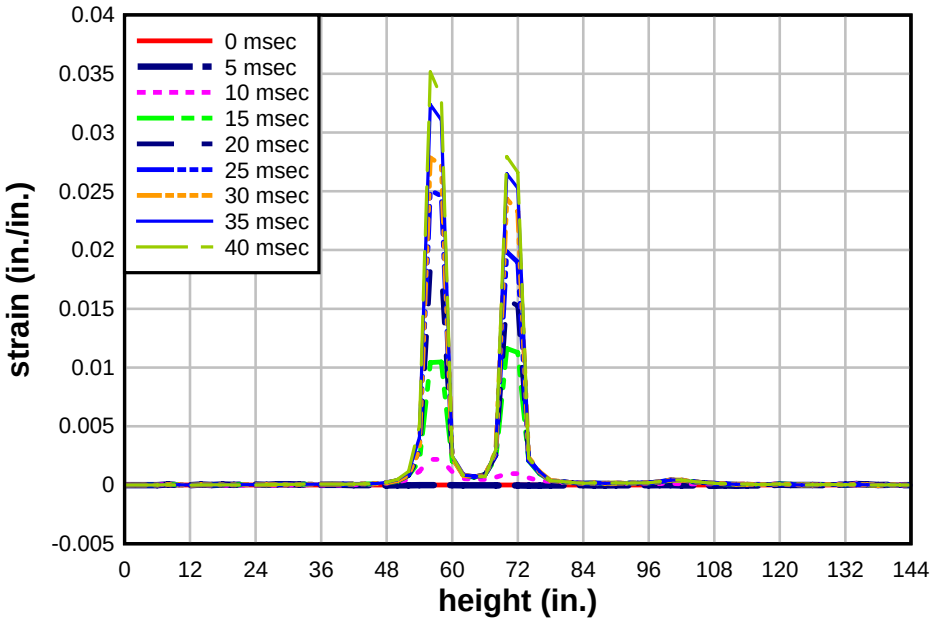

Fig. 4.4. SS4 – Experiment 1**:** Strain of reinforcement of interior concrete wythe across panel height over time

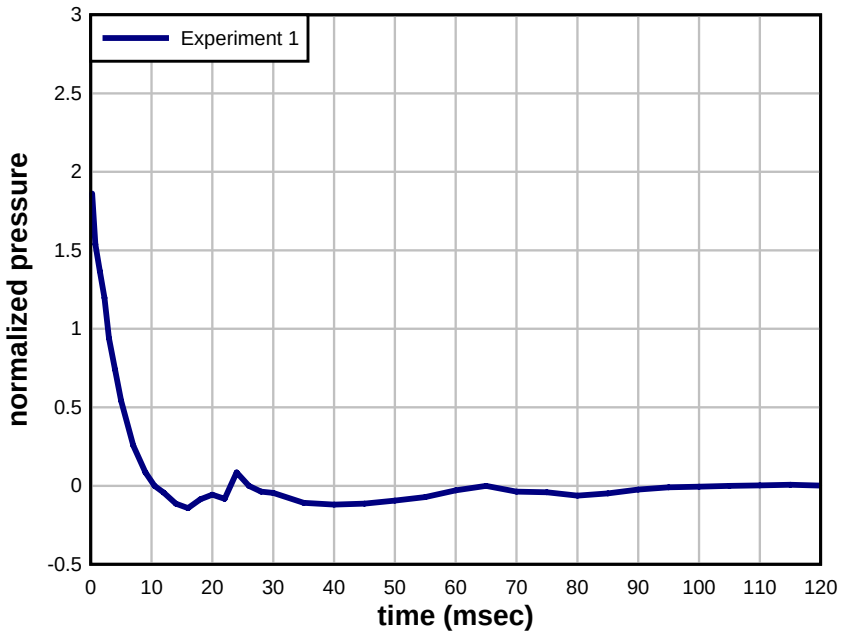

Fig. 4.5. Average pressure for Experiment 1 used for finite element models simulating single span test specimens

4.4 Reaction Force vs. FE Models

For Dynamic Series II experiments, reaction force was measured at the top of all single span specimens using two load cells as seen in Figure 4.6. FE models were prepared with rigid boundaries mirroring the load cell locations of the experimental panels. Overall reaction force was recorded on the rigid boundaries throughout time. FE models showed higher reactions than those recorded in full-scale dynamic experiments. Comparisons of measured reaction force and FE models were done for Experiment 1 of Dynamic Series II and results can be seen in Figures 4.7 through 4.10. For panel SS4, one load cell was not operational during the experiment; in order to make a comparison, the recorded reaction from the one load cell that was operational is compared against its representative rigid boundary in the model in Figure 4.10.

Commonly, concrete structural components are designed to withstand both inbound flexural response and outward rebound of the component. This design criterion usually means reinforcing is symmetric since stresses reverse on the rebound response of the component. Connections used for precast components subjected to blast are normally designed with small to zero dynamic increase factor. Ductility of the flexural resistance of the component is just as important to the connection as the ductility of the connection itself. If the component is too rigid, more force will be transmitted to reactions, possibility causing connection failure.

Figure 4.6. Load cells recording reaction force for single span specimens

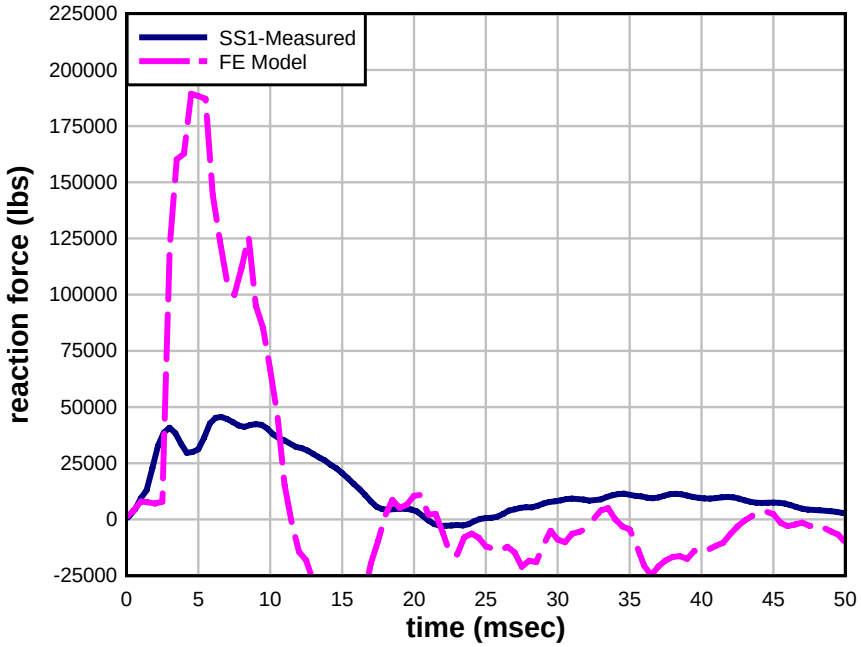

Fig 4.7. Comparison of measured total reaction force and recorded FE model reaction forces for Experiment 1 – SS1

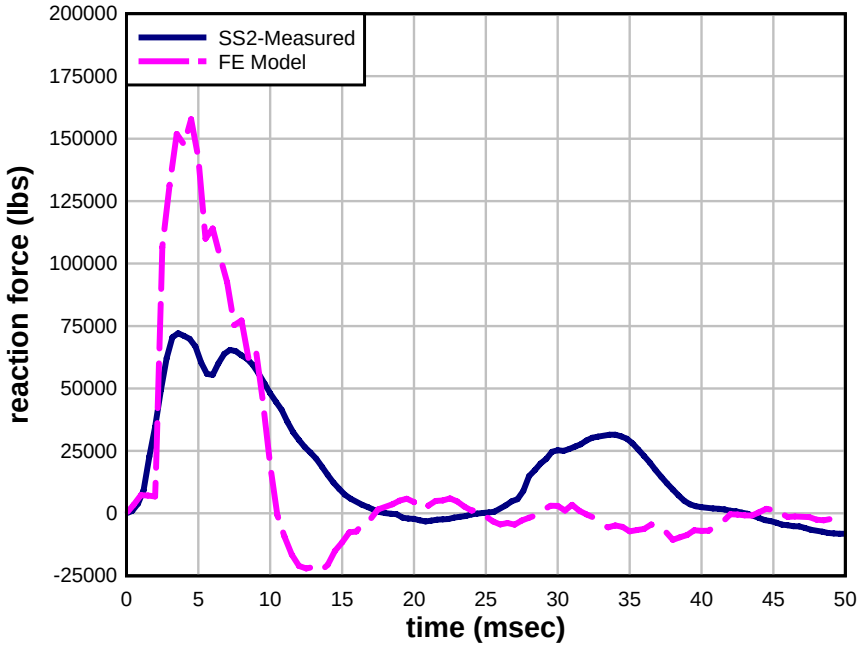

Fig 4.8. Comparison of measured total reaction force and recorded FE model reaction forces for Experiment 1 – SS2

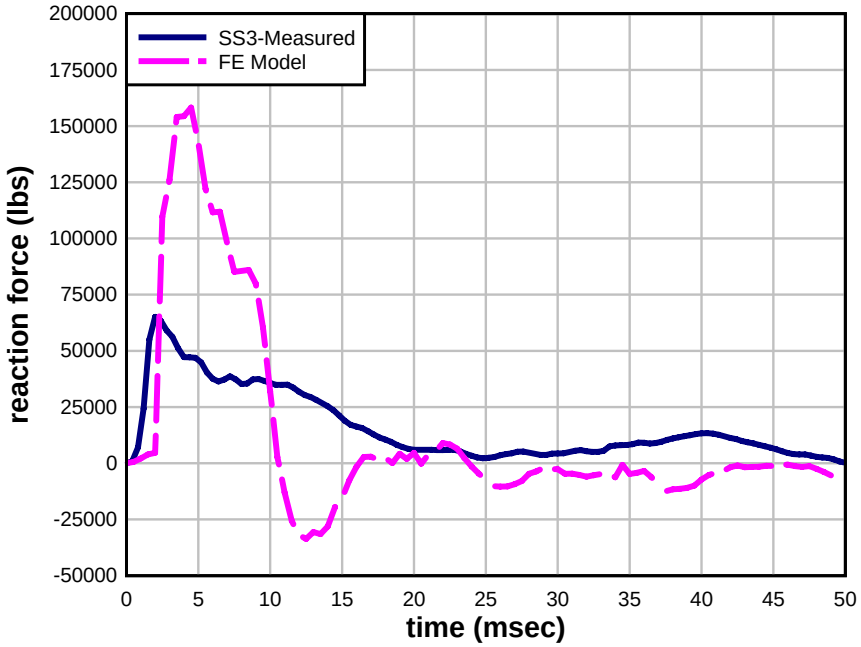

Fig 4.9. Comparison of measured total reaction force and recorded FE model reaction forces for Experiment 1 – SS3

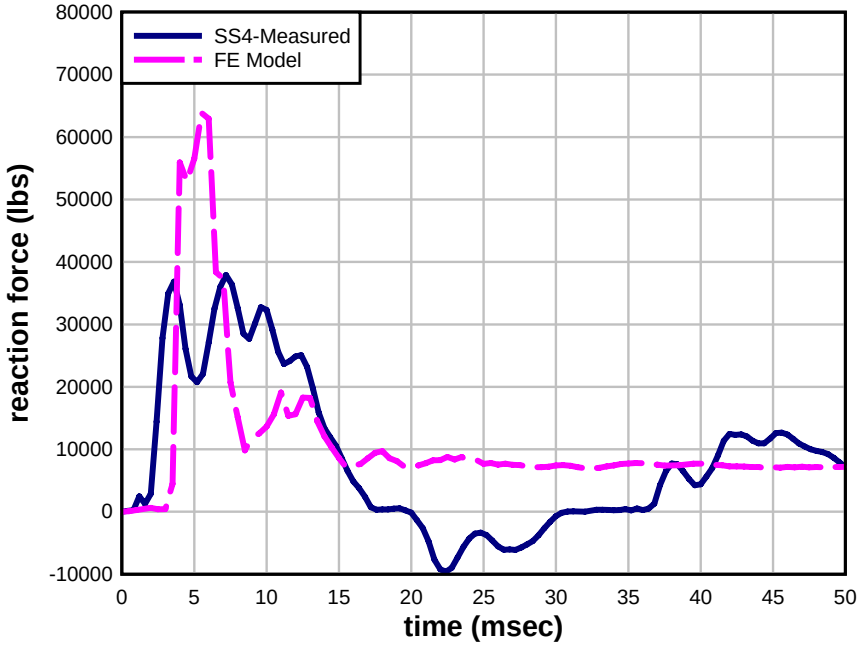

Fig 4.10. Comparison of measured reaction force and recorded FE model reaction force for Experiment 1 – SS4

CHAPTER 5

SINGLE-DEGREE-OF-FREEDOM MODEL DEVELOPMENT

5.1 Introduction

The most common design approach for structures subjected to impulse loads is to develop a single-degree-of-freedom (SDOF) system that will represent the displacement response of the structure. The central-difference numerical method can be used to integrate the equation of motion at discrete time intervals. This chapter will focus on the development of SDOF models for examining the blast response of precast sandwich panels in comparison to current design tools. Previously developed finite element models were used to expand the amount of data points used in comparison to SDOF predictions. Development of resistance curves used in SDOF models was based on upon current Army Corps of Engineers design methodology. Two resistances were produced: a composite resistance based upon one-hundred percent composite action of concrete wythes and a non-composite resistance based upon zero composite action. From analysis of these curves, a weighted resistance was calculated by weighting composite and non-composite response with percentages that represent approximate composite action of the system.

5.2 General SDOF Methodology

Structural systems can be broken down into infinite degrees of freedom; however, it is useful to simplify the motion of an object to a single-degree-of-freedom. Structural components subjected to blast are commonly designed with the midspan displacement as the single-degree-of-freedom in consideration. SDOF methodology is based upon the equation of motion of an object subjected to a force which causes an acceleration of the mass of the object (Equation 5-1).

$$m\ddot{x} + c\dot{x} + kx = F(t) \tag{4-1}$$

The force $F(t)$ is resisted by the mass of the object (m), damping constant (c), and spring/stiffness constant (k), multiplied by the acceleration ($\ddot{x}$), velocity ($\dot{x}$), and displacement (x), respectively. A system with the corresponding equation of motion is represented with a free-body diagram as shown in Figure 5.1.

An equivalent SDOF equation of motion can be developed from the characteristics of the structural component (Figure 5.1). An arbitrary beam with length *l* and shape function $\psi(y)$ with arbitrary mass per unit length $\bar{m}$ that resists the arbitrarily distributed load *v(y)* represents the structural system which must be effectively described as a single-degree-of-freedom. As previously discussed, the midspan displacement is commonly the degree of freedom under consideration. The SDOF equation of motion must be transformed from characteristics of the real component to equivalent characteristics of the SDOF system. Therefore, the characteristics of mass (m), damping constant (c), and spring/stiffness constant (k) and dynamic load (*F)* are multiplied by constants such that

$$K_M = \frac{m_e}{m} \tag{4-2}$$

$$K_D = \frac{c_e}{c} \tag{4-3}$$

$$K_S = \frac{k_e}{k} \tag{4-4}$$

$$K_L = \frac{F_e}{F} \tag{4-5}$$

where F and m are the total force ($F=vl$) and total mass ($m=\bar{m}\,l$) of the system. The constants K_S and K_D can be replaced with the constant K_L. This is done because K_S and K_L can be shown to be equal to each other (Biggs, 1964) and although mathematically it is not correct to replace K_D with K_L, is does not affect the outcome of the systems peak dynamic response since damping is usually negligible in this stage of response. The equation of motion can then be written as:

$$K_M m\ddot{x} + K_L c\dot{x} + K_L kx = K_L F(t) \tag{4-6}$$

A structure with continuous mass and distributed force will have both equivalent mass and equivalent force as follows:

$$M_e = \int^{l} \bar{m}\psi^2(y)dy \tag{4-7}$$

$$F_e = \int^{l} v(y)\psi(y)dy \tag{4-8}$$

where, $\psi(y)$ is the equivalent assumed-shape function of the system.

By dividing the equation of motion of Eq. 5-6 with K_L, the equation of motion can now be written as the following:

$$\frac{K_M}{K_L} m\ddot{x} + c\dot{x} + kx = F(t) \tag{4-9}$$

where $\frac{K_M}{K_L} = K_{LM}$ is the load-mass factor. Biggs (1964) presents several load-mass factors for beams and slabs having various types of support conditions.

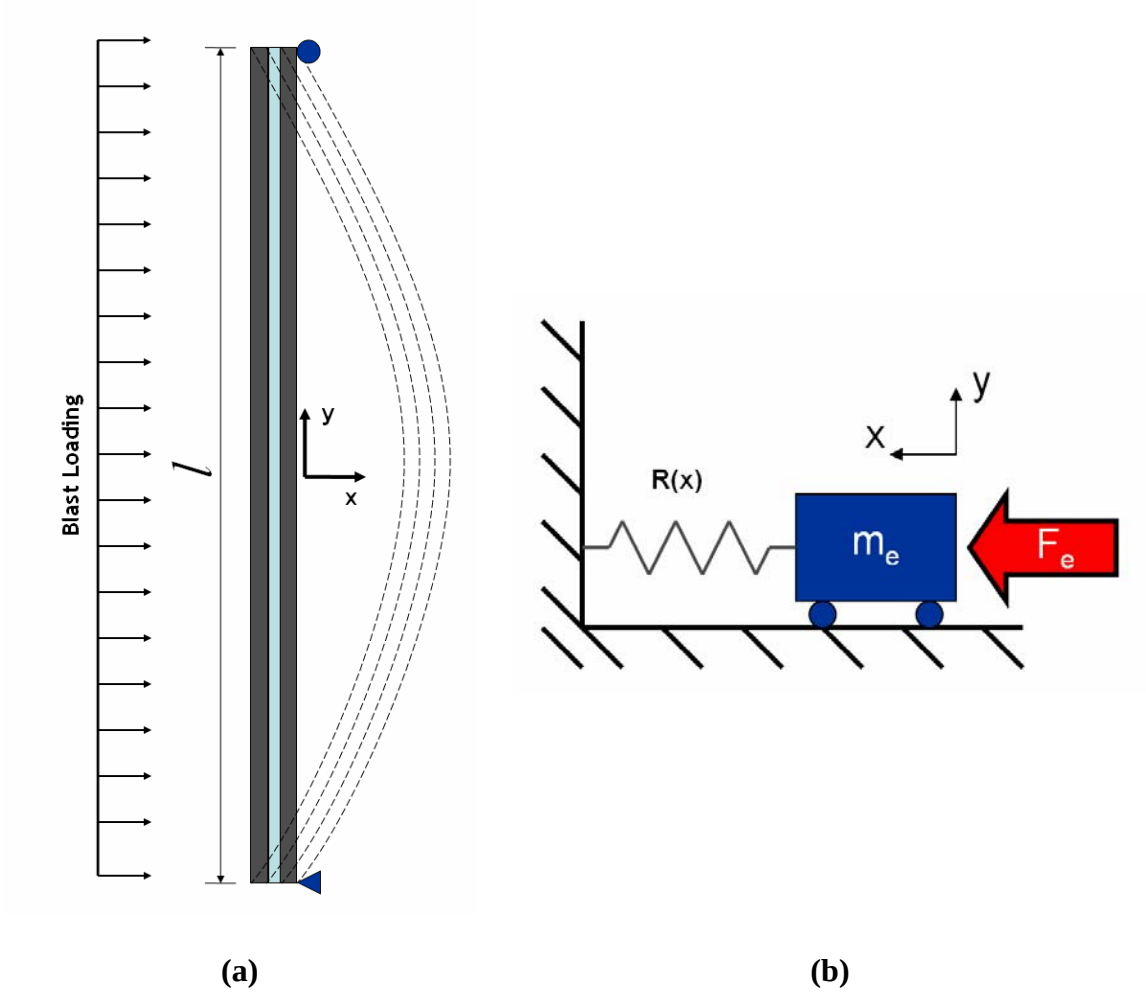

(a) **(b)**

Fig. 5.1. (a) Displacement representation of sandwich panel subjected to blast load (b) Equivalent single-degree-of-freedom system

As discussed in Chapter 2, safety is the most important aspect of systems subjected to blast loads. Therefore, the peak deflection (generally the first peak of

response history) is important; if the wall component fails, occupants will suffer serious injury. Since damping has a negligible effect on the first peak response of a structural system (USACE PDC, 2006), it was not considered in the computation of SDOF models used in this analysis. In design it is common to simplify the positive phase as a triangular load with an equivalent impulse (area under the pressure-time curve) and not consider the negative phase, which is a conservative assumption. For this study, as should be the case for any research involving response of structures to blast loads, both positive and negative phases of blast loads were used in SDOF models to achieve greater accuracy.

5.2.1 Central Difference Numerical Method

Closed form solutions for the equation of motion for single-degree-of-freedom systems is impossible if the force acting on the system is arbitrary with respect to time or if the system has nonlinearities (Chopra, 2007). A practical means of solving the non-homogeneous differential equation of motion is the central difference method. A numerical integration solution, the central difference method works well with nonlinear dynamic problems.

The central difference method is based upon a finite difference approximation of the velocity and acceleration of the structure. If the time step, Δt, is chosen correctly, the time derivatives of displacement (i.e. velocity and acceleration) can be approximated as:

$$\dot{x}_i = \frac{x_{i+1} - x_{i-1}}{2\Delta t} \tag{4-10}$$

$$\ddot{x}_i = \frac{x_{i+1} - 2x_i + x_{i-1}}{(\Delta t)^2} \tag{4-11}$$

Substituting these values for acceleration and velocity into Equation 5-1 gives

$$m\frac{x_{i+1}-2x_i+x_{i-1}}{(\Delta t)^2}+c\frac{x_{i+1}-x_{i-1}}{2\Delta t}+kx_i=F_i \tag{4-12}$$

Disregarding the damping term due to its negligible contribution to first peak response and solving for x_{i+1} gives

$$x_{i+1}=\left(\frac{F_i}{m}-\frac{kx_i}{m}\right)(\Delta t)^2+2x_i-x_{i-1} \tag{4-13}$$

It should be noted that by placing initial conditions within Equation 5-1 and continuing to disregard damping, it can be found that

$$\left(\frac{F_i}{m}-\frac{kx_i}{m}\right)=\ddot{x} \tag{4-14}$$

The SDOF model used in analysis uses equation 5-13 to solve for response but with a few modifications. First, the mass is the effective mass of the system, $K_{LM}m$. The initial location at t_{i-1} is input as 0, and the displacement after the first time step (t_i) is input as half (1/2) the $\frac{F_i(\Delta t)^2}{m}-\frac{kx_i(\Delta t)^2}{m}$ term of equation 5-13 as is suggested in Biggs (1964). This ensures that all terms are present after the second time step to calculate response. The pressure is called from the input load curve according to the appropriate time, t_i, then divided by the effective mass factor. The effective mass, m_e, is calculated by finding the unit mass of the wall and then dividing by the appropriate transformation factor (either elastic or plastic). The resistance is initially input as zero and called from the input resistance curve according to the appropriate previous steps displacement, then divided by the effective mass. Within the prediction model, the effective mass is

manually changed from the elastic effective mass to the plastic effective mass at the point where resistance is no longer elastic. The acceleration, $\ddot{x}$, is calculated as with equation 5-14, with the exception that kx_i is the appropriate called upon resistance as discussed previously. The term $\ddot{x}(\Delta t)^2$ is needed to calculate the appropriate displacement, x, for each time step.

Time (msec)	θ	p(t)	p(t)/m	R(y)	R(y)/m	ÿ	ÿ(Δt)^2	y		*m*	1051
0	0.0000	1.3442	0.0013	0.0000	0.0000	0.0013	0.0000	0.0000			890
0.02	0.0000	1.3442	0.0013	0.0000	0.0000	0.0013	0.0000	0.0000			
0.04	0.0000	1.3442	0.0013	0.0000	0.0000	0.0013	0.0000	0.0000		KLM Elastic	0.78
0.06	0.0000	1.3442	0.0013	0.0000	0.0000	0.0013	0.0000	0.0000		KLM Plastic	0.66
0.08	0.0000	1.3442	0.0013	0.0000	0.0000	0.0013	0.0000	0.0000			

Figure 5.2. Screenshot of SDOF model in Microsoft Excel spreadsheet format

5.3 Development of Sandwich Panel SDOF Prediction Models

The difficulty in developing an SDOF prediction model for sandwich panels subjected blast loads arises from the ambiguity in describing the resistance of the sandwich panel system. Current prediction tools were used to create a similar prediction model. A prediction model was produced using a combination of theoretical fully composite and non-composite resistance to create a bilinear weighted resistance.

5.3.1 Static Resistance of Sandwich Panels and SDOF Models

The static resistance of sandwich panels does not follow a traditional reinforced concrete mechanics path. Sandwich panels are designed to withstand lateral forces that typically do not cause midspan displacement beyond fractions of an inch. In fact, sandwich panels are designed to withstand any handling/erection loads and not to crack due to lateral forces for aesthetic reasons. Displacements for sandwich panels, both

conventionally reinforced and prestressed, can reach several inches when subjected to blast loads. During the response, sandwich panels lose the ability to behave compositely, making the calculation of resistance a matter of concern.

Several possible factors lead to the loss of composite action. First, discrete shear ties are often used to allow concrete wythes to act compositely. Local composite action may occur at the location of each shear tie but not in the spaces between ties, causing increased concrete stresses at areas where plane sections do not remain plane. Also stress concentrations at the location of discrete ties may lead to failure of concrete sections at these locations. All possible factors contribute to the failure of the sandwich panel before reaching the plastic limit calculated through general reinforced concrete mechanics theory.

In experimental static testing of panels, it was often seen that shear ties failed due to shear or concrete around tie embedment failed, causing the panel to lose composite behavior and strength as load increased (Naito et al., 2010a). This has proven to be very difficult to characterize and makes development of SDOF design methodology of sandwich panels complex. In design, the resistance of most structural components is characterized as bilinear for determinate systems or multi-linear depending upon the indeterminacy of the system. All systems have an ultimate resistance that remains constant at a strength based upon nominal resistance. Experimental testing of sandwich panels proves that loss of composite action due to shear tie failure and other factors leads to a decreasing resistance until failure (Figure 5.3). Although a bilinear approximation of this is not ideal, it is commonly used in SDOF prediction models and is an approximation

that can be created using previously established concrete mechanics, as will be presented later.

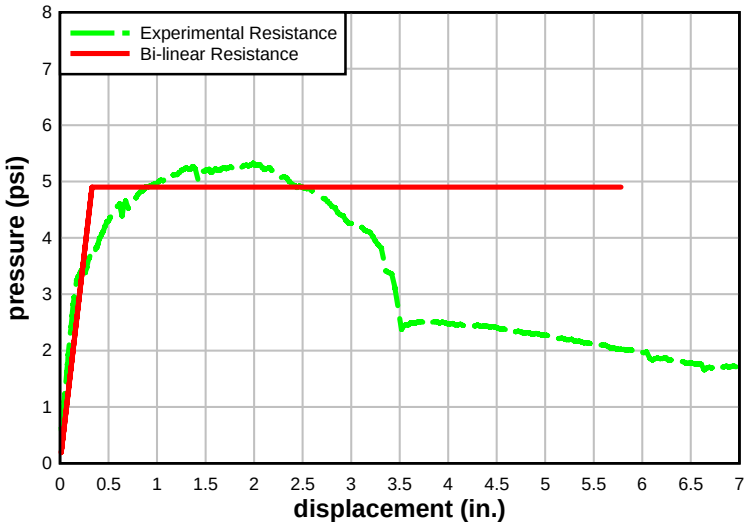

Figure 5.3. Comparison of experimental resistance to bilinear resistance curve

5.3.2 Correlation With Current Prediction Methods

The Protective Design Center (PDC) of the Army Corps of Engineers developed a tool entitled SBEDS (Single-Degree-of-Freedom Blast Effects Design Spreadsheet) which creates SDOF models used for prediction of response for a wide range of structural components. The mechanics and structural dynamics of the systems was based upon the technical manual titled "Structures to Resist the Effects of Accidental Explosions" (formally reference as TM5-1300, it has been entered into the Unified Facilities Criteria as UFC 3-340-02).

5.3.3 Resistance Calculation

The PDC has published a document entitled "User's Guide for the Single-Degree-of-Freedom Blast Effects Design Spreadsheet (SBEDS)" describing the methods incorporated from UFC 3-340-02 in the development of predictive SDOF models for

structural components (USACE PDC, 2006). From this document, SDOF models were developed for the prediction of sandwich panel designs used in full-scale experiments. The sandwich panel SDOF model resistances were created by calculating a 100% composite resistance and a 0% composite resistance, and creating a weighted average resistance, represented as a bilinear resistance for experimental samples. This bilinear resistance was then used to determine a response of the dynamic samples subjected to the two experimental blast loads.

5.3.4 Material Dynamic Properties Calculation

As previously discussed, both concrete and reinforcing steel strengths are sensitive to the rate of loading. It is known that, as strain rate increases, the concrete compressive strength also increases; there is some debate upon the factor that should be used. Often the dynamic increase factor (DIF) is chosen to be 1.19 for design purposes, and this factor was used in all SDOF models for this analysis. The equation for calculating dynamic concrete strength is

$$f'_{dc} = f'_c K_e K_a (DIF) \tag{4-15}$$

where f'_{dc} is the concrete dynamic compression strength, f'_c is the concrete minimum specified compression strength, K_a is the concrete aging factor, and K_e is the static strength increase factor, and the DIF is described above. The factor K_a accounts for the observed increase in concrete compressive strength over time and is conservatively taken as 1.1 in most cases. The factor K_e accounts for the observation that most material strengths exceed specified minimums and is conservatively taken as 1.1 unless in-field material testing leads one to use another value.

Like concrete strength, reinforcing steel dynamic strength uses a static strength increase factor and a DIF.

$$f_{dy} = f_y K_e (DIF) \tag{4-16}$$

Factors used depend upon the reinforcement type as seen in Table 5.1 (USACE PDC, 2006). Most prestressed sandwich panels use seven-wire strand of either Grade 250 or Grade 270; it is customary to give prestressing strand DIF and K_e values of 1.0.

Table 5.1. Dynamic yield strength for conventional reinforcement (USACE PDC, 2006)

Type of Steel	Yield Strength (psi)	Ultimate Strength (psi)	K_e	DIF
ASTM A615, A616, A706 (Grade 60)	60,000	90,000	1.1	1.17
ASTM A615 (Grade 40)	40,000	75,000	1.1	1.17
ASTM, A496 (Welded Wire Fabric)	70,000	80,000	1.0	1.1

The ultimate dynamic moment capacity of a conventionally reinforced concrete beam or slab is represented by equation 5-17, where A_s is the area of steel, d is the depth of tension reinforcement, and b is the width of concrete compression block. Singly reinforced cross-sections (described as Type I cross-sections in PDC 6-02) are often assumed for all cross-sections as a conservative approach. The ultimate dynamic moment capacity for reinforced concrete slabs and beams described in equation 5-17 is utilized by SBEDS without any consideration of a Type II cross section (Type II cross-sections are doubly reinforced and also assumes concrete cannot carry compression due to crushing).

$$M_{du} = A_s f_{dy}\left(d - \frac{A_s f_{dy}}{1.7 b f_{dc}^{'}}\right) \tag{4-17}$$

The ultimate dynamic moment capacity of prestressed concrete beams and slabs is represented by equation 5-18, where A_{ps} is the area of prestressed reinforcement, a (Equation 5-19) is the depth of the equivalent rectangle compression stress block, d_p is the distance from the extreme compression fiber to the centroid of the prestressed reinforcement and f_{ps} (Equation 5-20) is the average stress in the prestressed reinforcement at ultimate load.

$$M_u = A_{ps} f_{ps}\left(d_p - \frac{a}{2}\right) + A_s f_{dy}\left(d - \frac{a}{2}\right) \tag{4-18}$$

$$a = \frac{\left(A_{ps} f_{ps} + A_s f_{dy}\right)}{0.85 f_{dc}^{'} b} \tag{4-19}$$

$$f_{ps} = f_{pu}\left\{1 - \frac{\gamma_p}{\beta_1}\left[\rho_p \frac{f_{pu}}{f_{dc}^{'}} + \frac{d f_{dy}}{d_p f_{dc}^{'}}\left(\rho - \rho'\right)\right]\right\} \tag{4-20}$$

For conventionally reinforced sandwich panels, the moment of inertia used to calculate displacements used in resistance curves is an average (Equation 5-21) of total gross moment of inertia and a cracked moment of inertia (Equation 5-22).

$$I_a = \frac{\left(I_g + I_c\right)}{2} \tag{4-21}$$

$$I_c = F d^3 \tag{4-22}$$

Equation 5-22 is an approximation of cracked moment of inertia and uses the factor F chosen from the charts taken from UFC 340-02. The modular ratio used in conjunction with the cracked moment of inertia factor charts is stated as the following:

$$n = \frac{E_s}{E_c} \tag{4-23}$$

The modulus of elasticity for concrete is equal to:

$$E_c = 33 w_c^{1.5} \sqrt{f_c'} \tag{4-24}$$

where w_c is the unit weight of concrete – normally 145 lbs/ft^3. The moment of inertia of prestressed beams or slabs is also an average of gross and cracked moment of inertia as shown in Equation 5-21 with the cracked moment of inertia as follows:

$$I_c = nA_{ps}d^2\left[1-(\rho_p)^{1/2}\right] \tag{4-25}$$

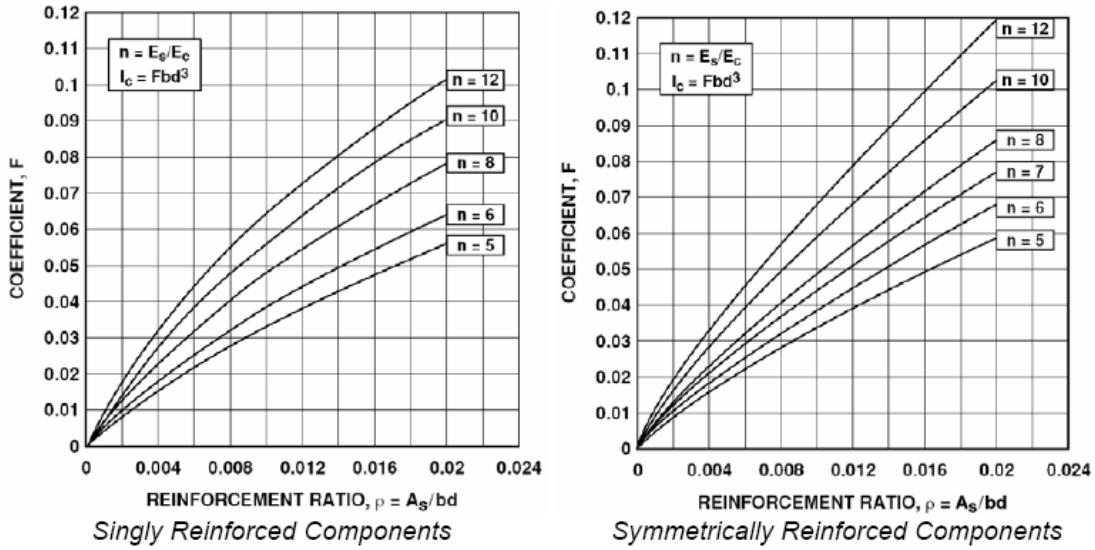

Figure 5.4. Coefficients of cracked moment of inertia (UFC 3-340-02)

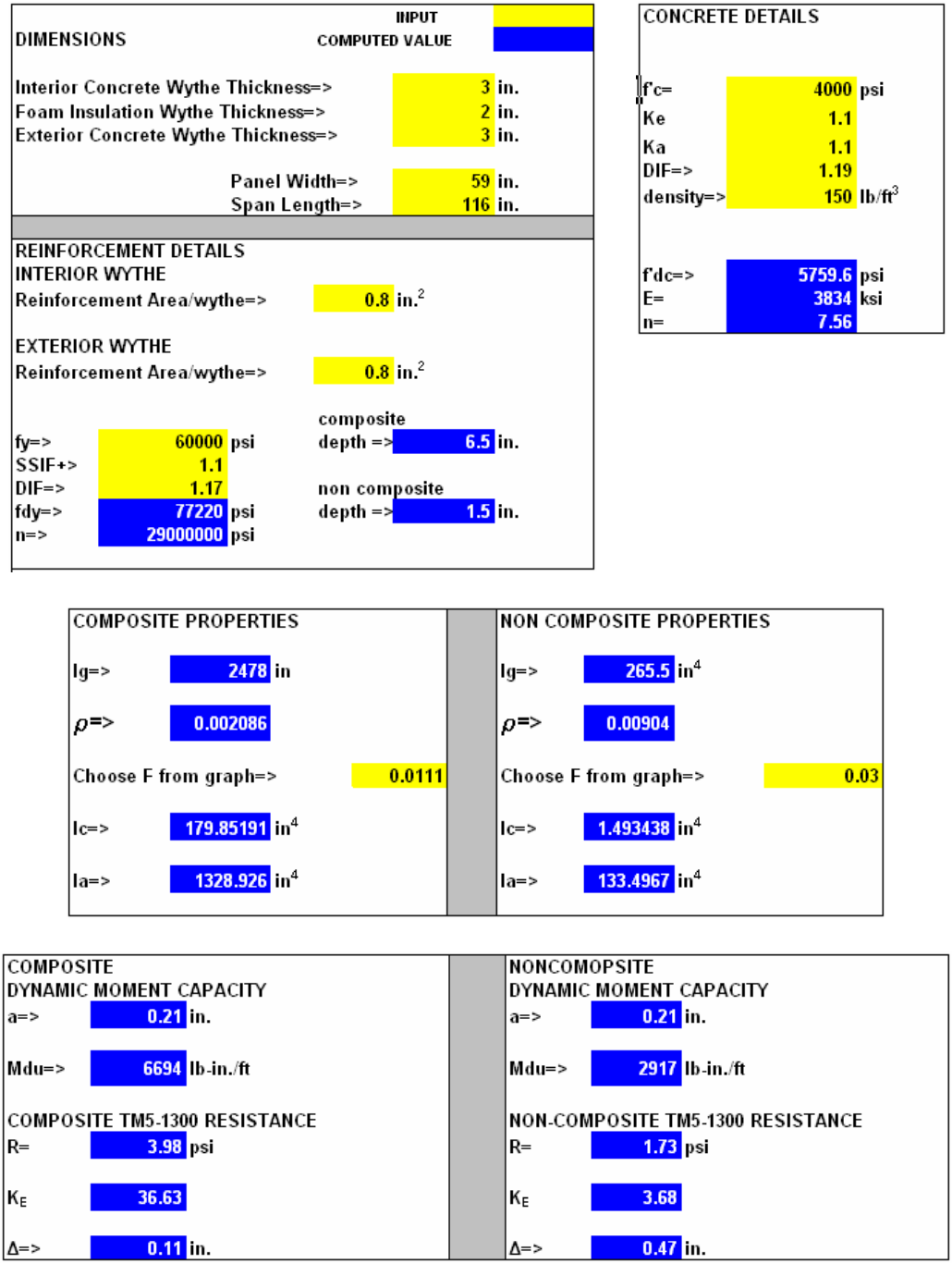

Fig. 5.5. Screenshots of SDOF prediction analysis spreadsheet resistance input

5.4 SDOF Prediction Model Comparisons

SDOF prediction models using the aforementioned bilinear weighted resistance were compared against full-scale dynamic tests and FE models.

5.4.1 SDOF Prediction Model Matrix

Full-scale dynamic tests were completed in two series. The first series of tests were completed in 2006 and included tests of two precast/prestressed sandwich panels subjected to various blast pressures and compared to standard conventionally reinforced concrete panels used as controls (Naito et al. 2009b). Test specimens were 30 feet tall with support conditions approximated as simple supports. In total, Dynamic Series I consisted of five separate detonations. Prediction models were used to predict responses for panels subjected Detonations 2 and 3.

Dynamic Series II consisted of two experiments each consisting of a pre-detonation loading and a primary loading as discussed in Chapter 3. Only single span specimens subjected to primary detonations were used for SDOF predictions. All single span Dynamic Series II specimens had a clear span of 9.7 feet and simple supports assumed (Naito et al., 2010b).

In order to increase the amount of data points to compare SDOF prediction models, FE modeling was used to test a different span length than was used in either dynamic full-scale test. Also, fixed-fixed boundary conditions were attempted in modeling to compare prediction models ability in simulating such conditions. In total, 22 SDOF prediction models were compared against either full-scale measured displacements or FE models. Table 5.2 shows all prediction models and their comparative bases.

5.4.2 SDOF Prediction Model Comparisons – Dynamic Series I

The first precast/prestressed test specimen used solid concrete sections as connectors between the interior and exterior concrete wythes. Panels using solid concrete sections for shear transfer are considered to give the panel composite behavior only during service loads; therefore, the SDOF prediction model used a weighted average with 65% composite, 35% non-composite resistance. These percentages were first chosen to match the Dynamic Series I data set, and was continuously used throughout all predictions for prestressed sandwich panels using some type of composite connector due to the overall acceptance of this percentage being adequate in prediction. The solid-zone panel was subjected to two detonations of varying pressures, the first being very small and causing very minimal damage. The second detonation was larger and considered a more viable data set for comparison of SDOF prediction models developed. As seen in Figure 5.6, the SDOF prediction is accurate for the measured response. It should be noted that since this panel had endured a previous detonation, there is a possibility that measured displacement may be higher than would be expected without previous testing. Figure 5.6 compares the SDOF responses with a composite resistance, a non-composite resistance, the weighted resistance, and the measured solid-zone panel response from Dynamic Series I, Detonation 2.

Table 5.2. SDOF Prediction Model Comparison Matrix

Dynamic Series I					
Specimen	Clear Span (ft)	Wythe Configuration	Tie Type	Boundary Conditions	Reinforcement Type
Detonation 2	30	3-2-3	Solid concrete zones	simple	prestressed
Detonation 3	30	3-2-3	carbon fiber composite	simple	prestressed
Dynamic Series II -Experiment 1 & 2					
Specimen No.	Clear Span	Wythe Configuration	Tie Type	Boundary Conditions	Reinforcement Type
SS1	9.7	3-2-3	carbon fiber composite	simple	prestressed
SS2	9.7	3-2-3	fiberglass composite	simple	prestressed
SS3	9.7	3-2-3	fiberglass composite	simple	conventional
SS4	9.7	6-2-3	fiberglass non-composite	simple	conventional
FE Modeling Data Expansion Set					
Specimen No.	Clear Span	Wythe Configuration	Tie Type	Boundary Conditions	Reinforcement Type
FE-1	18.7	3-2-3	carbon fiber composite	simple	prestressed
FE-2	18.7	3-2-3	fiberglass composite	simple	prestressed
FE-3	18.7	3-2-3	fiberglass composite	simple	conventional
FE-4	18.7	6-2-3	fiberglass non-composite	simple	conventional
FE-5	18.7	3-2-3	carbon fiber composite	fixed-fixed	prestressed
FE-6	18.7	3-2-3	fiberglass composite	fixed-fixed	prestressed
FE-7	18.7	3-2-3	fiberglass composite	fixed-fixed	conventional
FE-8	18.7	6-2-3	fiberglass non-composite	fixed-fixed	conventional
FE-9	9.7	3-2-3	carbon fiber composite	fixed-fixed	prestressed
FE-10	9.7	3-2-3	fiberglass composite	fixed-fixed	prestressed
FE-11	9.7	3-2-3	fiberglass composite	fixed-fixed	conventional
FE-12	9.7	6-2-3	fiberglass non-composite	fixed-fixed	conventional

The second precast/prestressed panel tested in Dynamic Series I was subjected to Detonations 3, 4, and 5. The panel used a composite carbon fiber shear connector as a

means of connecting concrete wythes and as a shear transfer mechanism. The shear tie provides composite action to panels subjected to their designed service loads, therefore the prestressed/composite weighted resistance of 65% composite resistance, 35% non-composite resistance was used. The prediction was lower than the measured response, which in general is not a good qualifier when creating a prediction method for structural systems subjected to blasts. As seen in Figure 5.7, the prediction was accurate, within the acceptable margin of error in such dynamic, nonlinear systems. Table 5.3 demonstrates the percent difference between weighted resistance predictions and measured data for Dynamic Series I tests.

No other detonations were considered for the CFRP panel due to the large permanent displacement seen after each detonation. The panels tested in Dynamic Series I represent the largest clear spans (30 feet) tested in a full-scale dynamic experiment. Sandwich panels become more efficient to build, transport, and erect as span length increases. Although the full-scale dynamic data set for sandwich panels of this height is small, their importance is large due to the common use of large span lengths in practice.

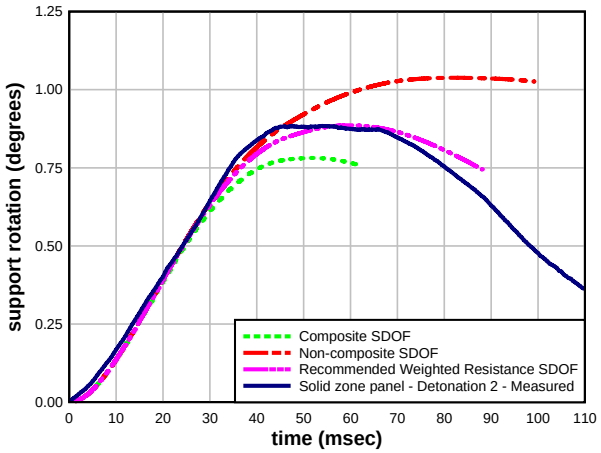

Fig. 5.6. Dynamic Series I, Detonation 2 measured displacement comparison to SDOF prediction using weighted resistance

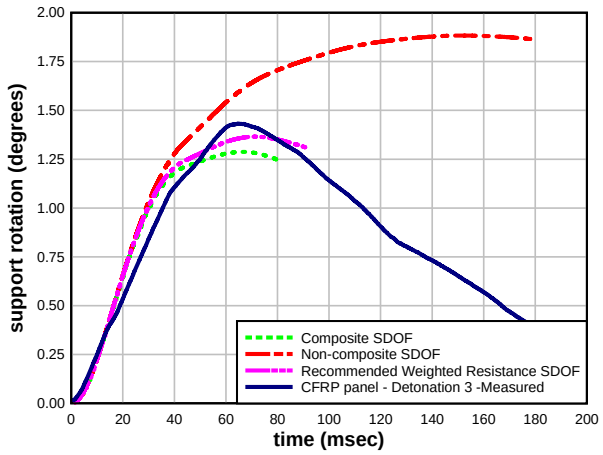

Fig. 5.7. Dynamic Series I, Detonation 3 measured displacement comparison to SDOF prediction using weighted resistance

Table 5.3. Percent Difference, Dynamic Series I SDOF prediction vs. measured support rotation

Panel	Predicted Support Rotation, degrees	Measured Support Rotation, degrees	% Difference
Solid-Zone Panel	0.886	0.884	0.2%
CRFP Panel	1.365	1.432	4.7 %

5.4.3 SDOF Prediction Model Comparisons – Dynamic Series II

Next, SDOF predictions using weighted resistances were compared for all single span specimens tested in Dynamic Series II. As mentioned before, Dynamic Series II consisted of two experiments. SDOF predictions using weighted resistances were created for primary detonations of both experiments. All composite panels used a weighted resistance of 65% composite resistance, 35% non-composite resistance was used. Predictions for the only non-composite panel in Dynamic Series II used a weighted resistance of 30% composite resistance, 70% non-composite resistance. As can be seen in Figure 5.8, Figure 5.9, Table 5.4, and Table 5.5, all weighted resistance predictions

accurately predicted response within the acceptable margin of error in such dynamic, nonlinear systems.

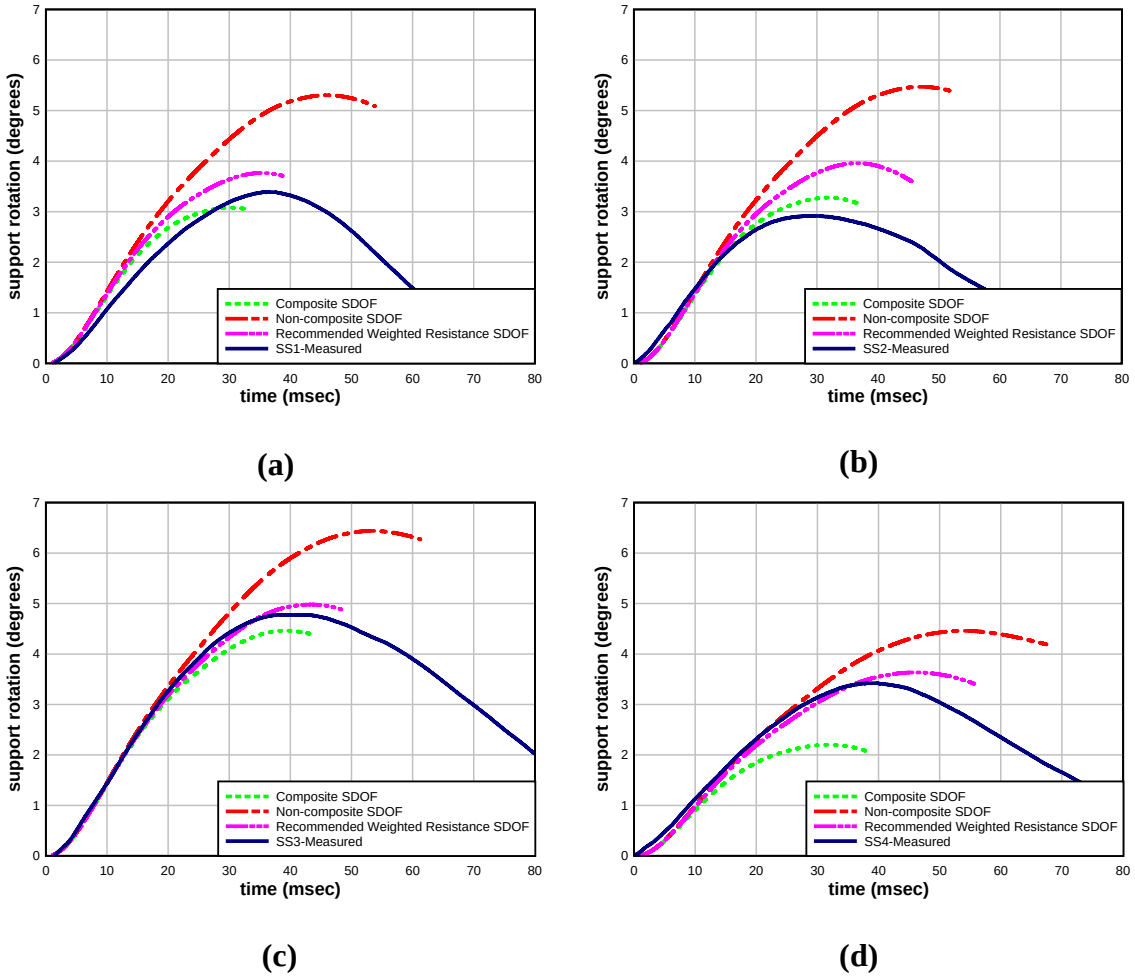

Figure 5.8 Evaluation of weighted resistance prediction method vs. measured data. Dynamic Series II - Experiment 1 – (a) SS1 (b) SS2 (c) SS3 (d) SS4

Table 5.4. Percent Difference, Dynamic Series II - Experiment 1 SDOF prediction vs. measured support rotation

Panel	Predicted Support Rotation, degrees	Measured Support Rotation, degrees	% Difference
SS1	3.77	3.39	11.2
SS2	3.96	2.92	35.6
SS3	4.98	4.78	4.2
SS4	3.64	3.42	6.4

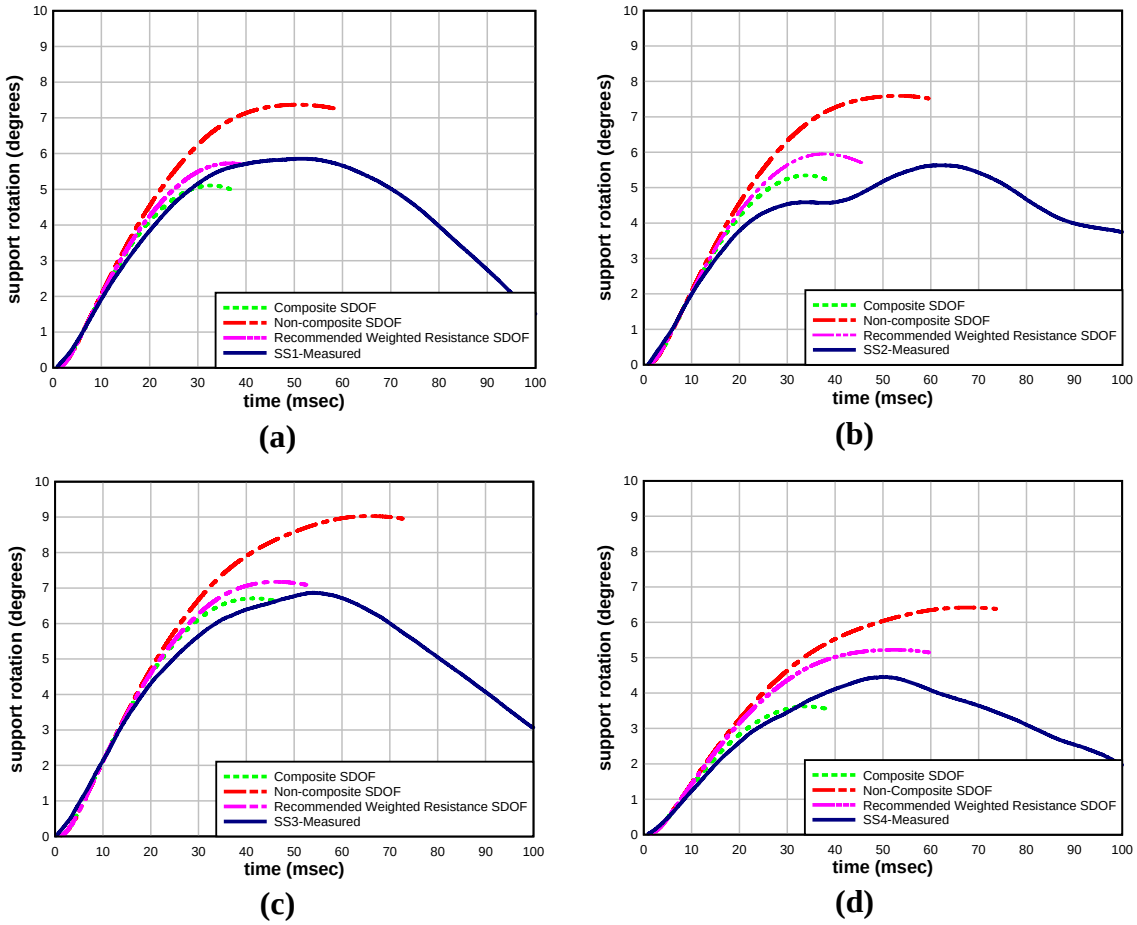

Figure 5.9. Evaluation of weighted resistance prediction method vs. measured data, Dynamic Series II - Experiment 2 – (a) SS1 (b) SS2 (c) SS3 (d) SS4

Table 5.5. Percent Difference, Dynamic Series II - Experiment 2 SDOF prediction vs. measured support rotation

Panel	Predicted Support Rotation, degrees	Measured Support Rotation, degrees	% Difference
SS1	5.72	5.86	-2.4
SS2	5.95	5.63	5.7
SS3	7.17	6.87	4.4
SS4	5.22	4.45	17.3

5.4.4 Resistance and Energy Comparisons

SDOF predictions were created for each specimen using recorded experimental resistance in order to study the viability of using a bilinear weighted resistance curve to

replace actual resistance in the SDOF system. After support rotation comparison, an SDOF model was created using the experimental resistance of each panel. The predicted response from the weighted resistance SDOF was compared against the response from the experimental resistance SDOF. As seen in Figure 5.10 and Figure 5.11, weighted resistance SDOF predicted a response similar to that of the experimental resistance SDOF.

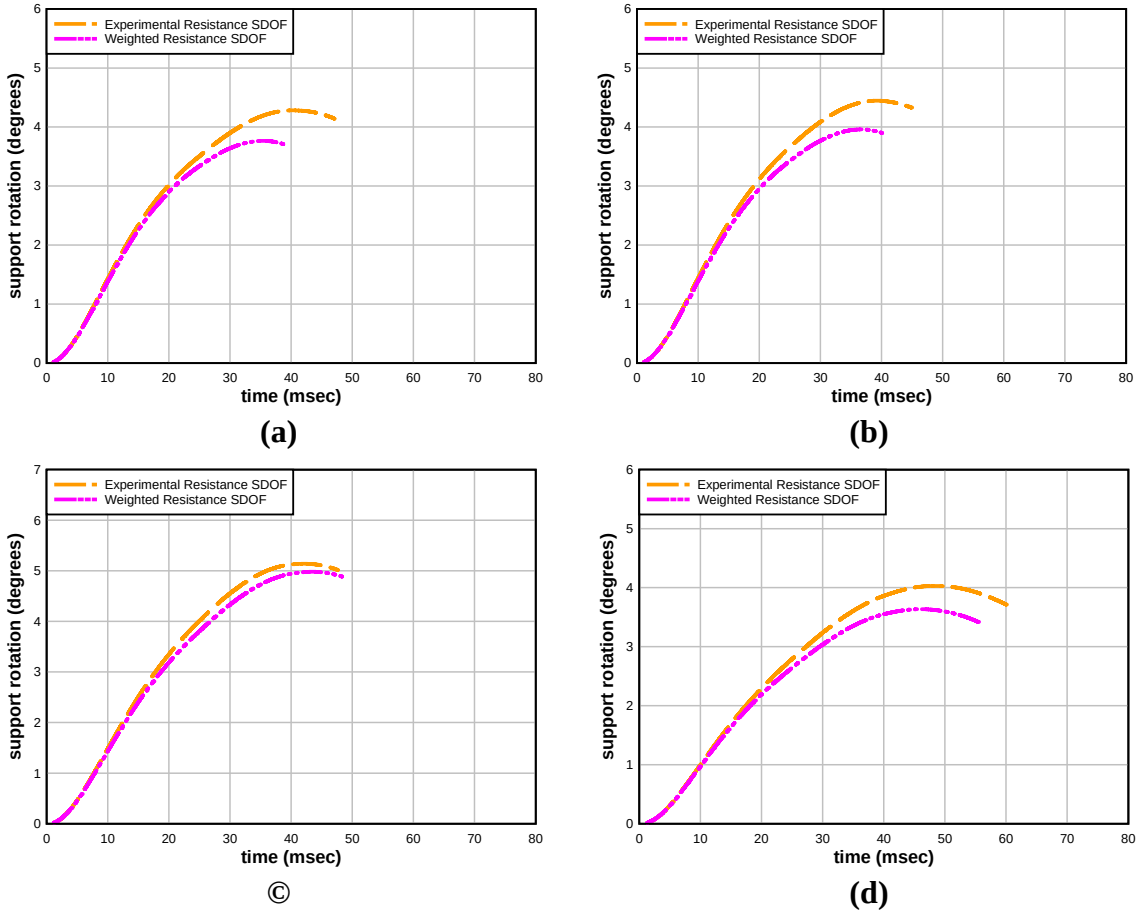

Figure 5.10. Experiment 1 loading: Predicted response comparisons of weighted resistance SDOF and experimental resistance SDOF – (a) SS1 (b) SS2 (c) SS3 (d) SS4

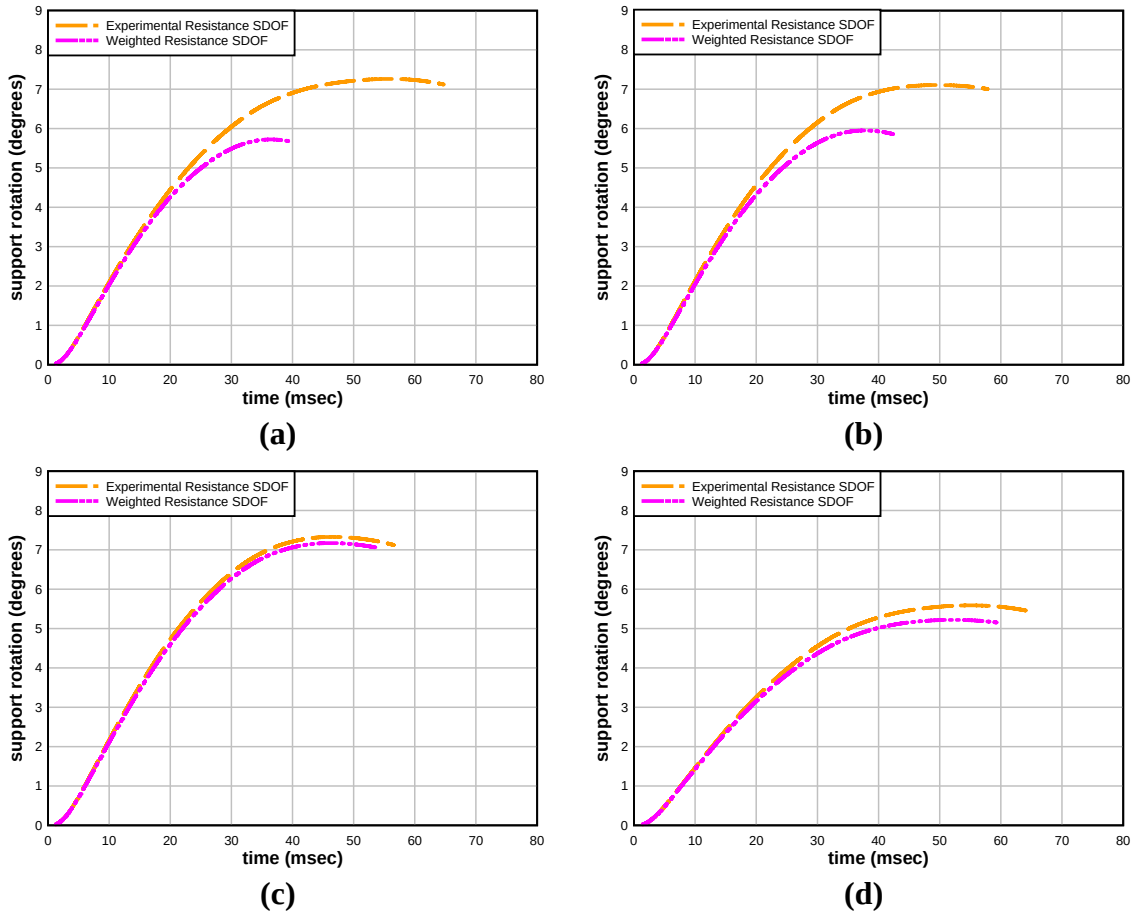

Figure 5.11. Experiment 2 loading: Predicted response comparisons of weighted resistance SDOF and experimental resistance SDOF – (a) SS1 (b) SS2 (c) SS3 (d) SS4

Next, the weighted and experimental resistances were directly compared for all specimens using loadings from both experiments. Both weighted and experimental resistances were recorded until maximum SDOF predicted displacement response was reached. Figure 5.12, Figure 5.13, Figure 5.14 and Figure 5.15 show the resistance and energy comparisons for Experiment 1 loading; Figure 5.16, Figure 5.17, Figure 5.18, and Figure 5.19 show the resistance and energy comparisons for Experiment 2 loading. Also, the area under the resistance curves were integrated, giving the total amount of energy absorbed through resistance. This serves as a good comparative basis since the bilinear

resistance can be conservative or un-conservative depending upon the displacement of the system as seen in Figure 5.20. In this case, a resistance is considered conservative when it would lead to a larger displacement in the SDOF model. If the bilinear weighted resistance is lower than the experimental resistance at the same displacement it is therefore called conservative. It should be noted Figure 5.20 is only an example and that bilinear weighted resistance for other designs does not always follow the path of being unconservative initially and becoming more conservative as displacement increases. In Figure 5.12 for instance, the bilinear resistance begins slightly conservative, then become unconservative, returns to conservative, and then become highly unconservative as displacement reaches higher. The bilinear weighted resistance was chosen as a means of creating resistance not for its accuracy of determining resistance as any one displacement, but as a global representation of energy absorbed by the system. The only specimen examined using the weighted resistance SDOF prediction methods that exhibited high amount of variability was panel SS4, the non-composite conventionally reinforced panel. Non-composite panels, as seen in testing, have high rates of variability when it comes to resistance, due to the differing degrees of a non-composite action.

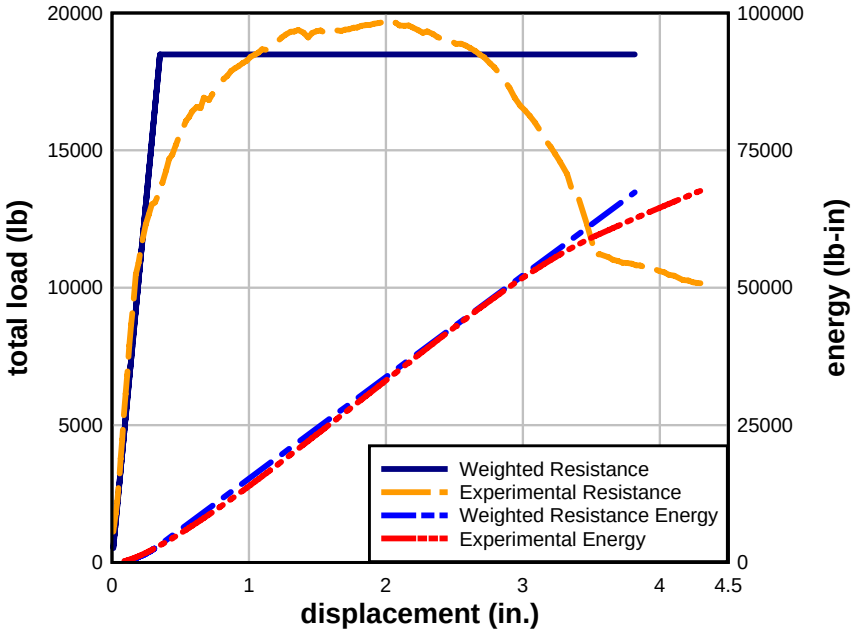

Fig. 5.12. Experiment 1 loading: resistance and energy comparisons for SS1

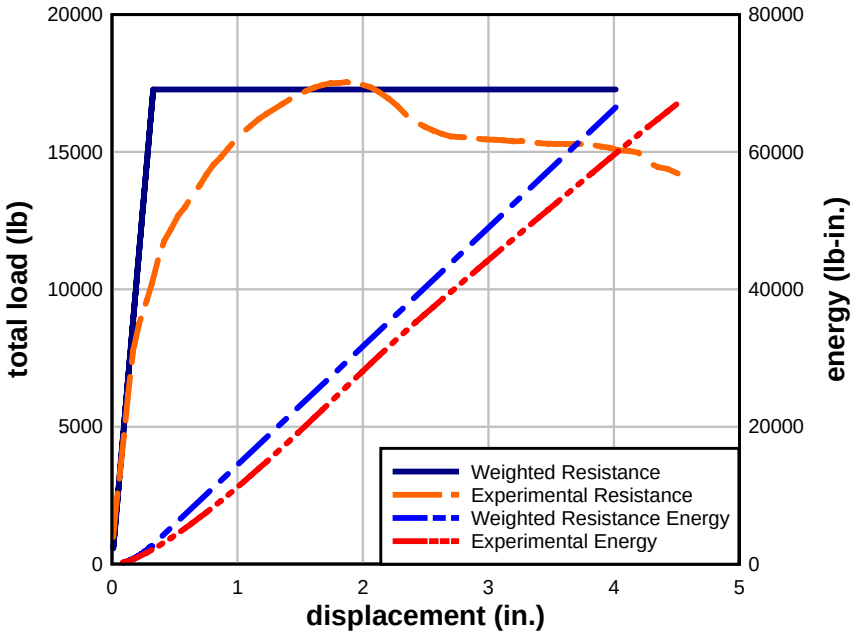

Fig. 5.13. Experiment 1 loading: resistance and energy comparisons for SS2

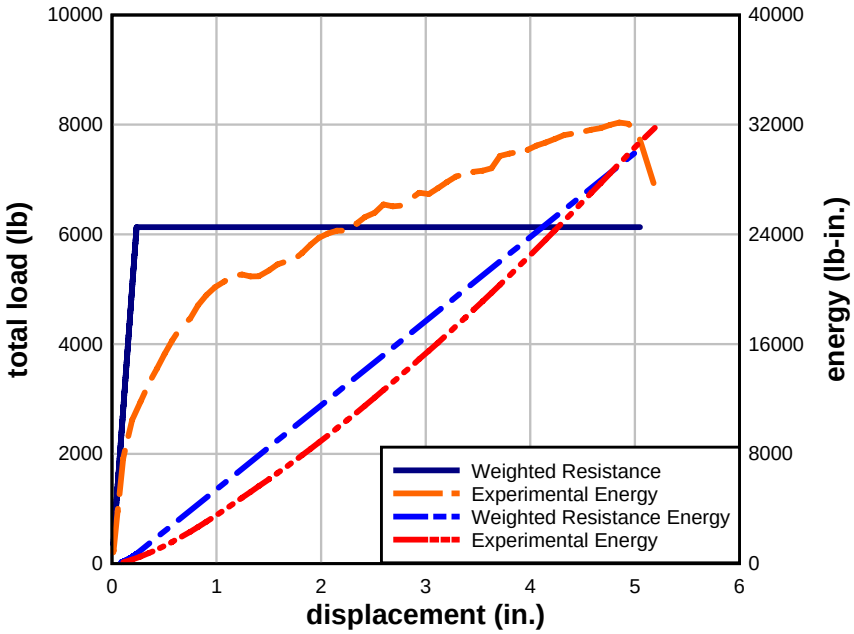

Fig. 5.14. Experiment 1 loading: resistance and energy comparisons for SS3

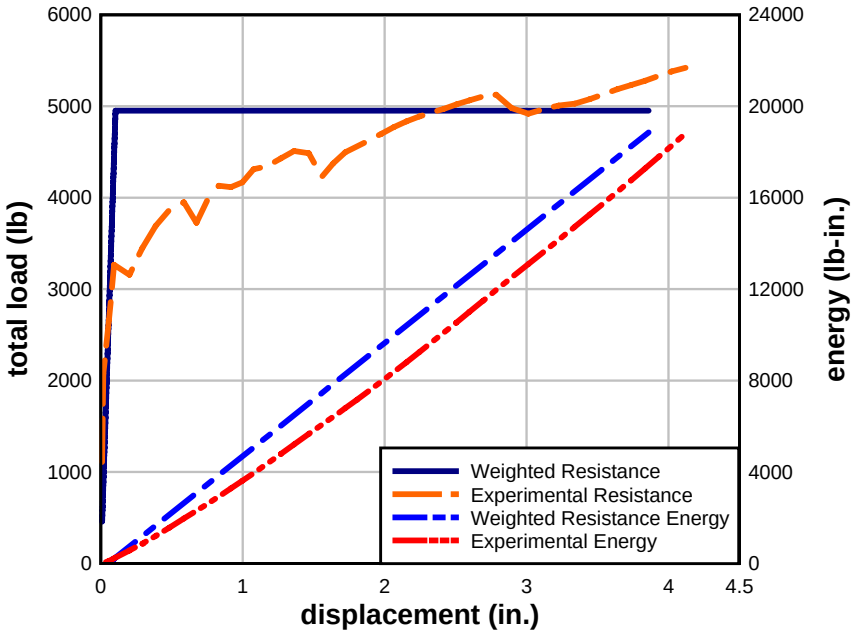

Fig. 5.15. Experiment 1 loading: resistance and energy comparisons for SS4

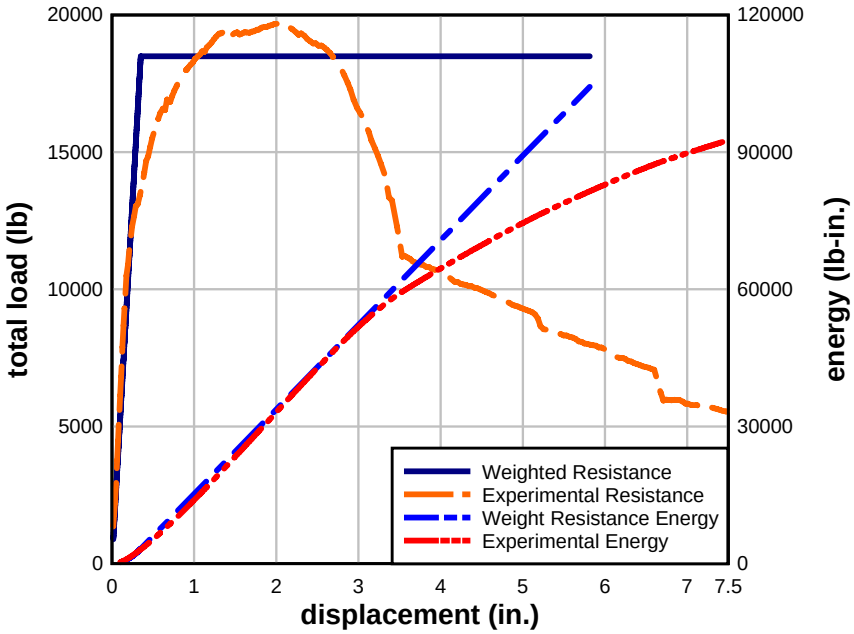

Fig. 5.16. Experiment 2 loading: resistance and energy comparisons for SS1

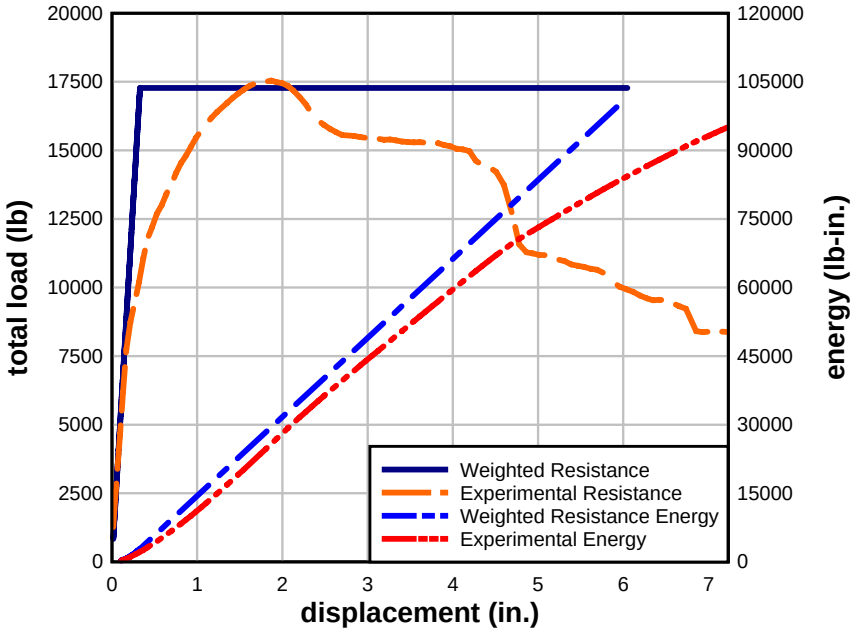

Fig. 5.17. Experiment 2 loading: resistance and energy comparisons for SS2

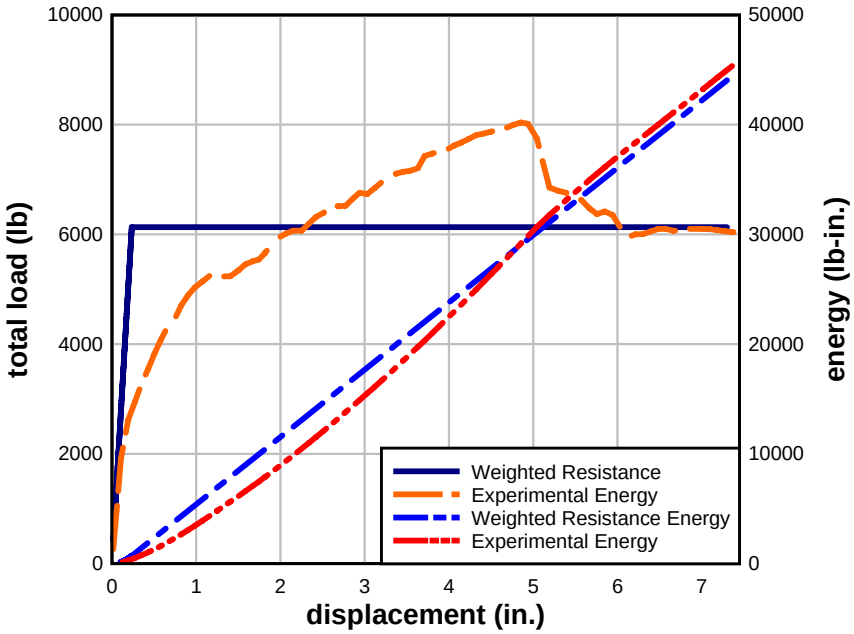

Fig. 5.18. Experiment 2 loading: resistance and energy comparisons for SS3

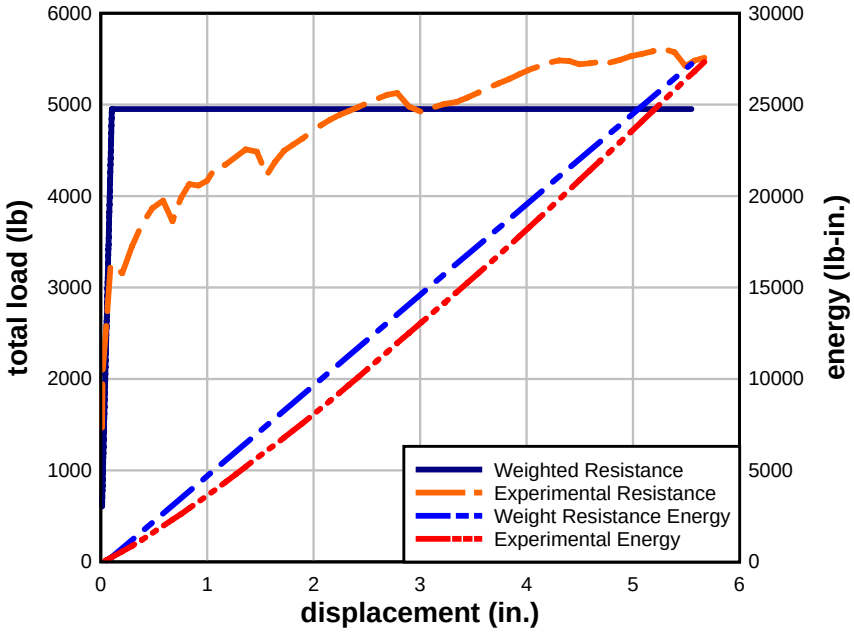

Fig. 5.19. Experiment 2 loading: resistance and energy comparisons for SS4

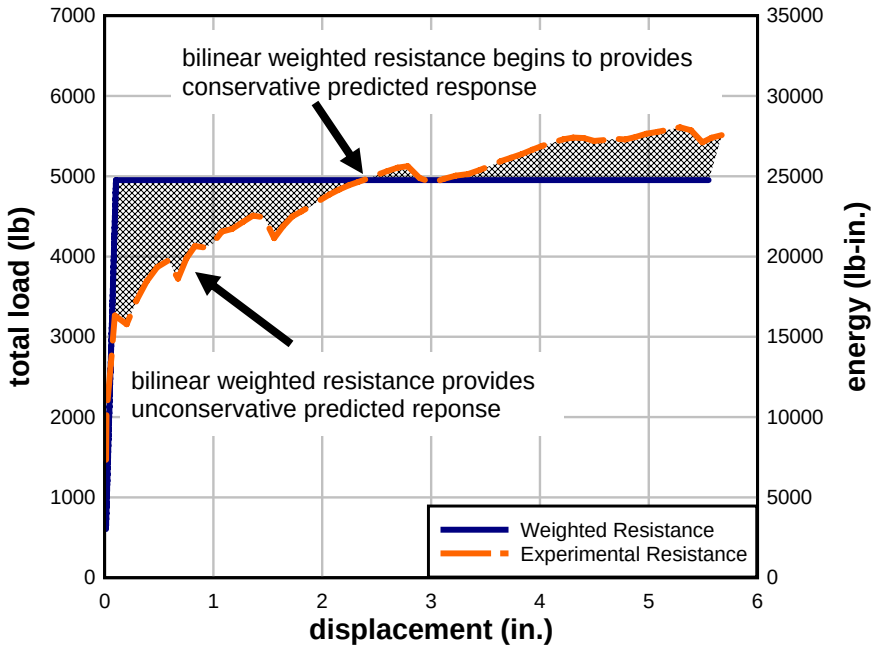

Fig. 5.20. Demonstration of bilinear resistance impact on conservative response prediction

5.4.5 SDOF Prediction Model Comparisons – FE Modeling

Finite element modeling is a less expensive means of studying structural components subjected to blast loads. In order to increase the amount of data points for weighted resistance SDOF prediction comparison, FE models with boundary conditions and span lengths that varied from full-scale dynamic tests were created. FE models were created with the same reinforcement schedules and shear connectors. Weighted resistance SDOF comparisons were previously completed for sandwich panels with span lengths of 9.7 ft and 30 ft. An intermediate span length of 18.67 ft was studied using FE models. Also, models using fixed-fixed connections were created and compared against weighted resistance SDOF responses.

Every finite element model created for the purpose of comparison to SDOF prediction had a response greater than that of the prediction. Some of this variability

between FE models and predictions can be explained. Much greater variability was seen between FE models and predictions with fixed boundary conditions due to the inability to accurately model fixed boundary conditions. FE models were created with an artificial fixed-fixed boundary condition formed from two objects at each end that restricted the boundaries; this is somewhat inaccurate since the weighted resistance SDOF prediction methodology considers fixed boundary condition to be more similar to continuous beams or columns. Figure 5.21 and Table 5.6 present the comparisons between FE model responses and weight resistance SDOF prediction for 18 ft. clear span, simply-supported sandwich panels. Figure 5.22 and Table 5.7 present the comparisons between FE model responses and weight resistance SDOF prediction for 18 ft. clear span sandwich panels with fixed-fixed boundary conditions. Figure 5.23 and Table 5.8 present the comparisons between FE model responses and weight resistance SDOF prediction for 9.7 ft. clear span sandwich panels with fixed-fixed boundary conditions.

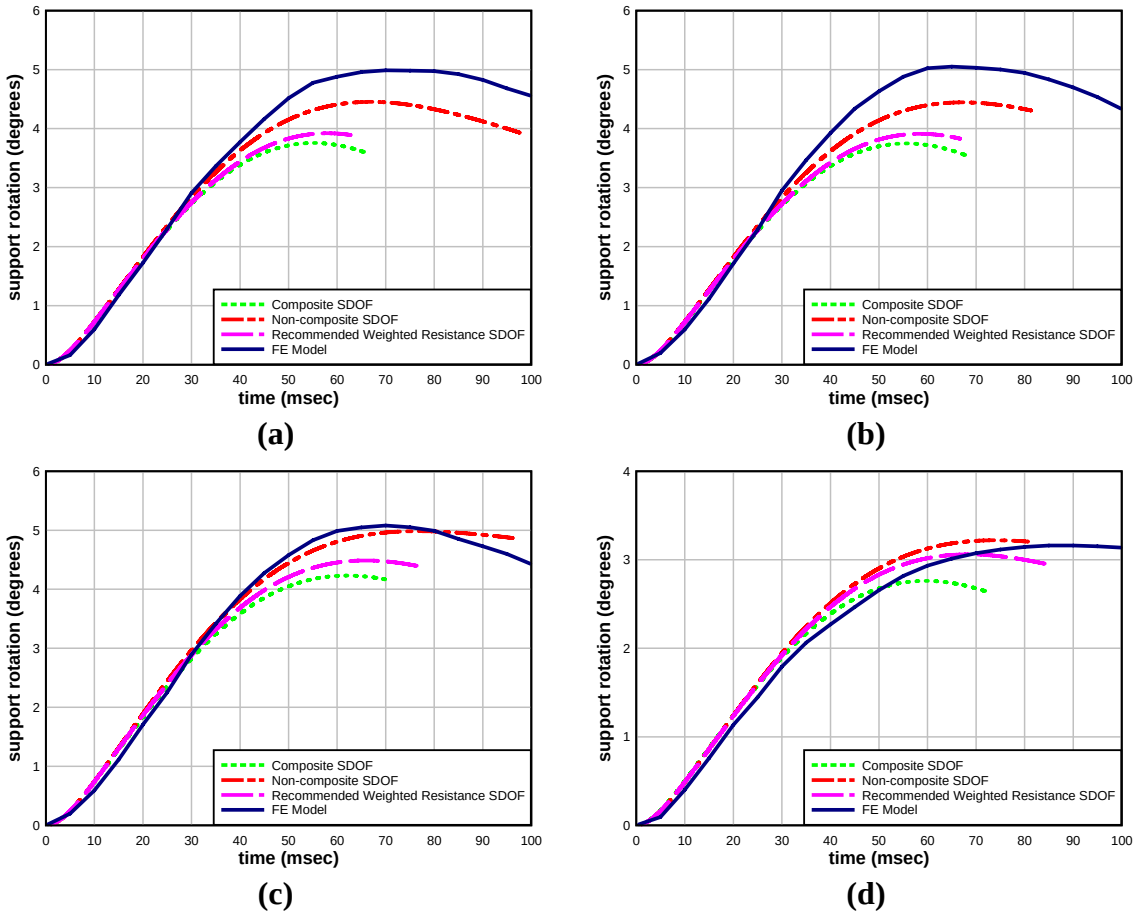

Fig 5.21. FE model response vs. SDOF prediction using weighted resistance for (a) FE-1 (b)FE-2 (c) FE-3 (d) FE-4

Table 5.6. Percent Difference, SDOF prediction vs. FE model response

Panel	Predicted Support Rotation, degrees	Measured Support Rotation, degrees	% Difference
FE-1	3.92	4.99	-21.4
FE-2	3.91	5.05	-22.6
FE-3	4.49	5.08	-11.6
FE-4	3.06	3.16	-3.2

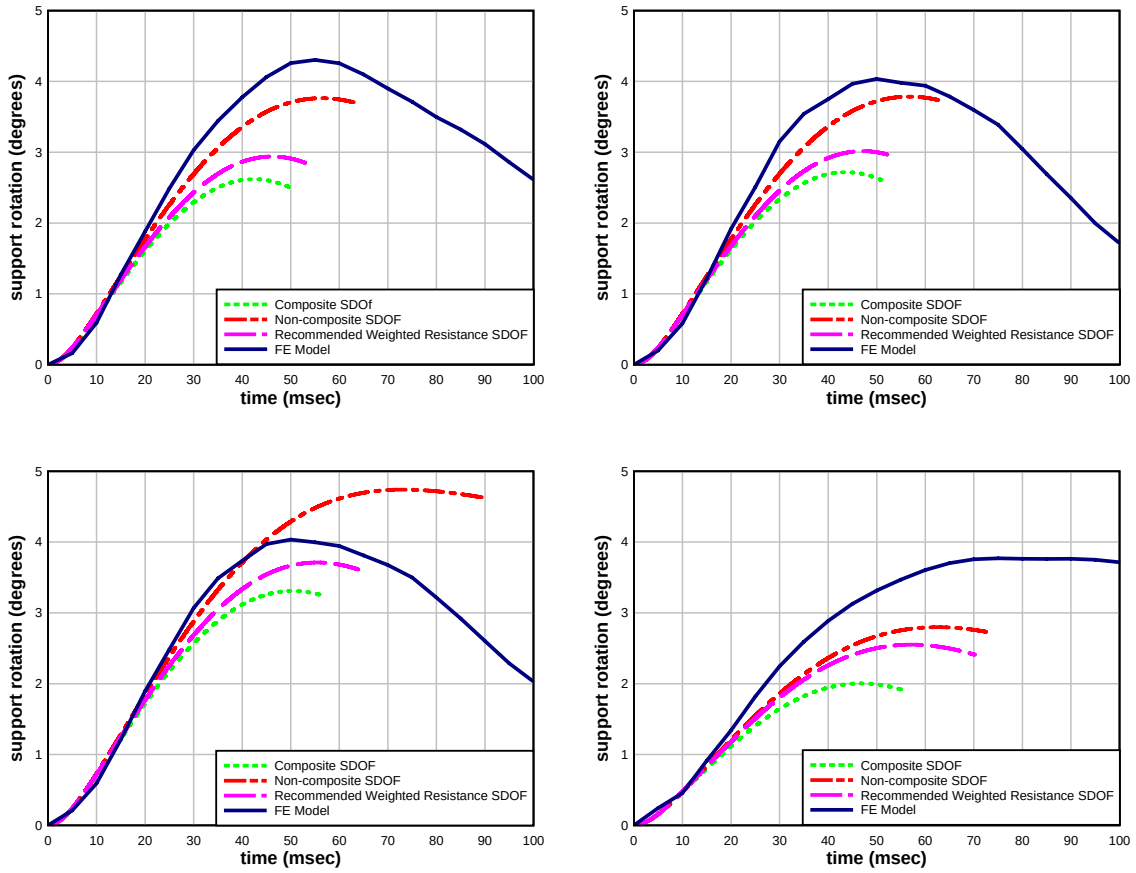

Fig 5.22. FE model response vs. SDOF prediction using weighted resistance for (a) FE-5 (b)FE-6 (c) FE-7 (d) FE-8

Table 5.7. Percent Difference, SDOF prediction vs. FE model response

Panel	Predicted Support Rotation, degrees	Measured Support Rotation, degrees	% Difference
FE-5	2.94	4.30	-31.7
FE-6	3.02	4.03	-25.1
FE-7	3.71	4.03	-7.9
FE-8	2.55	3.77	-32.4

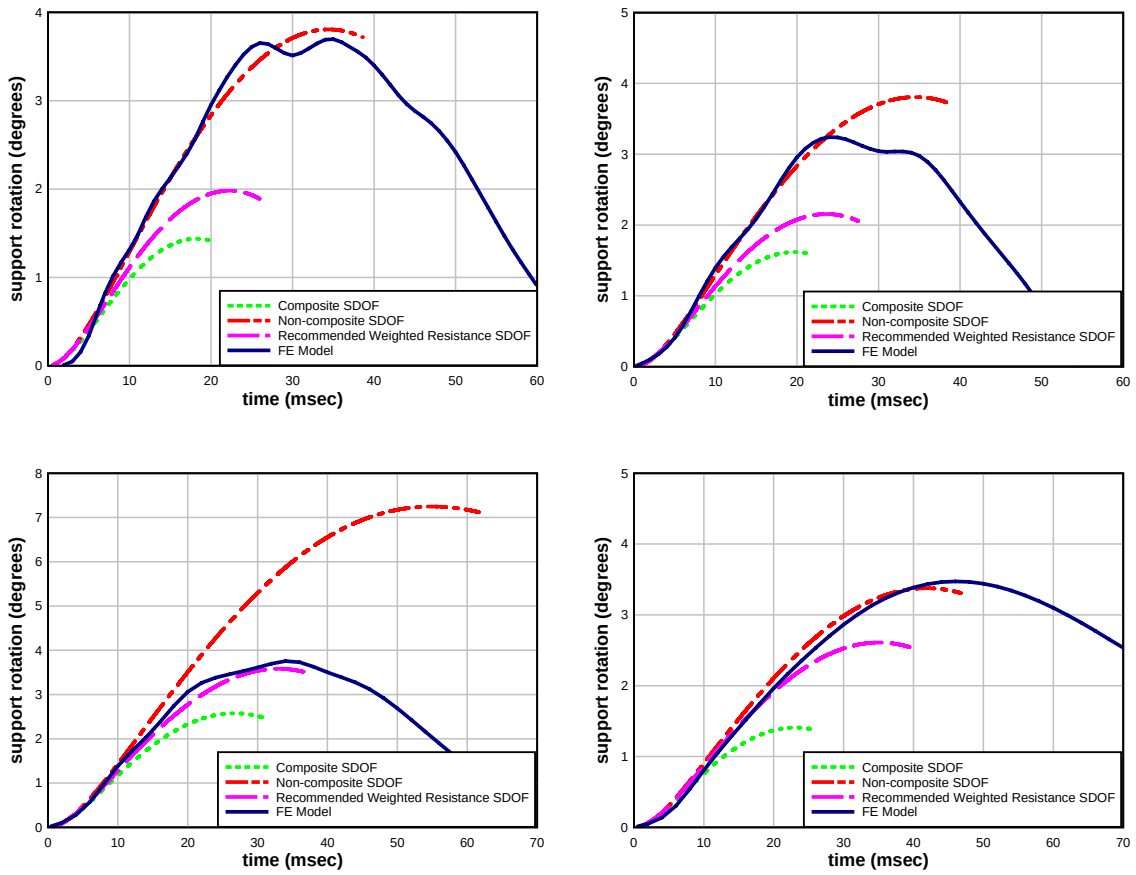

Fig 5.23. FE model response vs. SDOF prediction using weighted resistance for a) FE-9 , b)FE-10, c) FE-11 d) FE-12

Table 5.8. Percent Difference, SDOF prediction vs. FE model response

Panel	Predicted Support Rotation, degrees	FE Model Support Rotation, degrees	% Difference
SS1	1.98	3.70	-46.5
SS2	2.16	3.24	-33.3
SS3	3.58	3.75	-3.73
SS4	2.61	3.47	-23.9

CHAPTER 6

CONCLUSIONS AND RECOMMENDATIONS

6.1 Conclusions

Both static and full-scale dynamic testing of insulated concrete sandwich panels was conducted. A variety of shear connectors were tested to better understand the overall resistance of sandwich panels. Finite element models were created to understand failure mechanisms and characteristics of sandwich panel blast response behavior.

It became clear from static testing that understanding composite action of sandwich panels was crucial to understanding the resistance. Shear connectors are designated composite and non-composite, however composite connectors do not reach allow panels to achieve full composite action under large displacements. Panels using composite shear connectors will act composite while under service loads, but when subjected to large displacement, full composite action between concrete wythes does not occur. Likewise, panels using non-composite shear ties will incur some composite action when subjected to large displacements. Understanding and developing methods to model such behavior are key to predicting sandwich panel behavior.

Finite element modeling methodology was established in four steps: 1) concrete damage model validation using reinforced concrete beam testing as a comparison basis, 2) development of the multi-point constraint approach used to simulate shear connector resistance, 3) static modeling of both conventionally reinforced and prestressed sandwich

panels, 4) dynamic modeling of both conventionally reinforced and prestressed sandwich panels. Static models were validated using laboratory test data. Dynamic models were compared against full-scale dynamic test data to test their viability.

In depth analysis of sandwich panel response behavior was accomplished after comparison to full-scale dynamic tests. From this analysis it was apparent that shear connectors greatly affect the behavior of sandwich panels which aligned with previous static testing analysis.

SDOF prediction methodology was examined using a bilinear weighted resistance to estimate the sandwich panel global resistance. Comparisons between full-scale dynamic test and SDOF predictions demonstrated SDOF prediction models using weighted resistances are a viable option.

6.2 Recommendations

It is recommended that an in-depth look of panels with spans on the larger end of standard sandwich panel design (perhaps >20 ft). This would include both static and full-scale dynamic experiments. Also, a more in-depth study of material properties could be used to increase the effectiveness of finite element models. The effectiveness of SDOF predictions using bilinear weighted resistance could also be increased with continued study of sandwich panels and increased effectiveness of finite element models.

REFERENCES

ABAQUS Standard User's Manual Version 6.7. (2008). Hibbit, Karlsson & Sorensen, Inc., Pawtucket, R.I.

Alaoui, S.and Oswald, C. (2007). "Blast-resistant Design Considerations for Precast, Prestressed Concrete Structures," PCI Journal, vol. 52, pp. 53-65

Biggs, J. M. (1964). "Introduction to Structural Dynamics," McGraw-Hill, New York.

Chopra, A.K., (2001). "Dynamics of Structures," 3rd Edition, Prentice Hall, Upper Saddle River, New Jersey

Department of Defense (2008). "Structures to Resist the Effects of Accidental Explosions," UFC 3-340-02, Whole Building Design Guide, http://dod.wbdg.org/ (accessed Feb. 2010).

Drucker, D. C. and Prager, W, (1952). Solid mechanics and plastic analysis for limit design. Quarterly of Applied Mathematics, vol. 10, no. 2, pp. 157–165.

Franz, U., Schuster, P., Stahlschmidt, S. (2004). Influence of pre-stressed parts in dummy modeling-simple considerations. LS-DYNA Anwenderforum, Bamberg.

Jankowiak, T., and Lodygowski, T (2005). "Identification of Parameters of Concrete Damage Plasticity Constitutive Model," Foundations of Civil and Environmental Engineering, No.6

Jamieson, P. (1998). Khobar Towers : Tragedy and Response, Air Force History and Museums Program. Washington, D.C.

Jenkins, R.S. (2008). Compressive Properties of Extruded Expanded Polystyrene Foam Building Materials. M.S.C.E. report, University of Alabama at Birmingham.

Lee, J., and G. L. Fenves (1998). "Plastic-Damage Model for Cyclic Loading of Concrete Structures," Journal of Engineering Mechanics, vol. 124, no.8, pp. 892–900, 1998.

Livermore Software Technology Corporation (LSTC) (2009). LS-DYNA Keyword User's Manual.

Lubliner, J., J. Oliver, S. Oller, and E. Oñate, (1989). "A Plastic-Damage Model for Concrete," International Journal of Solids and Structures, vol. 25, pp. 299–329.

Malvar, L. Javier and John E. Crawford (1998). "Dynamic Increase Factors for Concrete," Twenty-Eighth DDESB Seminar, Orlando, FL August 1998.

Naito, C., Hoemann, J., Bewick, B., and Hammons, M., (2009a). "Evaluation of Shear Tie Connectors for Use in Insulated Concrete Sandwich Panels," Air Force Research Laboratory Report, AFRL-RX-TY-TR-2009-4600, December 2009, 31 pages.

Naito, C., Dinan, Robert J., Fisher, J., and Hoemann, J., (2009b). "Precast/Prestressed Concrete Experiments - Series 1 (Volume 1)" Air Force Research Laboratory Report, AFRL-RX-TYTR-2008-4616, August 2009, 38 pages.

Naito, C., Hoemann, J., Shull, J., Saucier, A., Salim, H., Bewick, B., and Hammons, M. (2010a). "Static Performance of Non-Load Bearing Insulated Concrete Sandwich

Panels Subject To External Demands," Air Force Research Laboratory Report, AFRL-RX-TY-TR-2009-XXXX, July 2010, 164 pages.

Naito, C., Hoemann, J., Shull, J., Beacraft, M., Bewick, B., and Hammons, M. (2010b). "Dynamic Performance of Non-Load Bearing Insulated Concrete Sandwich Panels Subject To External Demands," Air Force Research Laboratory Report, AFRL-RX-TY-TR-2009-XXXX, September 2010, 123 pages.

National Research Council (1995). "Protecting Buildings from Bomb Damage: Transfer of Blast-effects Mitigation Technologies from Military to Civilian Applications Washington," Washington D.C. : National Academy Press.

Nawy, Edward G. (1996). "Prestressed Concrete: A Fundamental Appraoch," Upper Saddle River, New Jersey: Prentice-Hall Inc.

PCI Committee on Precast Sandwich Wall Panels (1997). "State-of-the-Art of Precast/Prestressed Sandwich Wall Panels," Journal of the Precast/Prestressed Concrete Institute, 42 (2).

PCI Industry Handbook Committee (2004). PCI Design Handbook Precast and Prestressed Concrete, 6th Edition. PCI MNL 120-04, Chicago, IL, USA.

Pessiki, S. and Mlynarczyk, A. (2003). "Experimental Evaluation of the Composite Behavior of Precast Concrete Sandwich Wall Panels," PCI Journal, Precast/Prestressed Concrete Institute, Vol. 48, No. 2, March-April 2003, pp. 54-71.

Stouffer, D. and Dame, L. (1996). "Inelastic Deformation of Metals: Models, Mechanical Properties, and Metallurgy," John Wiley and Sons, Inc.

Tedesco, J. W., McDougal, W. G., and Ross, C. A. (1999). "Structural Dynamics:

Theory and Applications," Addison Wesley Longman, California.

U.S. Army Corps of Engineers Protective Design Center (2006). "User's Guide for the Single-Degree-of-Freedom Blast Effects Design Spreadsheets (SBEDS)." PDCTR 06-02.